EXCEEDINGLY BIOCOMPATIBLE AND THIN-LAYERED REDUCED GRAPHENE OXIDE NANOSHEETS AND ITS APPLICATION IN CO-DELIVERY OF CURCUMIN AND PACLITAXEL SHOWS HIGHLY POTENT SYNERGISTIC ANTICANCER EFFECTS IN A549 AND MDA-MB-231 CELLS

KASTURI MUTHOOSAMY

EXTENDED ABSTRACT SUBMITTED TO THE
UNIVERSITY OF NOTTINGHAM FOR THE DEGREE OF
DOCTOR OF PHILOSOPHY

OCTOBER 2015

The University of Nottingham
UNITED KINGDOM · CHINA · MALAYSIA

Exceedingly Biocompatible and Thin-layered Reduced Graphene Oxide Nanosheets and its Application in Co-delivery of Curcumin and Paclitaxel Shows Highly Potent Synergistic Anticancer Effects in A549 and MDA-MB-231 cells

by

Kasturi Muthoosamy

Under the advisory of

Prof. Dr Sivakumar Manickam

Extended abstract submitted in fulfilment of the requirements for the degree of Doctor of Philosophy in Chemical Engineering

Department of Chemical and Environmental Engineering
Faculty of Engineering
The University of Nottingham Malaysia Campus

2015

Abstract

Delivery of anti-cancer drugs using graphene and its derivatives: graphene oxide (GO) and reduced graphene oxide (RGO) has sparked major interest in this emerging field. The anti-cancer therapies often pose a limitation of insolubility, administration problems and cell-penetration ability. In addition, systemic toxicity caused by lack of selective targeting towards cancer cells and inefficient distribution limits its clinical applications. Graphene nanocomposite is a promising tool to address these drawbacks. Graphene is a flat monolayer of carbon atoms that holds many promising properties such as unparalleled thermal conductivity, remarkable electronic properties, and most intriguingly high planar surface and superlative mechanical strength, which are attractive in biotechnology applications.

However the synthesis route for the production of GO or RGO often involves the use of harsh chemicals which jeopardize its further application as a drug delivery cargo. To overcome these limitations, a simple one-pot strategy was used to synthesize RGO nanosheets by utilizing an easily available over-the-counter medicinal and edible mushroom, *Ganoderma lucidum*. The produced RGO was readily dispersible in water and various solvents. The RGO was highly biocompatible towards colon (HT-29), brain (U87MG) and normal cells (MRC-5). By functionalization of RGO with an amphiphilic polymer, PF-127, a more stable RGO was produced, called GP. Curcumin (Cur) and Paclitaxel (Ptx) was then loaded onto the GP cargo, resulting in a nano-sized GP-Cur-Ptx sytem with the particle size of 140 nm. A remarkably high drug loading was also achieved with 678 wt.%, highest thus far, compared to any other Cur nanoformulations. Based on cell proliferation assay, the GP-Cur-Ptx is a synergistic treatment and is highly potent towards A549 (lung) and MDA-MB-231 (breast) cancer cells. These positive findings are further confirmed by increased reactive oxygen species (ROS); mitochondrial membrane potential (MMP) depletion; and cell apoptosis. The same treated with normal cells (MRC-5) shows that the system is biocompatible and cell-specific.

Keywords: reduced graphene oxide, synergistic treatment, A549, MDA-MB-231, Curcumin, Paclitaxel

Graphical abstracts

1. Synthesis of biocompatible RGO

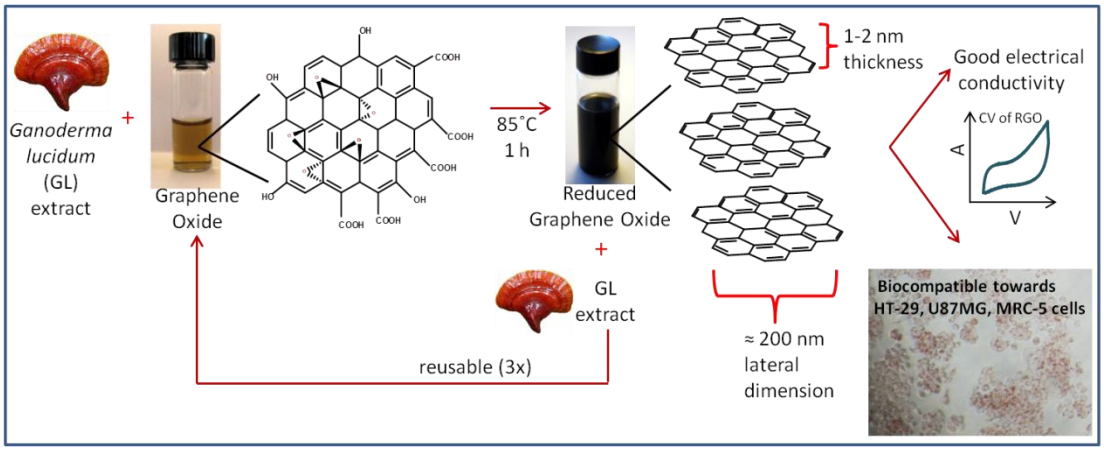

2. Application of RGO as a drug delivery cargo for anticancer drugs

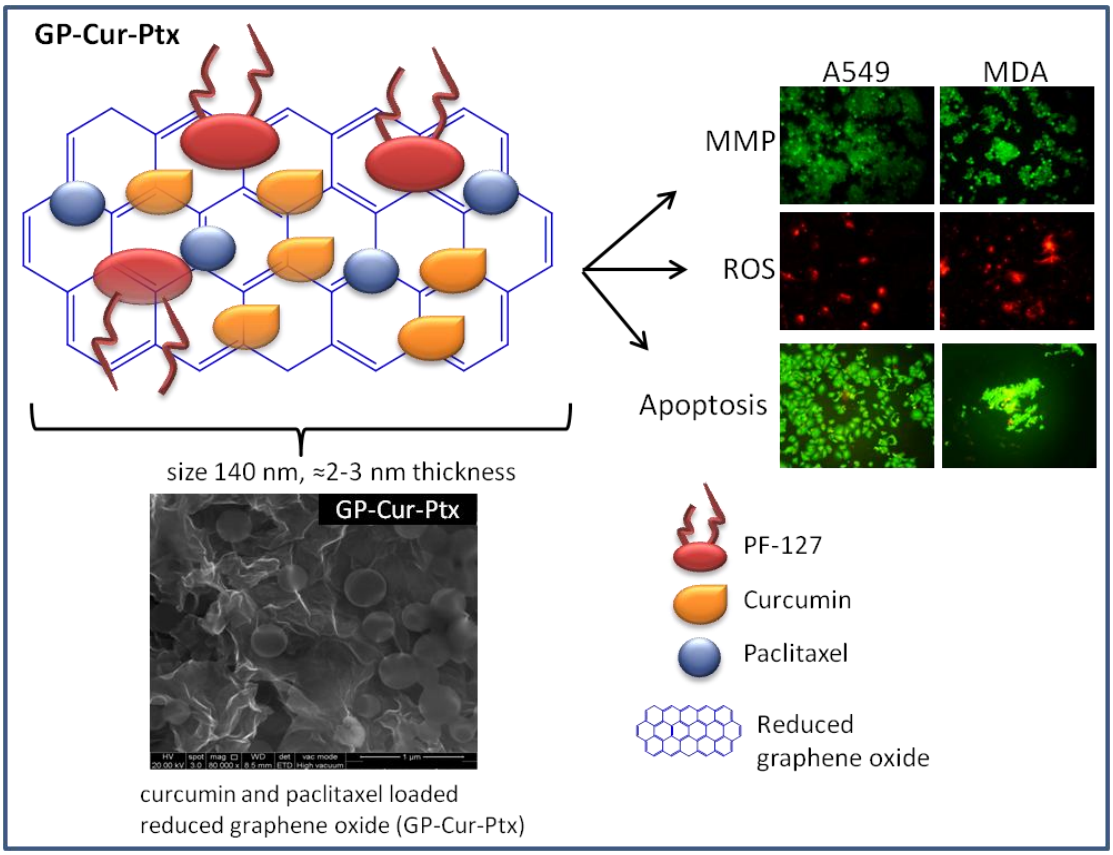

Declaration

This is to certify that:

This extended abstract comprises of only my original work that has been published in journals as listed below. Further details of this PhD investigation can be obtained from the published papers, as attached in Appendix. This extended abstract which serves as a summary of the findings for the whole PhD duration is comprised of 10,000 words in alignment with the University of Nottingham's requirements.

Kasturi Muthoosamy

List of publications:

Peer-reviewed Journal Publications

[1] K. Muthoosamy, R. G. Bai, S. Manickam. Graphene and graphene oxide as a docking station for modern drug delivery system. *Current Drug Delivery* 2014;11;1-18.

[2] K. Muthoosamy, R. G. Bai, I. B. Abubakar, S. M. Sudheer, H. N. Lim, H. S. Loh, S. Manickam, N. M. Huang, C. H. Chia. Exceedingly biocompatible and thin-layered reduced graphene oxide nanosheets using an eco-friendly mushroom extract strategy. *Int. Journal of Nanomedicine*. 2015;10:1505-1519.

[3] K. Muthoosamy, I. B. Abubakar, R. G. Bai, H. S. Loh, S. Manickam. Engineered design for the exceedingly higher co-loading of Curcumin and Paclitaxel onto polymer-functionalized reduced graphene oxide cargo shows highly potent synergistic anticancer effects in lung and breast cancer cells. *Under review @ Scientific Reports, Mar 2016.*

[4] R. G. Bai, N. Ninan, **K. Muthoosamy**, S. Manickam. Graphene: a versatile platform for nanotheranostics and tissue engineering. *Under review, Progress in Materials Science, Oct 2015.*

[5] S. Afreen, **K. Muthoosamy**, S. Manickam and U. Hashim. Functionalized fullerene (C60) as a potential nanomediator in the fabrication of highly sensitive biosensors. *Biosensors & Bioelectronics*. 2015; 63: 354-64.

[6] C. M. Ng, **K. Muthoosamy**, H. S. Loh, S. Manickam, N. Sridewi. Conjugation of insulin onto the sidewalls of single-walled carbon nanotubes (SWCNTs) through functionalization and diimide-activated amidation. *Int. Journal of Nanomedicine.* 2016; 11: 1607-14.

[7] S. Afreen, **K. Muthoosamy**, K. Kokubo, S. Manickam. Hydration or hydroxylation: A quantitative study towards a facile approach of producing Fullerenol by introducing hydroxyl groups onto C60 cage via acoustic cavitation in presence of hydrogen peroxide. *Under review, RSC Advances, Dec 2015.*

[8] R. G. Bai, **K. Muthoosamy**, F. N. Shipton, A. Pandikumar, P. R. Kumar, N. M. Huang, S. Manickam. Biogenic synthesis of reduced graphene oxide-silver (RGO-Ag) nanocomposite and its dual applications as antibacterial agent and cancer biomarker sensor. *RSC Advances*. 2016; 6: 36576-87.

[9] S. N. Ariffin, H. N. Lim, F. A. Tumeri, A. H. Abdullah, M. Ahmad, N. A. Ibrahim, N. M. Huang, P. S. Teo, **K. Muthoosamy**, I. Harrison. Modification of polypropylene filter with metal oxide and reduced graphene oxide for water treatment. *Ceramics Int*. 2014; 40(5): 6927-36.

Book chapter

[10] R. G. Bai, **K. Muthoosamy**, S. Manickam. *Nanomedicine in Theranostics*. *Nanotechnology Applications in Tissue Engineering. Publisher: Elsevier* http://store.elsevier.com/Nanotechnology-Applications-for-Tissue-Engineering/isbn-9780323328890/, Editors: Neethu Ninan, Sabu Thomas, Yves Grohens, **2015**. pp.195-213.

Conference Proceedings

[11] R. G. Bai, **K. Muthoosamy**, S. Manickam. Development of stable aqueous Graphene dispersion by ultrasonic cavitation *In:* 1st International Conference on Ultrasonic based Applications: from Analysis to Synthesis. (Ultrasonic 2014), Lisbon, Portugal, Sep 15-17.

[12] K. Muthoosamy, R. G. Bai, H. N. Lim, N. M. Huang, C. H. Chia, S. Manickam. Biocompatible silver decorated reduced graphene oxide for antimicrobial and biosensing applications *In*: Proceedings of 5th EuCheMS Chemistry Congress, Istanbul, Turkey, 2014; Aug 31- Sep 4.

[13] S. Manickam, R. G. Bai, **K. Muthoosamy**, Exfoliation and generation of nanographene sheet dispersion induced by greener ultrasound cavitation *In:* Proceedings of 5th International IUPAC conference on Green Chemistry (ICGC5), Durban, South Africa, 2014; Aug 17-21.

[14] K. Muthoosamy, S. Manickam, H. N. Lim, N. M. Huang. A Novel multifunctional template using graphene oxide and fluorescent probe as a biomedical cargo for better visualization of curcumin into cancer cells *In:* Proceedings of 3rd Conference on Innovation in Drug Delivery: Advances in local Drug Delivery, Pisa, Italy, 2013; Sep 22-15.

[15] K. Muthoosamy, H. N. Lim, N. M. Huang, S. Manickam. Nano-hybrid graphene and graphene oxide as a biomedical cargo for enhanced delivery of curcumin into cancer cells *In:* Proceedings of the 7th World Congress on Biomimetics, Artifical muscles and Nano-Bio, South Korea, 2013;Aug 26-30.

[16] K. Muthoosamy, R. G. Bai, S. M. Sudheer, H. N. Lim, N. M. Huang, S. Manickam, In-situ green synthesis of reduced graphene nanosheets using medicinal mushroom *In:* Proceedings of 4th International Conference on Nanotechnology: Fundamentals and Applications (ICNFA 2013), Toronto, Canada, 2013; Aug 12-14.

[17] R. G. Bai, **K. Muthoosamy**, S. Manickam. Green synthesis of graphene nanosheets using a medicinal mushroom extract *In:* Proceedings of 3rd Euro-India International Conference on Nanomedicine and Tissue Engineering, Amrita University, India, 2013; Aug 9-11.

[18] K. Muthoosamy, R. G. Bai, S. M. Sudheer, H. N. Lim, N. M. Huang, S. Manickam. Graphene and graphene oxide as docking station for modern drug delivery system In: Proceedings of the NanoBio 2013 (Advances in Biomedical and Pharmaceutical Nanotechnologies), Anna University, Thiruchirappalli, India, 2013; June 27-29.

[19] K. Muthoosamy, H. N. Lim, S. Manickam. Designing a novel nanoscale drug delivery platform using graphene, dye and pluronic PF-127 as a nanohybrid vehicle for improved efficacy of curcumin into cancer cells In: Proceedings of the European Conference/Workshop on the Synthesis, Characterizations and Applications of Graphene, Greece, 2012; Sept 27-30.

[20] R. G. Bai, **K. Muthoosamy**, S. Manickam. Development of stable aqueous graphene dispersion by ultrasonic cavitation In: 2nd Asia-Oceania Sonochemical Society Conference, Kuala Lumpur, Malaysia, 2015; Jul 25-28.

[21] S. Afreen, **K. Muthoosamy**, K. Kokubu, S. Manickam. Quantification of hydroxyl groups on C60 molecular cage generated by acoustic cavitation in aqueous media in presence of hydrogen peroxide In: 2nd Asia-Ocenia Sonichemical Society (AOSS-2) Conference, Kuala Lumpur, Malaysia; Jul 25-28.

[22] R. G. Bai, **K. Muthoosamy**, S. Manickam. Development of metal nanoparticle incorporated graphene sheets and its applications In: National Seminar on "Advanced materials and their applications", Edakochi, Kochi, Kerala, India, 2015; Sep 10-11.

[23] R. G. Bai, **K. Muthoosamy**, S. Manickam. Development of silver nanoparticles by a facile green chemistry approach using a Mushroom - Ganoderma lucidum extract In: WSED (World Sustainable Energy Days), Wels, Austria 2015; Feb 25-27.

Acknowledgements

I would like to extend my deepest gratitude to my PhD Advisor, Prof. Dr Sivakumar Manickam who have guided me from the beginning of my research career and has tirelessly given enormous support, bright ideas and has spent a lot of time providing motivation and advice. Besides providing prompt replies to my questions, Prof Sivakumar always has a solution when I'm caught in crossroads. I am indeed lucky to have such an advisor who noticed my hidden potential and nourished it further.

This work would not have been successful without the support of my fellow PhD colleagues, Renu Geetha Bai, Ibrahim Babangida Abubakar, Surya Mudavasseril Sudheer and Sadia Afreen who worked alongside with me and has given huge support both mentally and physically. Working with them has been a good experience as each brought new ideas to the table and strengthened the research work.

I would like to also express my sincere thanks to the technical staffs, Andrew Yakin, Nurzulaika Rosli, Noor Fatihah Suhaimi, Ahmad Fareez Rawi and Mayhan, who have provided solutions to all the technical issues when it comes to handling analytical equipments. Without your quick action, I would not have finished this research work on time.

A big thank you also goes to my collaborators and my fellow friends, namely Dr Sandy Loh Hwei San, Dr Lim Hong Ngee, Dr Huang Nay Ming, Dr Lim Siew Shee and Suganthi Ramarad, who has always been there to provide me with all support that I need, be it in terms of providing technical advice or mental support.

Last but not least I would like to thank the Dean of Faculty of Engineering, Prof. Ian Harrison, who has given me the opportunity for Staff PhD by Publication and who also recognized my capabilities and gave the room for career growth. I also would like to thank my fellow colleagues in the Faculty of Engineering who have in some way contributed to the success of this project.

Thank you All.

Abbreviations

0D	zero dimensional
1D	one dimensional
2D	two dimensional
3D	three dimensional
6-CFDA	6-carboxyfluorescein diacetate
10x IC_{50}	ten-fold the concentration of IC_{50} values
A549	lung cancer cells
AFM	atomic-force microscopy
CI	combination index
CO_2	carbon dioxide
Cur	curcumin
CNTs	carbon nanotubes
CVD	chemical vapour deposition
DI	distilled water
DLS	dynamic light scattering
DMSO	dimethyl sulfoxide
FBS	fetal bovine serum
FESEM	field emission scanning electron microscope
FRET	Förster resonance energy transfer
FTIR	Fourier transform infrared spectroscopy
GL	*Ganoderma lucidum*

GO	graphene oxide
GP	polymer functionalized RGO
GP-Cur	curcumin loaded onto a polymer-functionalized RGO
GP-Ptx	paclitaxel loaded onto a polymer-functionalized RGO
GP-Cur-Ptx	curcumin and paclitaxel loaded onto a polymer-functionalized RGO
H_2SO_4	sulfuric acid
H_2O_2	hydrogen peroxide
H_3PO_4	phosphoric acid
HCl	hydrochloric acid
HPLC	high performance liquid chromatography
HRTEM	high-resolution transmission electron microscopy
HT-29	colon adrenocarcinoma
IC_{20}	20% inhibitory concentration
IC_{50}	50% inhibitory concentration
JC-10	5,5′,6,6′-tetrachloro-1,1′,3,3′-tetraethylbenzimidazolcarbocyanine iodide
$KMnO_4$	potassium permanganate
MDA-MD-231	breast cancer cells
MDR	multidrug resistance
MMP	mitochonria membrane potential
MRC-5	normal human cells
MTT	3-(4,5-dimethylthiazol-2-yl)-2,5-diphenyltetrazolium bromide

MW cut-off	molecular weight cut-off
NaOH	sodium hydroxide
NFκB	nuclear factor-κB
P	PF-127 polymer
PBS	phosphate buffered saline
PDI	polydispersity index
PEO	polyethylene oxide
PPO	polypropylene oxide
Ptx	paclitaxel
RGO	reduced graphene oxide
ROS	reactive oxygen species
RP-HPLC	reversed phase HPLC
RT	room temperature
TGA	thermal gravimetric analysis
U87MG	brain cancer cells
UV-Vis spectroscopy	ultraviolet–visible spectroscopy
XPS	X-ray photoelectron spectroscopy
XRD	X-ray powder diffraction

Table of Contents

1.0 Introduction

Graphene, a 'wonder material' of this decade has gained tremendous interest from researchers across the globe since its discovery in 2004, using a sticky tape and a pencil [1]. Graphene is a two-dimensional (2D) sheet with one atom thickness and consists of sp^2 hybridized carbon atoms, arranged in a honeycomb network [2]. It is also the building block of other carbon allotropes, whereby wrapping of graphene forms 0D fullerene [3], rolling forms 1D carbon nanotubes (CNTs), and stacking can produce 3D graphite [4].

In this short period of time, extensive research has been carried out on graphene and its derivatives, with the number of publications exceeding 23,000 (Science Direct), closely catching up on CNTs' 33,000 publications, which was discovered back in 1991 [5]. The explosion of interest in this new nanomaterial is due to its properties such as superlative mechanical strength (Young's modulus of 1100 GPa) [6], unparalleled thermal conductivity (5000 W/m/K) [7], electrical conductivity (mobility of charge carriers of 200,000 $cm^2V^{-1}s^{-1}$) [8,9], high planar surface area (2630 m^2/g) [6], ease of functionalization [10,11], low cost and easy scalability on its production [12-15].

As graphene research has expanded, many potential applications were discovered such as new energy storage devices, sensors, transparent electrodes, photodetectors [6,16-18], as well as recent advances in medical applications such as drug or gene delivery, biosensor, medical imaging, tissue engineering, photothermal therapy, antibacterial applications and water treatment [2,14,15,19-26].

Graphene oxide (GO) and reduced graphene oxide (RGO) is part of the graphene family, besides other derivatives such as graphene nanosheets, few-layer graphene and ultrathin graphite [27]. GO, in particular is the most researched material in the graphene family due to its ease of functionalization. GO consists of carboxylate groups on the periphery as well as epoxide, hydroxyl and graphenic domains on the basal plane. The graphenic domain exhibits hydrophobicity and displays pi-pi

interactions with other aromatic molecules, whereas the remaining functional groups provide hydrophilicity. However, most of the routes for synthesizing GO involve strong oxidizing agents which are ultimately carried forward to the end-product. Moreover, GO is highly acidic which could cause damage to the normal cells, thus jeopardizing its role as a carrier in drug delivery system. Moreover, presence of hydroxyl and epoxide groups on the basal plane in GO hinders effective pi-pi interactions with other aromatic molecules due to steric hindrance, as compared to preferable drug carrying capacity in RGO (Figure 1) [28,29].

On the other hand, RGO is the reduced form of GO that contains only the graphenic domains on the basal plane, without any oxygen functional groups. Hence, RGO is hydrophobic and tends to agglomerate irreversibly or even transforms back to graphite due to its van der Waals' interaction and its stronger π-π stacking, which limits its further applications. Therefore, the route of synthesis of RGO is of vital importance to impart stability as most of its unique electrical and mechanical properties are associated only with the individualised graphene sheets [30-32]. In addition, imparting solubility in water is also crucial as a well-dispersed RGO would allow further functionalization and open opportunities for various technological applications.

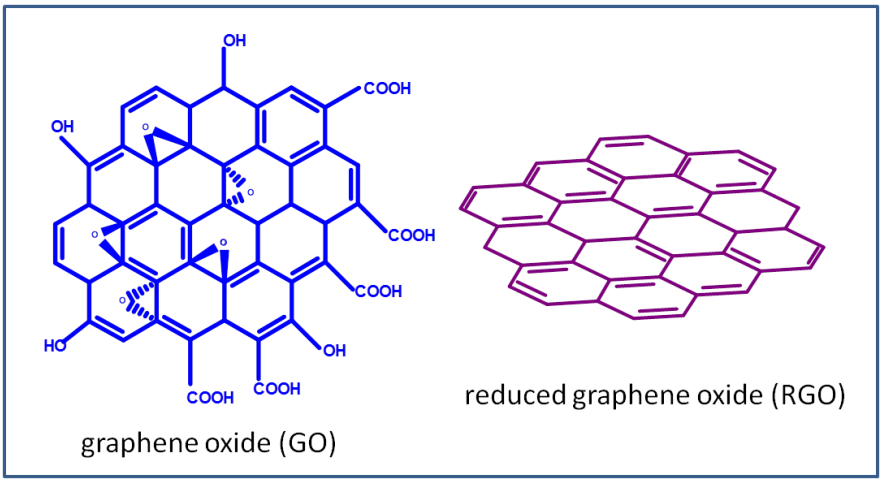

Figure 1 Graphical illustration of GO and RGO.

Several methods have been reported to obtain RGO such as micromechanical cleavage [1], epitaxial growth [33], chemical vapour deposition (CVD) [34], un-zipping of carbon nanotubes (CNTs) [35] and chemical reduction of GO [36]. Micromechanical method suffers from low yield and hinders large scale applications [37]; the epitaxial growth method produces graphene with random and uncontrollable thickness [4]; whereas the methods of CVD and un-zipping of CNTs involve using several chemicals and lengthy reaction steps. Hence, much focus has been emphasized on solution-based reduction of GO which generally produces single to few-layer graphene sheets. Conventional thermal reduction, however requires higher temperatures and pressures for the removal of intercalated water molecules and oxide functional groups such as epoxides, hydroxides and carboxylic acids [37,38]. In addition, it requires a specific reaction vessel and may cause environmental and economic concerns when large scale production is considered.

Therefore, researchers are more intrigued in finding out suitable reducing agents. The most commonly used chemical reducing agents are anhydrous hydrazine [39], hydrazine monohydrate [40], sodium borohydrate [41], and hydroquinone [42]. These reducing agents are highly toxic, harmful and explosive. Moreover, hydrazine-reduced graphene tends to agglomerate irreversibly and converts into graphite [43]. Metal/hydrochloric acid reduction is another alternative, however impurities formed from the residual metal hinders further applications [44,45].

Recently, reduction of GO using environmentally friendly organic agents such as vitamin C [46], amino acid [47], glucose [48], protein [49], plant extract [50-52], dextran [53], bacterial respiration [54] and *E-coli* [38] have taken a centre stage and have been proposed as alternatives. Although these methods are green, they demand lengthy experimental procedures; require expensive reagents and longer reaction times. Besides, some of these methods introduce foreign materials to RGO that may reduce its purity and limit its further applications. An additional step of sonication is often necessary to produce good dispersion in water. Moreover, incomplete reduction and formation of large graphene aggregates hamper its good electrical conductivity [55]. Most of the reports also claim their suitability for drug delivery; however cytotoxicity studies on normal healthy cells have never been looked into. Thus, there

is an impending demand to develop an easy approach which can produce RGO with good purity but without losing its excellent electrical properties and its biocompatibility.

Ganoderma lucidum (GL) or widely known as Reishi in Japan, or Ling Zhi in China, has been a popular mushroom often used in many medicinal applications. It is used in the treatment of a variety of ailments such as hypertension, diabetes, hepatitis, cancer and AIDS. In Asia and North America, usage of this mushroom extends to nutraceuticals and food processing due to many of its astounding properties such as anti-oxidant, anti-inflammatory, anti-bacterial, and anti-viral [56-59]. One of the interesting properties of this mushroom extract is its high content of polysaccharides which exhibit strong anti-oxidant properties [60,61]. Thus, GL extract is a promising prospect to be used as a reducing agent in an eco-friendly RGO synthesis. In addition to this, the polysaccharide is highly soluble in water and does not react with RGO and as a consequence, a simple ultracentifugation step can be carried out to separate the reducing agent (extract) after the reaction [28]. From our investigation, it was found that the GL extract can be used at least three times with good conversion efficiency (75%), as depicted in Figure 2.

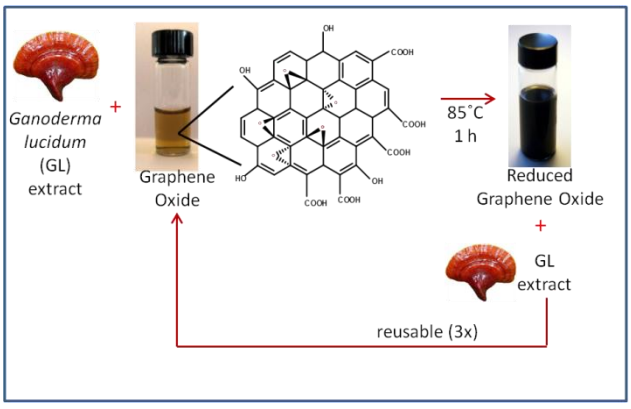

Figure 2 Schematic representation of RGO production from the reduction of GO.

Following the synthesis of RGO which was found to be highly biocompatible towards cancer cells (colon, HT-29 and brain, U87MG) as well as normal (MRC-5) cell lines

[28], the possibility of employing RGO as a drug delivery cargo was investigated. 2 types of hydrophobic drugs were employed, i.e. curcumin (Cur) and Paclitaxel (Ptx) in terms of drug loading efficiency, and synergistic effect of these 2 drugs on lung (A549) and breast (MDA-MD-231) cancer cells as well as MRC-5 cells were also determined.

Curcumin (Cur) is a yellow colored naturally occurring polyphenolic phytoconstituent purified from the rhizome of the plant, *Curcuma longa*. Cur, despite being well-known for its anti-inflammatory, anti-oxidant and anti-bacterial properties, it is also an anticancer agent which has gained much attention. It was reported to be able to suppress and treat various types of malignancies such as breast, cervical, lung, prostate, kidney, pancreatic and colorectal epithelial carcinoma [62-66]. This multi-targeting property is mainly contributed by Cur's ability to regulate about 100 cell signalling pathways [67-69]. Paclitaxel (Ptx), on the other hand is a highly potent and toxic anticancer drug isolated from the bark of *Taxus brevifolia*. Ptx has often been studied in various nanoformulations and in conjunction with other chemotherapeutic agents to enhance its therapeutic effectiveness. It was reported to be able to inhibit breast cancer metastasis [70] and has been used in the treatment of lung, prostate, ovarian, and neck carcinomas, however chemoresistance was also observed in some instances [71-75].

Combination drug therapy with the use of Cur and Ptx has proven as an attractive anticancer modality [76,77]. In this synergistic treatment approach, the co-delivered drug regimen serves as a complimentary effect by targeting different pharmacological pathways. At the mechanistic level, Ptx is a potent microtubule-stabilizing agent that triggers cell cycle arrest which subsequently leads to cell death via apoptosis [78]. In addition to stabilizing microtubules, Ptx up-regulates the expression of nuclear factor-κB (NFκB) which subsequently leads to the enhanced expression of multidrug resistance (MDR) protein, thus promoting cancer cell survival, proliferation, invasion and metastasis [79]. On the other hand, Cur attacks biologically by regulating multiple signal transduction pathways, including the ability to down-regulate the transcriptional factor NFκB, thus eventually inducing cell apoptosis [80]. At the same

time, Cur also sensitizes cancer cells so that its response to anticancer drugs increases and thus improves the therapeutic potential of Ptx [79,81]. Moreover, Cur also overcomes the MDR effect of Ptx by down-regulating the P-glycoprotein production and increase the accumulation of Ptx in cancerous cells [82]. By co-delivery, both of these drugs enhance caspase-3/7 activity, thus significantly increases apoptosis and inhibit lung and breast cancer metastasis [83].

With the simple functionalization of RGO with an amphiphilic triblock co-polymer, such as PF-127 (P), a polymer-functionalized RGO cargo can be produced called GP. In GP enhanced stability and solubility can be attained, whereby the polypropylene oxide (PPO) groups of the polymer will be adsorbed on the surface of RGO via hydrophobic interaction, whereas the polyethylene oxide (PEO) brush will extend out imparting solubility [84]. The hydrophobic drugs, Cur and Ptx can then be loaded to the empty spaces on the RGO via pi-pi interactions between the drugs and the aromatic structures of RGO, as shown in Figure 3.

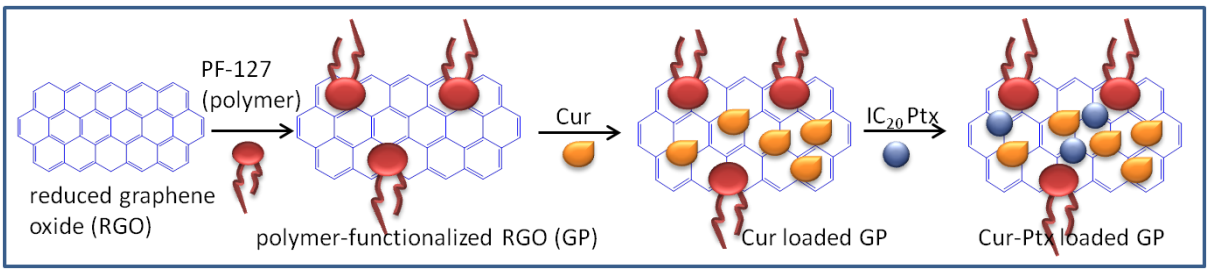

Figure 3 Schematic representation of hydrophobic drugs loaded onto the polymer-functionalized RGO (GP).

Studies have shown that the drug delivery vehicles that are administered intravenously will immediately be cleared from the blood by opsonisation of the mononuclear phagocytic system (MPS), also known as reticuloendothelial system (RES). To overcome this, stealth coating of the delivery vehicles with polymers such as PEG or pluronic allows extended half-life and blood circulation for more than 40 h [85,86]. A pluronic polymer or PEG coated drug delivery vehicle was found to be able to significantly increase the level of recirculation and accumulation of drugs in

tumor and RES organs. In addition, it was found to have extended presence in the systemic circulation at higher concentrations, compared to non-functionalized ones [87-89].

In this engineered design, it is hypothesized that apart from enhanced solubility of Ptx and Cur, exceedingly high drug loading on the GP cargo can also be achieved. The vast unhindered surface on RGO would allow effective and maximal drug loading via pi-pi interactions, which would otherwise be marginally detrimental in GO due to the interference of epoxide and hydroxyl functional groups on its surface. Although there are many reports on combined drug regimen using Cur and Ptx, the dose tested was often random, sometimes in the ratio of 1:1, contradicting the main aim of reducing systemic toxicity. An attempt to use the lowest possible amount of Ptx, such as at the amount of sub-inhibitory concentration of 20% or sub-effective dose of IC_{20} along with abundance of Cur has never been tested, thus far. In addition, the polymer-functionalized RGO (GP) cargo is hypothesized to be non-toxic to normal cells and thus, this nano-sized material is expected to contribute a better drug delivery into cancer cells with increased effectiveness on cancer cell inhibition, compared to treatments with single drug agents [90].

2.0 Methodology

2.0 Methodology

2.1 Materials

Graphite was purchased from Asbury Graphite Mills, Inc. (Asbury, USA). *Ganoderma lucidum* (commercial grade) was contributed by Ganofarm Sdn. Bhd., Malaysia. Typically, mushrooms (including stalk, gills and cap) were dried and ground into powder form and sold to the commercial market. Other reagents employed were of analytical grade and used as-received. Anhydrous D-Glucose was purchased from Fisher Scientific (UK) and PBS buffer was obtained from Sigma Aldrich (USA). Ultrapure deionized water was obtained from a Milli-Q Plus system (Millipore Corp., USA).

2.2 Characterization

The reduction of GO was monitored by measuring the UV-Vis spectrum of the reaction at predetermined time intervals using a Lambda 35 Spectrophotometer (Perkin Elmer). FTIR spectra of solid samples were recorded on a FTIR Spectrometer (Spectrum RX1, Perkin Elmer) in the frequency range of 4000-400 cm^{-1}. The crystalline nature of synthesized RGO was investigated by using a PANalytical X'Pert Pro diffractometer. The XRD was operated at 45 kV with a current of 35 mA and using Cu/kα radiation (λ=1.54060). TGA was performed under a nitrogen flow (50 mL/min) using a TGA/DSC 1, Star^{e} System (Mettler Toledo). Samples were heated from room temperature to 1000°C at 5 °C/min. Ultrasonication was employed by using an ultrasonic bath (Elma, Germany, 130 and 35 kHz, 200 W). Zetasizer Nano ZS (Malvern Instruments, UK) was used to analyse the hydrodynamic diameter of the particles. Samples dispersed in absolute ethanol were drop-casted on Si substrate and dried in air before subjecting to Raman and XPS analysis. Raman spectra were acquired on a inVia Raman Microscope (Reinshaw) with 514 nm laser excitation source. XPS measurements were performed using a Kratos Axis Ultra (Shimadzu, Japan) spectrometer equipped with a monochromatized Al kα radiation (hv = 1486.6 eV). The graphene/ethanol suspension was also drop-casted on Cu grid

(3 nm thick) and mica substrate for HRTEM, AFM and SEM analysis. High-resolution TEM images were acquired using a Philip model (JOEL, Japan) operating at an accelerating voltage of 120 kV. The thickness of graphene materials was examined using 5500 Agilent Technologies AFM System (USA) using a nanosensor NCH with ultrasharp tips. Morphological analysis was carried out using field emission gun SEM (Quanta FEI 400 instrument).

2.3 Preparation of Graphene Oxide (GO)

GO was produced at room temperature based on the modified Hummer's method [91]. Briefly, to a 3 g of graphite, H_2SO_4 (95%) and H_3PO_4 (88%) were added in the ratio of 9:1, followed by a slow addition of 18 g of $KMnO_4$. The resulting inhomogeneous solution was allowed to stir. After 72 h, the reaction was terminated with the addition of 400 g of ice cubes followed by 18 ml of H_2O_2 (30%). The mixture was then centrifuged at 6,000 rpm for 10 min. To the supernatant, 1 M HCl was added to discard the sulphate and phosphate ions followed by centrifugation at 11,500 rpm for 30 min. This was repeated three times followed by washing with DI water for six times. The final mixture was a viscous brown GO solution. A standard calibration curve of GO was generated by measuring the characteristic absorbance of GO at 230 nm by using UV-Vis spectrophotometer. The concentration of the prepared GO was found to be 10 mg/ml.

2.4 Preparation of GL extract

To 1 g of GL mushroom powder, 100 ml of Milli Q water was added and the mixture was allowed to boil at 95°C for 3 h. To remove the spent powder, the mixture was centrifuged at 10,000 rpm for 15 min. The solution was then stored at 4°C and used directly for the reduction of GO as mentioned in section **2.6**.

2.5 Determination of the concentration of GL extract

Concentration of the GL mushroom extract was determined using the phenol-sulphuric acid assay [92] with glucose as a reference. Briefly, to a 10 ml of GL extract, 30 ml of ethanol was added and stored overnight at 4°C. The crude polysaccharide precipitate was then separated by centrifugation at 10,000 rpm for 15

min and the clear supernatant was then subjected to vacuum drying at 40°C to obtain a solid powder. The powder was then dissolved in 1 ml of Milli Q water and 0.1 ml was taken to determine the concentration following the method as reported by [92] The concentration obtained was found to be 1 mg/ml.

2.6 Preparation of RGO using GL extract

pH adjustments were carried out on the GO solution (0.1 mg/ml) by using NaOH to obtain a pH of 7. 50 ml of GL extract was then added to a 50 ml of GO solution and transferred to a water bath which was pre-heated to 85°C and allowed to react for 16 h at 120 rpm. The resulting black dispersion was then ultracentrifuged at 10,000 rpm for 20 min to remove the GL extract. The product was then washed three times with water to further remove the residual GL extract. The resulting black RGO dispersion was then re-dispersed in water.

2.7 Reusability of GL extract

The GL extract which was separated in section **2.6** was reused for 2 more cycles to reduce the freshly prepared GO using the same reduction protocol. UV-Vis measurements were used to determine the amount of GO that was converted to RGO by determining the intensity of RGO peak at 260 nm. In each case, the amount of GO converted to RGO was calculated. The first use of GL extract was considered as 100% conversion from GO to RGO. The yield (%) was determined by drying the obtained RGO in an oven for 48 h at 60 °C.

2.8 GO and RGO size analysis and solubility test

5 min of ultrasonication (20 kHz, 45% amplitude, 750 W) with a microtip was carried out to disperse the GO and RGO before subjecting to size distribution by dynamic light scattering (DLS). For solubility test, RGO was dispersed in water, PBS buffer, ethanol, methanol and acetone by ultrasonication for 5 min. The dispersed samples were kept at RT and observation was continued for 12 months.

2.9 Cell lines and culture conditions

Human grade IV glioblastoma (U87MG), colon adenocarcinoma (HT-29) and normal lung fibroblast (MRC-5) cells were used in this study. HT-29 and MRC-5 cells were cultured with RPMI (Nacalai Tesque) whilst U87MG cells were cultured with MEM containing sodium pyruvate (Nacalai Tesque). The steps on propagation and maintenance of the cells were followed as described previously [93].

2.10 Neutral red uptake assay

Cell viability of GO and RGO treatments was performed by neutral red uptake assay on U87MG, HT-29 and MRC-5 cells as described by Lim et al. [94]. A total of 5 x 10^3 cells were seeded in 96 well plates (SPL Life Sciences, Korea) and incubated overnight for attachment. The cells were treated with 200 µl of media containing 0.1-50 µg/ml of GO and RGO, whereas the cells grown in media without any treatment were used as a negative control. Following 48 h of incubation at 37 ˚C, the percentage of cell viability was determined. All the experiments were carried out in triplicates in three independent experiments. Absorbance readings of the plates were captured by using a microplate reader (Thermo Fisher Scientific, USA) at 490 nm.

2.11 Statistics

Statistical analysis was performed using the Graphpad Prism (version 5) software. One way Anova was used to test for statistical significance between treated and untreated groups using Dunnet *t*-test. Meanwhile, comparison amongst the treatment groups was done by two way Anova using Bonferroni *t*-test.

2.12 Preparation of GP

PF-127 polymer (P) of 0.12 g were added to 20 ml of G (0.15 mg/ml), followed by bath sonication (35 kHz frequency, 100% amplitude, 200 W) for 3 h in a pulse mode with 3 min ‘on’ and 15 min ‘off’ to control the temperature which was maintained at 25±3 °C. The reaction was then left under a shaker overnight at 120 rpm. Subsequently, un-loaded P was removed by dialysis (MW cut-off = 14 kDa) against double-distilled water and left for a further 24 h. To further

remove the unbound polymer, ultracentrifugation at 10,000 rpm for 5 min was carried out. The final product, G functionalized with P will be named as GP hereafter.

2.13 Cur loading studies

Cur in ethanol (2 ml) of various concentrations (0.1-2 mg/ml) was mixed with 2 ml of GP (0.15 mg/ml) and bath sonicated for 1 h, followed by mixing under shaker for another 1 h at 120 rpm. The resulting solution was centrifuged at 10,000 rpm for 15 min. The supernatant was then subjected to UV-Vis analysis, which represents the amount of Cur in excess. A Cur in ethanol calibration curve was initially obtained for quantification. The Cur loading efficiency is determined as follows,

drug loading capacity = $[(W_{\text{initial Cur}} - W_{\text{Cur in excess}}) / W_{GP}]$ x 100
drug loading efficiency = $[(W_{\text{initial Cur}} - W_{\text{Cur in excess}}) / W_{\text{initial Cur}}]$ x 100

where, $W_{\text{initial Cur}}$ is the initial weight of Cur added, $W_{\text{Cur in excess}}$ is the weight of Cur in the supernatant and W_{GP} is the weight of GP. Samples were analyzed in triplicates.

2.14 Preparation of Cur loaded GP (GP-Cur) and Ptx loaded GP (GP-Ptx)

Synthesis of GP-Cur was based on the maximum loading obtained from the above Cur loading studies. Cur (2 mg) was initially dissolved in DMSO/distilled water (1:1) solution. GP (0.15 mg/ml) solution was then introduced and the mixture was bath sonicated (35 kHz frequency, 100% amplitude, 200 W) for 0.5 h before preparing various concentrations of GP-Cur with RPMI media as solvent. For comparison purposes, Ptx loaded onto GP (GP-Ptx) was also tested. For GP-Ptx, 1 ml of Ptx in DMSO (2 mg/ml) was added to 1 ml of GP (0.15 mg/ml), followed by bath sonication for 0.5 h and kept as aliquots at -20°C. Cur and Ptx loaded onto polymer (P-Cur and P-Ptx) was also prepared as controls using the same protocol by replacing GP solution with the polymer solution.

2.15 Preparation of Cur and Ptx co-loaded onto GP (GP-Cur-Ptx)

IC_{20} of Ptx (determined from the cell proliferation assay, **section 2.19**) was added to the GP-Cur solution, followed by bath sonication (35 kHz frequency, 100% amplitude, 200 W) for 0.5 h and dilutions as required in RPMI media. Briefly, IC_{20} of Ptx in A549 and MDA cell lines were determined as 69.7 and 46.7 ng/ml, respectively. Thus 69.7 and 46.7 ng/ml of Ptx were added to GP-Cur (0.2-200 µg/ml) to be tested against A549 and MDA cells, respectively.

2.16 Cell culture

MRC-5 (human normal lung fibroblast), MDA-MB-231 (MDA, human breast adenocarcinoma) and A549 (human lung adenocarcinoma) cell lines were obtained from ATCC (Manassas, USA) and cultured in RPMI media supplemented with 10% FBS and 1% penicillin/streptomycin. All cell lines were maintained at 37°C in a humidified 5% CO_2 atmosphere.

2.17 Determination of cell proliferation using neutral red uptake assay

A total of $5x10^3$ of MRC-5, MDA and A549 cells were cultured in 96-well plates, followed by incubation overnight for cell attachment. The cells were then exposed to 200 µL of various concentrations of the treatment groups (GP-Cur, GP-Ptx, GP-Cur-Ptx) and further incubated for 48 h. For comparison purposes, unmodified Cur and Ptx were also tested. Briefly, 2 mg/ml of Ptx was prepared in DMSO. To obtain the same drug concentration as in GP-Ptx, 1 ml of Ptx (2 mg/ml) was added to 1 ml of distilled water. Subsequent dilutions were made in the RPMI media. The same protocol was adapted to prepare unmodified Cur. Cells grown in the media without any treatment served as a negative control. Following 48 h of incubation, the cell viability was determined using the neutral red uptake assay according to the previously described protocol [95]. The IC_{50} values were determined using the non-linear regression curve fit of the Graphpad Prism5 software. Neutral red was used instead of MTT assay to avoid false positive reading as both the drug Cur and MTT solution are yellow-colored,

whereas the neutral red is a red-colored reagent that absorbs at a wavelength of 540 nm in the UV-Vis spectroscopy.

2.18 Determination of intracellular ROS generation

The generation of intracellular ROS was determined using MAK 142 fluorometric kit (Sigma Aldrich, USA). A549 and MDA cell lines were seeded at a density of $5x10^4$ cells in black 96-well plates with a clear bottom. In a preliminary study, the ROS generation peaked at 120 min, which was taken as the incubation time. Cells were treated with IC_{50} and 10-fold IC_{50} doses of respective treatments (Cur, GP-Cur, Ptx, GP-Ptx, GP-Cur-Ptx) and GP (0.15 mg/ml) as well as plain media (untreated) cells serving as negative controls. After 120 min of incubation, the ROS generated were determined according to the manufacturer's protocol. Subsequently, the fluorescence intensity was quantified using a fluorescence Varioskan flash microplate reader (Thermo scientific, USA) with excitation and emission wavelengths fixed at 650 and 765 nm, respectively. ROS generation was determined as the percentages of ROS compared to the control. For fluorescence microscopy imaging, A549 and MDA cell lines were seeded in 4-well chamber slides (SPL Life Sciences, South Korea). ROS reagents of 125 µL were used and images were captured using Nikon Az100 fluorescence microscope (Nikon, Japan).

2.19 Determination of MMP depletion

A total of $5x10^4$ A549 and MDA cell lines were seeded in black 96-well plates with a clear bottom and were allowed to attach overnight. The cells were then exposed to 200 µL of the treatment groups at concentrations of IC_{50}, 10-fold IC_{50} and plain media (untreated control) and GP (0.15 mg/ml) to monitor the effect of increased dose. After 48 h of incubation, MMP in terms of permeability of JC-10 dye was quantified using MAK159 MMP kit according to the manufacturer's protocol (Sigma Aldrich, USA). JC-10 forms reversible red-fluorescent aggregates in the healthy cells with polarized mitochondrial membrane, however, upon the collapse of MMP, JC-10 returns to its monomeric green-fluorescent form [96]. MMP loss for each treatment group is

calculated as a ratio of green (λ_{ex} = 490/λ_{em} = 525 nm) to red (λ_{ex} = 540/λ_{em} = 590 nm) fluorescence and was taken as a percentage over control.

2.20 Determination of apoptosis using Annexin-V assay

A549 and MDA cell lines were seeded at a density of $5x10^4$ cells in 4-well chamber slides and treated with IC_{50} and 10-fold IC_{50} doses in comparison with the untreated control and GP (0.15 mg/ml) for 24 h. Thereafter, apoptosis was detected using Annexin V-Cy3 apoptosis detection kit according to the manufacturer's protocol (Sigma Aldrich, USA) with slight modifications. Briefly, treated cells were washed twice with PBS (100 µL) and three times with 100 µL of binding buffer (0.1 M HEPES at pH 7.4, 1.4 M NaCl and 25 mM $CaCl_2$). Subsequently, 100 µl of double-label staining solution containing Annexin Cy-3 and 6- Carboxyfluorescein diacetate (6-CFDA) was then added and incubated for 10 min at RT to quantify the living cells from apoptotic and necrotic cells. The staining solution was then removed and the cells were washed five times with 50 µL of binding buffer. Finally, 50 µL of the binding buffer were placed in each well and protected with cover slips and images were captured using Nikon Az100 fluorescence microscope fitted with TRITC filter (Nikon, Japan). Annexin Cy3 stains red on necrotic cells, by binding to phosphatidylserine, which is present outside the plasma membrane of cells undergoing apoptosis. Upon entering the living cells, the non-fluorescent 6-CFDA is hydrolyzed by esters producing a green-fluorescent product. Cells in the early stages of apoptosis, however, stained yellowish-green [97].

3.0 Results and Discussion

3.1 Characterizations of RGO

The reduction of GO using GL extract was monitored by time-dependent UV-Vis spectroscopy as shown in Figure 4. The strong absorption peak at 230 nm (0 h) is a distinctive peak of GO which corresponds to π-π* transition of C=C bond and the shoulder at 300 nm is due to n-π* transition of the C=O bonds in GO. Gradual red-shifting of the 230 nm peak towards 260 nm can be seen during the reaction, suggesting the restoration of π-conjugation network of RGO after reduction. Moreover, the gradual disappearance of the plasmon peak at 300 nm confirms the removal of oxygen groups in RGO [30,98,99]. The formation of RGO was observed within 1 h with the red shift of a typical GO peak at 230 nm to 251 nm. The highest absorbance was observed at 16 h, which indicates that reaction time is directly proportional to the amount of RGO formed. A tested duration of 48 h gives ≈73% yield.

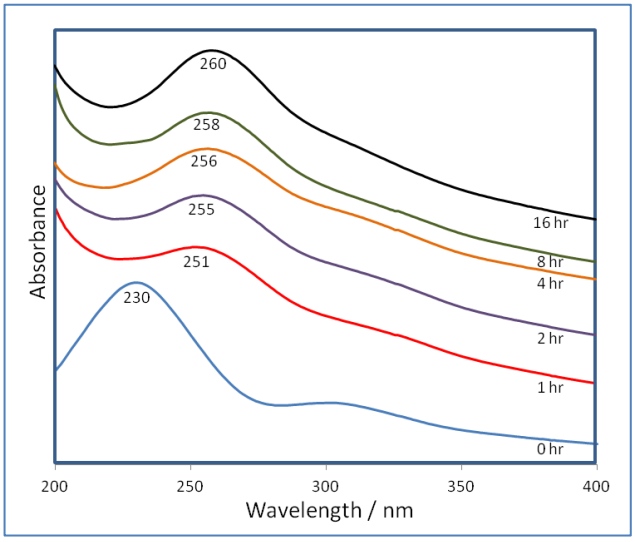

Figure 4 UV-Vis spectra of GO reduction with GL extract at different time intervals.

The formation of RGO is further confirmed by FTIR spectroscopy as shown in Figure 5a. FTIR spectra of GO shows a strong absorption peak of ν_{O-H} at 3412 cm^{-1} due to stretching vibrations and a deformation peak at 1396 cm^{-1} due to the hydroxyl groups located on the plane of GO. Carboxyl groups at the edges of GO sheets show stretching vibration and the $\nu_{C=O}$ peak appears at 1726 cm^{-1}. The spectra also exhibit several characteristic peaks of GO; $\nu_{C=C}$ at 1630 cm^{-1} due to the aromatic C=C bonds; ν_{C-O} at 1246 cm^{-1} due to the epoxy C-O stretching vibration; and ν_{C-O} at 1116 cm^{-1} due to the alkoxy C-O stretching vibration [31,38,100]. Compared to graphite the GO spectrum indicates successful oxidation with the presence of hydroxyl, epoxy, alkoxy and carboxyl functional groups. Successful deoxygenation could be seen for RGO with the disappearance and reduced intensities of all the oxide functional groups. A broad C-O band that appears from 1214 to 1000 cm^{-1} even after reduction could be attributed to oxygen atoms or cyclic ether accumulated at the edges of defects in RGO. This indicates that all the oxygen groups are removed from the region adjacent to edges and only clean graphene domains are present in RGO [4,101]. The spectra of GL extract exhibit a broad band around 3397 cm^{-1} due to the stretching of N-H and O-H groups, and a corresponding N-H bending at 1639.5 cm^{-1}. Other characteristic peaks of the GL extract are at 2930 cm^{-1} and at 2884.9 cm^{-1} due to the asymmetric stretching of CH_3 and symmetric stretching of CH_2, respectively. The sharp peaks at 1074.4 cm^{-1} and at 1046.5 cm^{-1} are due to C-O stretching and bending of C-OH in the polysaccharide [102,103]. The absence of these characteristic peaks in RGO confirms the complete removal of the GL extract after the reaction.

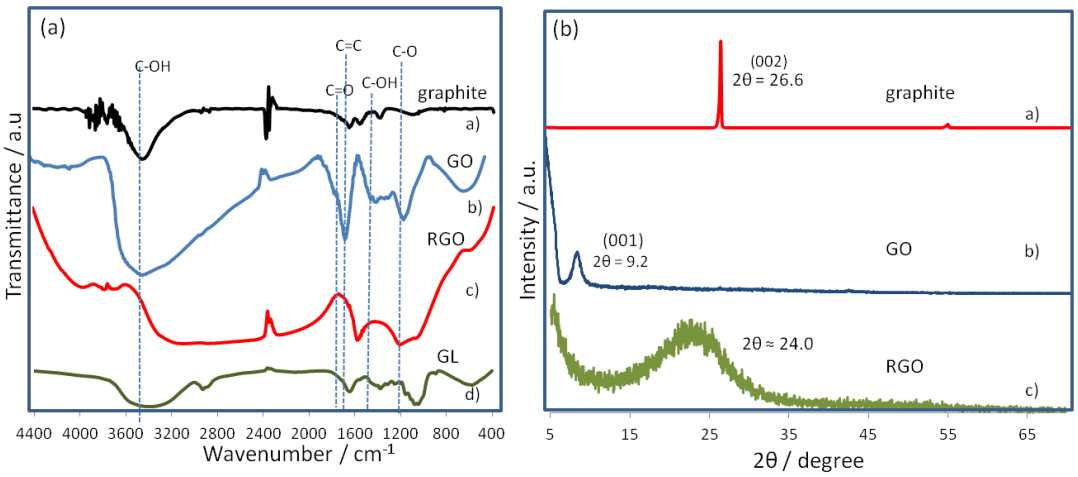

Figure 5 (a) FTIR spectra of (i) graphite, (ii) GO, (iii) RGO and (iv) GL extract; (b) XRD patterns of (i) graphite, (ii) GO and (iii) RGO.

The XRD analysis (Figure 5b) is a good tool to estimate the interlayer spacing between the graphitic layers, the crystalline properties as well as to determine the completion of reaction. Graphite exhibits a strong basal reflection (002) at 2θ = 26.6° with an interlayer distance (d-spacing) of approximately 0.33 nm. This intense crystalline peak is a characteristic peak of hexagonal pristine graphite. The disappearance of this peak in GO confirms the complete oxidation of graphite. Upon oxidation, the diffraction peak (001) of GO appears at a lower angle (2θ = 9.2°) with a d-spacing of 0.96 nm. The larger interlayer spacing after oxidation is due to the intercalation of oxide functional groups on both sides of GO sheets. In addition, structural defects (sp^3 bonding) generated on the originally flat graphite sheets contribute to an atomic-scale roughness and thus a larger d-spacing of GO [104]. After reduction, the distinctive GO peak of RGO disappears indicating reduction as well as exfoliation of the layered RGO sheets [49,105]. A broad peak has been observed for RGO, starting from 2θ = 15 to 30°, with the peak centred at 2θ = 24.0°, and a d-spacing of 0.37 nm. The appearance of this peak at 24.0° is due to restoration of van der Waals interaction between the carbon frameworks on the graphene sheets

upon reduction. The presence of a broad peak indicates the loss of a long range order in the graphene sheets and stacked with few layers thickness [43,100,106,107]. In addition, the significant reduction in the interlayer spacing of RGO as compared to GO suggests the removal of oxygen groups and water molecules from the interlayer of graphene sheets in RGO.

The formation of RGO was further confirmed by XPS analysis. The C1s of GO as shown in Figure 6a demonstrates the highest intensity at the binding energy of 287.8 eV, which belongs to carbonyl functional groups. Other peaks at 284.8, 286.3 and 289.1 eV correspond to C=C/C-C in aromatic rings; C-O in hydroxyl and epoxy groups; and O-C=O in carboxyl groups, respectively [38,43,108]. After reduction, the peak intensity for all the oxygen species has decreased dramatically suggesting the effective removal of oxygen containing groups in RGO. In addition, a sharp increase in the C=C/C-C peak at 284.4 eV and the appearance of a pi-pi* peak at 288.5 eV indicate the restoration of sp^2 carbon network [109]. C/O molar ratio calculated from the peak areas shows a very high content of oxygen species in GO (1:13.6), whereas in RGO the molar ratio was found to be only 1:2.16, again confirming the successful reduction of GO.

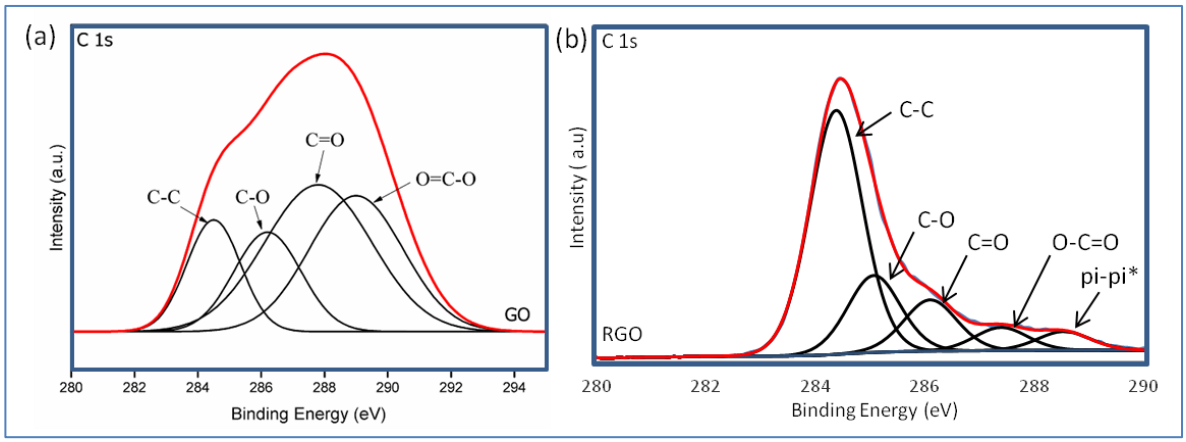

Figure 6 XPS spectra of C1s of (a) GO and (b) RGO.

Figure 7 shows the FESEM images of GO and RGO. It could be observed that GO (Figure 7a) has a continuous and smooth wave-like sheets, whereas a flake-like morphology could be noted in RGO (Figure 7b) which forms a disordered solid with

the individual sheets closely stacked [110,111]. With the removal of oxygen groups from the basal plane as well as from the edges of RGO, the graphene sheets are now allowed to closely associate and stack via van der Waals interactions. This finding is in good agreement with the results of XRD obtained for RGO, where the d-spacing or interlayer distance is smaller than GO, permitting the stacking of RGO flakes. The RGO flakes lie flat on top of each other suggesting the possibility of good electrical contact between them [112]. The microstructure of GO and RGO was further investigated by HRTEM. It could be seen that GO has a wavy structure with few well-defined layers of stacking at the edges (Figure 7c). The observed stacking could be due to strong hydrogen bonding interaction between the GO layers or with water molecules [113]. As for RGO, thin veil-like sheets were observed with scrolling and wrinkles which confirms that the reduction of GO has taken place. It was reported that scrolling is caused by the presence of isolated epoxy and hydroxyl groups, whereas the wrinkles are due to the removal of strain on the C-C bond in the epoxy groups which was created during the formation of three-membered epoxide ring in GO [114]. In addition, RGO appeared transparent which is similar to the graphene produced from electrolytic exfoliation of graphite. Lateral dimension of RGO in both FESEM and HRTEM was approximately 500 nm.

To further confirm the reduction of GO, Raman spectroscopy was used to investigate the nature of layering and defects on the graphitic sheets. The Raman spectra of graphite (Figure 8) displays a sharp G band at 1582 cm^{-1} due to in-phase vibration of the graphite lattice and a weak D band at 1370 cm^{-1} indicating low degree of defects that are mostly due to the sheet edges. In comparison, GO exhibits a prominent G band which is blue-shifted to 1586 cm^{-1} signifying the presence of isolated double bonds which resonate at higher frequencies than that of graphite. The intensity of D band at 1352 cm^{-1} was also increased which could be attributed to the decrease in size of in-plane sp^2 domains compared to graphite [38,43,49,104]. For RGO, the G band is broadened and shifted to 1611 cm^{-1} and moved closer to the G band of graphite attributed to graphitic self-healing and successful reduction [115], as the removal of oxygen groups allows the RGO to associate and re-stack. The D-band of RGO

becomes more prominent and remains almost at the same position as GO i.e. at 1351 cm^{-1}.

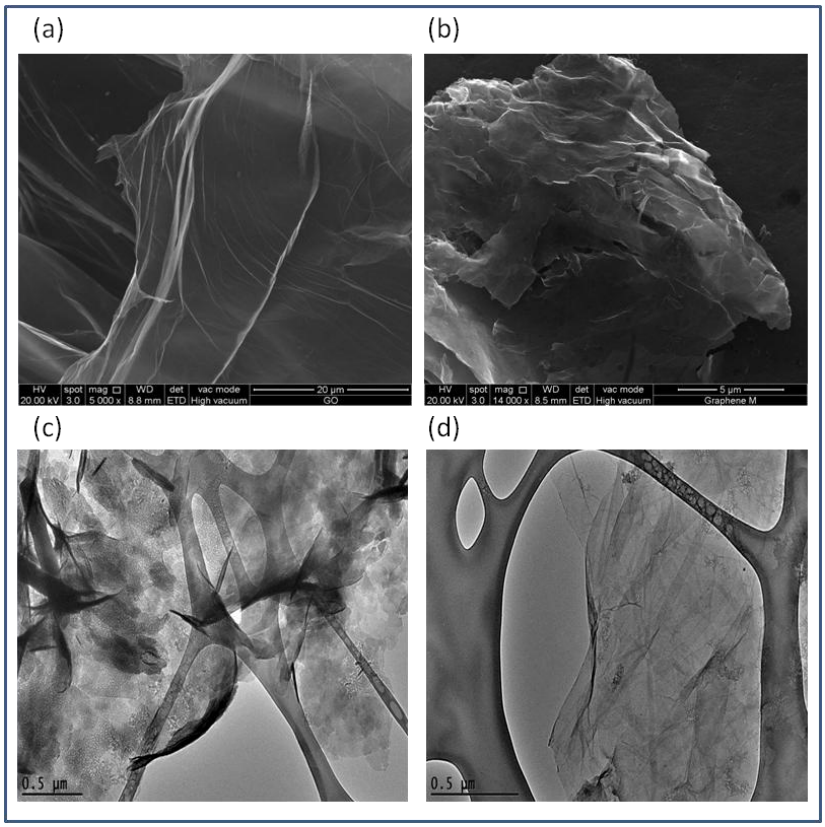

Figure 7 FESEM images of (a) GO and (b) RGO and HRTEM images of (c) GO and (d) RGO.

The intensity ratio of D to G (I_D/I_G) is a good indicator of the degree of distortion in the graphitic sheets. As expected, the intensity ratio of RGO has dramatically increased to 0.99 as compared to GO (0.94) and graphite (0.07). A higher intensity ratio as seen in GO compared to graphite is due to the introduction of defects after oxidation of graphite, whereas the highest intensity ratio seen in RGO indicates disorder on the graphene sheets after reduction and an increase in the number of sp^2 domain. It is suggested that the reduction of GO causes fragmentation and yields smaller RGO graphitic domains with different sizes [116,117].

The 2D band represents the symmetry-allowed overtone of the G band. The shift, shape and width of the 2D peak are sensitive to the stacking order of the graphene

sheets along the c-axis and the number of graphene layers, in which single-layered graphene has a single sharp Lorentzian peak below 2700 cm^{-1}. Multiple layered sheets have broader and up-shifted 2D peaks [30,100,104,118]. The broad 2D band of graphite from 2627 to 2776 cm^{-1} indicates the presence of multiple layered graphite sheets, whereas the 2D band of GO at 2700 cm^{-1} indicates a single layered sheet. After reduction, this peak has marginally broadened and shifted to 2769 cm^{-1} suggesting the presence of three-layered graphene sheets [119]. The cooperation between D and G peaks gives D + G combination band which indicates the presence of highly disordered and randomly arranged graphene sheets [30,31]. The D + G band is observed for GO at 2690 cm^{-1} and a slightly broader band is observed for RGO at 2692 cm^{-1} indicating the presence of more random arrangement in RGO. The absence of these peaks in graphite shows that it exists as a continuous long sheet.

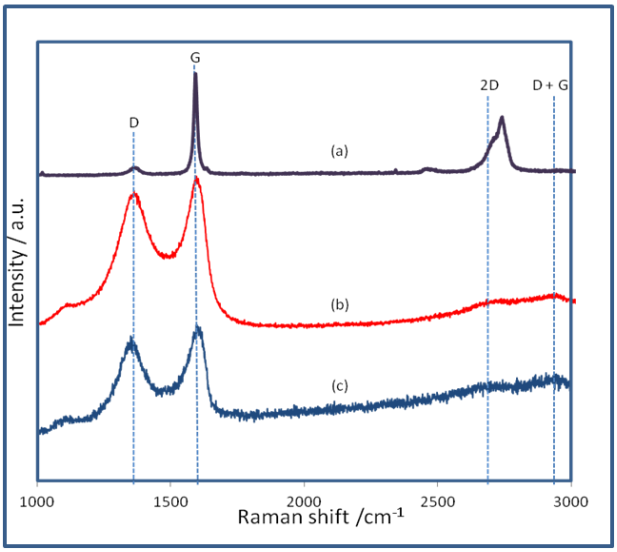

Figure 8 Raman spectra of (a) graphite, (b) GO and (c) RGO.

GO and RGO were then subjected to AFM to determine their respective topography as well as thickness (Figure 9). The cross-section from AFM analysis shows that the maximum thickness of GO is approximately 1 nm which is in compliance with the d-spacing of GO i.e. 0.96 nm as determined by XRD. After reduction, the RGO's thickness is approximately 1-2 nm. The thickness obtained is similar to those

produced from hydrazine reduced GO [120,121] and hydrothermally reduced GO [114].

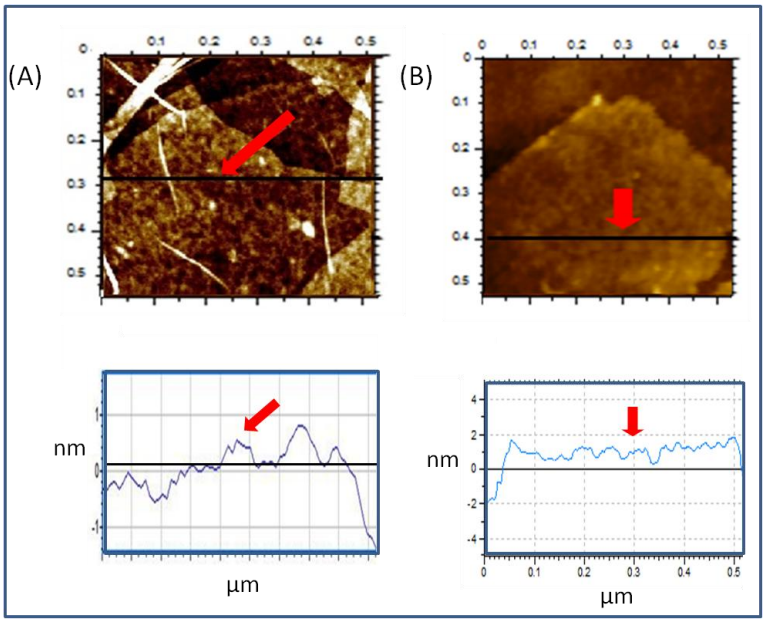

Figure 9 AFM images of (A) GO and (B) RGO with respective thickness measurements taken along the cross-section, as indicated by a line and a red arrow.

Based on the XRD analysis of RGO with 0.37 nm d-spacing, it could be estimated that RGO is few-layered (3-5 layers) similar to the observation made using Raman analysis.

The particle size distribution of aqueous dispersion of GO and RGO was determined by DLS analysis. Although DLS is more suitable for spherical particles rather than for planar sheets like graphene, it serves to indicate whether a uniformly-sized dispersion of graphene was produced in addition to demonstrating the changes in the size of GO and RGO. As shown in Figure 10, the average size of GO and RGO is 313 nm and 181 nm, respectively. In GO, the peak appearing after 1,000 nm could be due to the presence of remnants from the reaction of graphite oxidation. Also, the presence of undisrupted long continuous sheets in the GO results in larger size. RGO however shows a uniform size distribution with sizes generally at least two times smaller than

GO. This concludes that there is a loss of long range graphitic order in RGO and corroborates with the observation of a D+G peak in the XRD spectra. The smaller sized RGO observed could be mainly due to the method of synthesis employed and due to the effect of 5 min of ultrasonication. Generally, ultrasonication breaks the RGO nanosheets to smaller fragments, a similar observation was also noted in GO [122]. In addition, ultrasonication of RGO results in better dispersion in water. A solubility test conducted (Figure 10) shows that RGO is stable in the tested solvents for up to 12 months, without any visible aggregation or sedimentation. It is reported that ultrasonic treatment induces cavitation near surfaces of RGO sheets which inhibits the aggregation of RGO by weakening its van der Waals interactions and thus enhanced the formation of stable RGO dispersion [109].

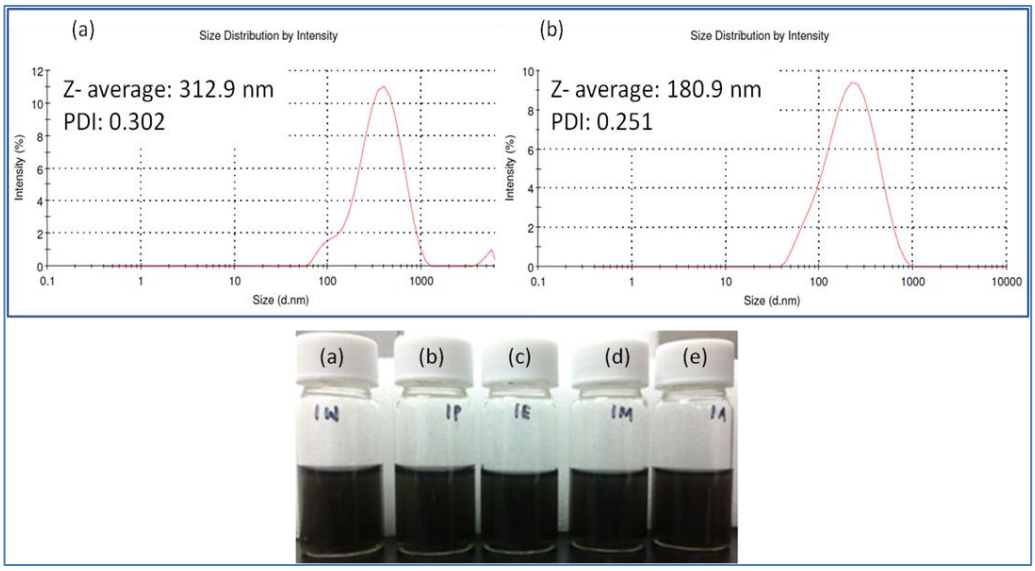

Figure 10 Above: Size distribution analysis on a) GO and b) RGO with its respective polydispersity index (PDI) and average size (Z). Below: Solubility of RGO in (a) water (b) PBS buffer (c) ethanol (d) methanol and (e) acetone.

3.2 Cell viability of GO and RGO on normal and cancer cells

Based on the fact that viable cells incorporate and bind more dye as compared to damaged or dead cells [123], the dose dependent cytotoxicity of GO and RGO can be determined by neutral red uptake assay. Cell viabilities were normalized using

untreated cell readings. Both GO and RGO showed no significant toxicity towards HT-29 cells as shown in Figure 11a. Over 90% cell confluence was observed at the highest concentration (50 µg/ml), even for GO. However, a different cytotoxicity pattern is seen in U87MG cells as shown in Figure 11b. A decrease in cell viability was observed for GO starting from 10 µg/ml when compared to untreated cells. GO has been largely reported to cause plasma membrane damage and oxidative stress, thus the anti-proliferative distress to the cells [124]. On the other hand, RGO was found to be biocompatible with almost 100% cell confluency even at the highest concentration (50 µg/ml). By comparing GO with RGO, significant difference in cell viability was observed starting from the concentration of 25 µg/ml ($p < 0.01$).

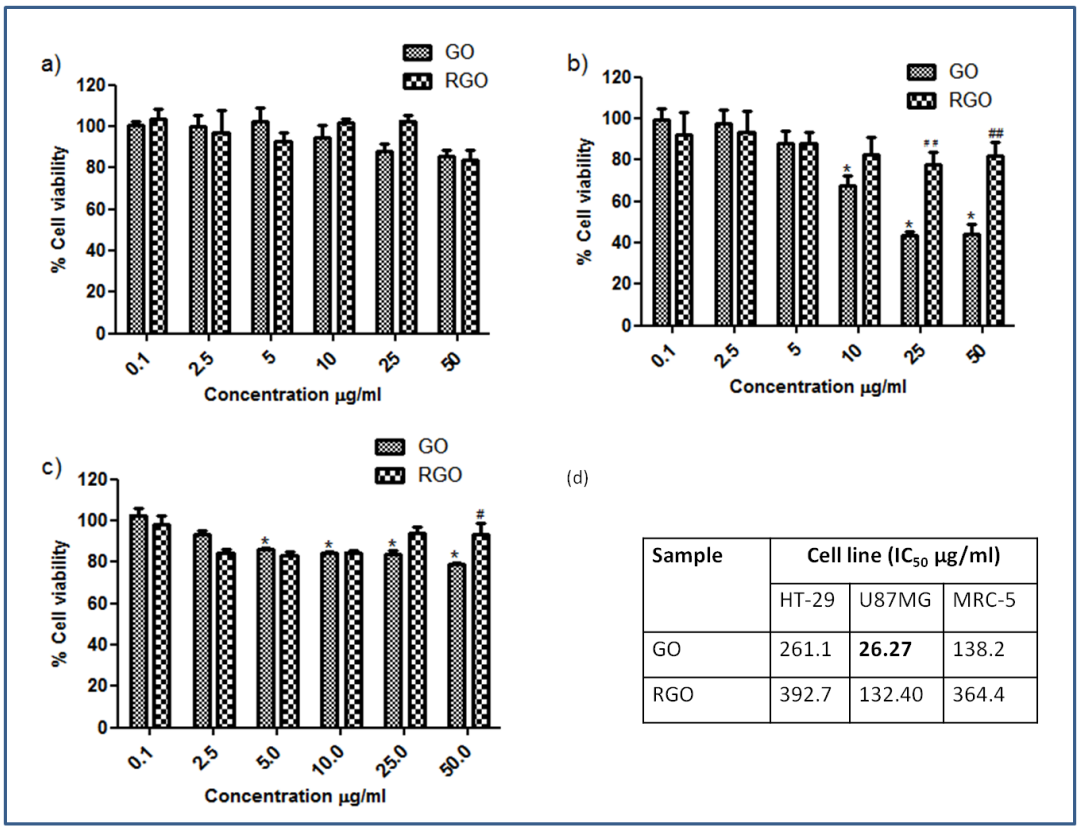

Sample	Cell line (IC_{50} µg/ml)		
	HT-29	U87MG	MRC-5
GO	261.1	**26.27**	138.2
RGO	392.7	132.40	364.4

Figure 11 The cell viability (%) on (a) HT-29, (b) U87MG and (c) MRC-5 cells and (d) overall IC_{50} values of GO and RGO treatments for 48 h generated by neutral red uptake assay. Bars represent mean±SEM of triplicates in three independent experiments (n=9). (*) = significant difference when treated groups were compared with untreated ($p < 0.001$) using one way Anova with Dunnel *t*-test. (#,##) = significant difference when GO was compared to RGO with $p < 0.5$ and $p < 0.01$, respectively, using two way Anova with Bonferroni *t*-test.

GO (Figure 11c) shows obvious toxicity towards MRC-5 as compared to the un-treated cells even from concentration as low as 5 µg/ml as GO was reported to induce cytotoxicity, genotoxicity and oxidative stress to MRC-5 cells. In contrast, RGO showed no cytotoxicity towards normal cell lines with the cell viability above 90%, even at 50 µg/ml.

GO was found to be toxic especially towards U87MG cells with IC_{50} at a very low concentration of 26.27 µg/ml (Figure 11d). This is due to the presence of oxygen functional groups in GO, which consequently lead to oxidative stress to cells and results in poor cell survival [99]. RGO shows better cell survival compared to GO for all the three cell lines with IC_{50} values beyond 50 µg/ml and up to 390 µg/ml. Since the cell viability assay is conducted only up to a concentration of 50 µg/ml, the concentration values in Fig. 9d only serve as an estimation generated by the software. Nevertheless, based on the current findings, our mushroom synthesized RGO, without the need of any functionalization shows good aqueous stability and is equally biocompatible similar to the functionalized ones such as carboxyl modified graphene [125]. Although our RGO does not pose any selectivity against the two cancer cell lines and normal cells tested, this feature is still of great value for the synthesized RGO to be a tool for protein/gene transfection as well as a drug delivery vehicle for cancer treatment, such as by the conjugation of an anticancer drug, as reported in subsequent section.

3.3 Charaterizations of polymer-functionalization of RGO forming a GP cargo

The successful functionalization of RGO with polymer was further validated using XRD (Figure 12a). The semicrystalline polymer, P, has two peaks at the same region of RGO starting at ≈19-36° [126,127]. Upon functionalization, these peaks appeared in the GP composite with an overlap of RGO and P bands at 15-19°. The peaks also appeared red-shifted compared to RGO and P alone, revealing successful functionalization.

The thermal stability of GP was analyzed by TGA as shown in Figure 12b. P suffered from 100% weight loss, with obvious weight drop seen from 270-400°C, which is due to the decomposition of the PEO and PPO copolymer [128]. However, upon functionalization with RGO, GP showed enhanced thermal stability.

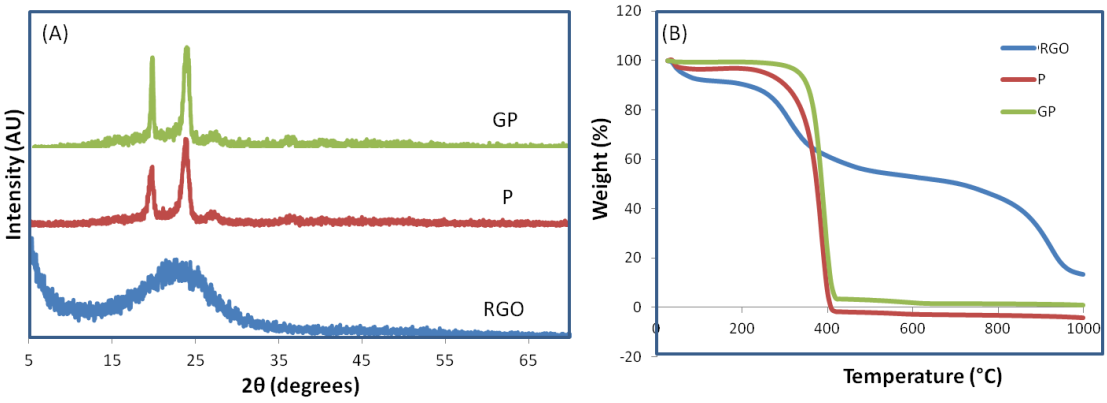

Figure 12 (a) XRD patters of RGO, P and GP. (b) TGA curves of RGO, P and the functionalized GP. **Note:** RGO: reduced graphene oxide; P: polymer; GP: polymer-functionalized reduced graphene oxide.

3.4 Characterizations of Cur and Ptx loaded onto GP

Upon modification of RGO with P resulting in GP, surface roughness was created with the presence of a porous structure, as shown in Figure 13b. In addition, the height profile shows increased thickness of ≈4 nm, which is due to the immobilization of P onto the surface of RGO. Accordingly, the height profile of GP-Cur is around 2 nm and upon introduction of Ptx has increased by ≈2-3 nm, confirming the non-covalent interaction of Cur and Ptx on the surface of GP. In addition, it is presumed that the molecules of Cur and Ptx, which are smaller in sizes, could have filled the pores that appear in GP.

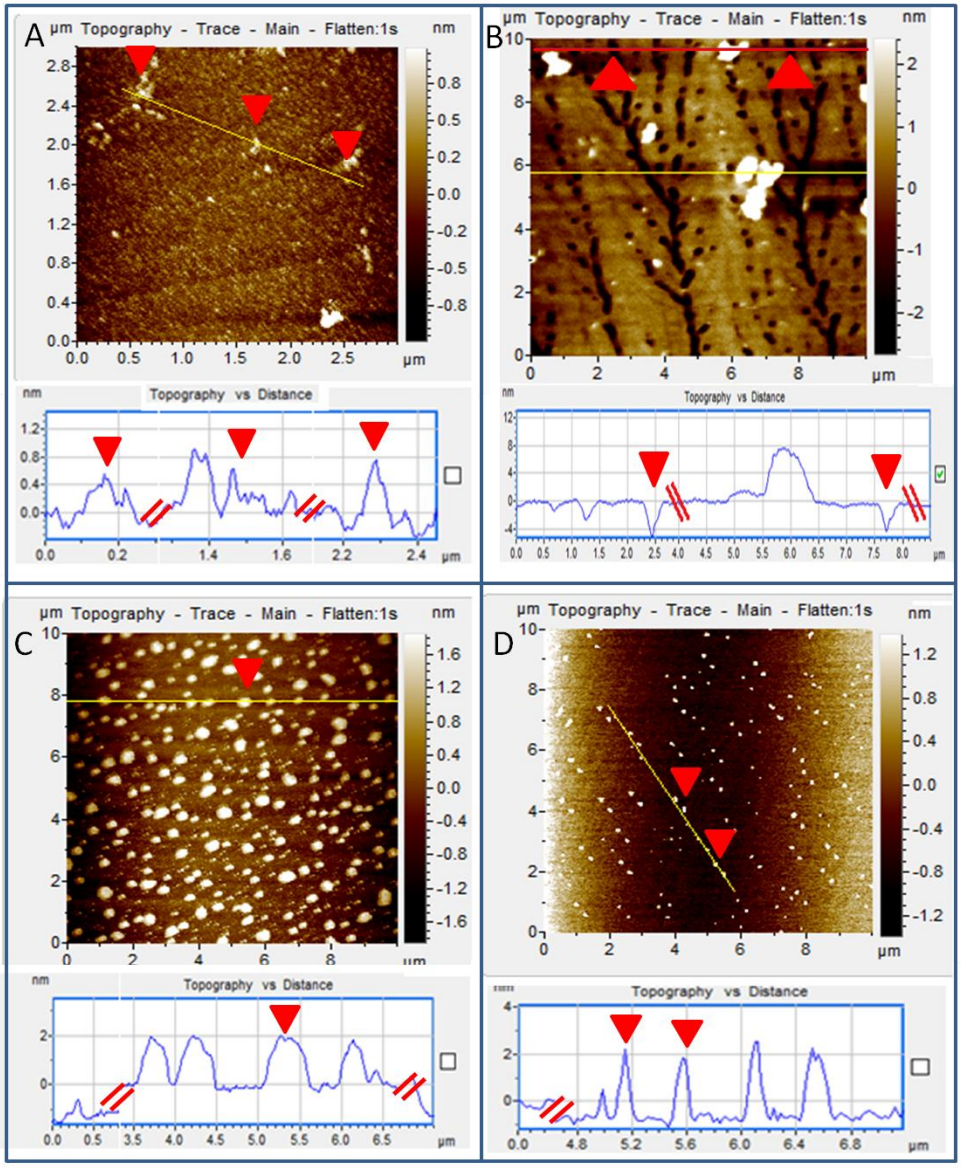

Figure 13 Tapping mode AFM images and its corresponding height profiles for (a) RGO, (b) GP, (c) GP-Cur and (d) GP-Cur-Ptx. **Note:** RGO: reduced graphene oxide; GP: polymer-functionalized reduced graphene oxide; GP-Cur: curcumin loaded onto GP; GP-Cur-Ptx: curcumin and paclitaxel co-loaded onto GP.

The hydrophobic interaction between Cur and the cargo GP can be further ascertained in fluorescence emissions (Fig. S1). Graphitic materials generally induce quenching upon interaction with aromatic or double bond conjugated materials, which is an

imperative tool to confirm loading of the fluorescent materials or drugs. At 420 nm excitation wavelength, Cur exhibited maximum fluorescence emission at ≈540 nm.

In GP-Cur however, a 93% quenching of fluorescence was observed which is due to the strong pi-pi interaction between the conjugated system in Cur and the aromatic structures in GP. As a result, a photoinduced electron-transfer process or fluorescence resonance energy transfer (FRET) takes place in the GP-Cur hybrid system that diminishes fluorescence [84,129,130]. Interestingly, the fluorescence signal was found higher (78% quenching) upon introduction of Ptx to the GP-Cur system. This phenomenon may be ascribed to the loading of Ptx molecules which interferes with the GP-Cur interaction, consequently releasing Cur from GP, which then exhibits increased fluorescence intensity [21]. In comparison, GP, Ptx and GP-Ptx did not demonstrate any fluorescence activity.

The surface morphology of the materials can be further elucidated using FESEM. As reported above, RGO has a flake-like structure with closely packed graphene sheets [28]. After functionalization with P, the GP has obvious surface roughness (Figure 14a) and with higher magnification, the microporous structure was observed, which is consistent with the topographical observation under AFM (Figure 14b). On the contrary, in the hybrid system, crystals of Cur in either rectangular or cubic shapes appeared to decorate the surface of GP, which is also in line with the observations reported in other studies [131,132]. Similarly, the appearance of granule like Ptx in the GP-Ptx hybrid system confirms the successful pi-pi interaction of Ptx and the GP. In GP-Cur-Ptx, more homogenous and non-aggregated drug loading was observed. Under higher magnification, the spherical structure of polymers can be seen adsorbed on the surface of G, together with the drugs which appeared brighter under the FESEM.

The lateral and size distribution of the aqueous dispersions of drug loaded GP were evaluated further using DLS. Upon modification with P, the size of GP slightly increased owing to the adsorption of polymer onto the flat surface of the RGO (Table 1). In their unmodified form, Cur and Ptx dissolved in ethanol/water (1:1) have

average sizes much larger than their hybrid form of GP-Cur and GP-Ptx, respectively. As both are hydrophobic drugs, the aqueous dispersion is somehow limited, however upon loading onto GP, the solubility of these drugs were significantly improved thus the lowered average sizes. A more convincing result can be seen in GP-Cur-Ptx, whereby upon loading of the drugs, the hydrodynamic average size was increased to ≈140 nm, which is higher than GP-Cur and GP-Ptx, proving the co-loading of Cur and Ptx onto the GP cargo system.

The size of the drug loaded GP carrier which is below 200 nm is highly advantageous for drug delivery applications as drug carriers within these sizes have been shown to have long half-life in the blood [133,314]. Since the tumor vasculature have defective architecture within these pore sizes, consequently this increases the propensity of the drugs to extravasate through vascular fenestrations of tumors and escape filtration by liver and spleen [86,135]. In addition, the poor lymphatic drainage of tumor cells prevents an efficient removal of the drug carrier and collectively <200 nm drug carrier allows enhanced permeability and retention (EPR) effect, which increases the drug's efficacy [136].

3.5 Drug loading studies of Cur onto GP cargo

From the various concentrations of Cur tested (0.1-2 mg/ml), the highest amount of Cur loading was 2 mg with the loading efficiency of ≈97% and loading capacity of 678 wt. %. Loading efficiency is determined as a percentage of experimental drug loading compared to theoretical drug loading, whereas loading capacity is determined as weight of the drug loaded compared to the weight of the GP cargo. As described earlier, this remarkably higher drug loading is mainly due to the unperturbed surface that is present on GP, contributing to efficient pi-pi interaction with Cur molecules.

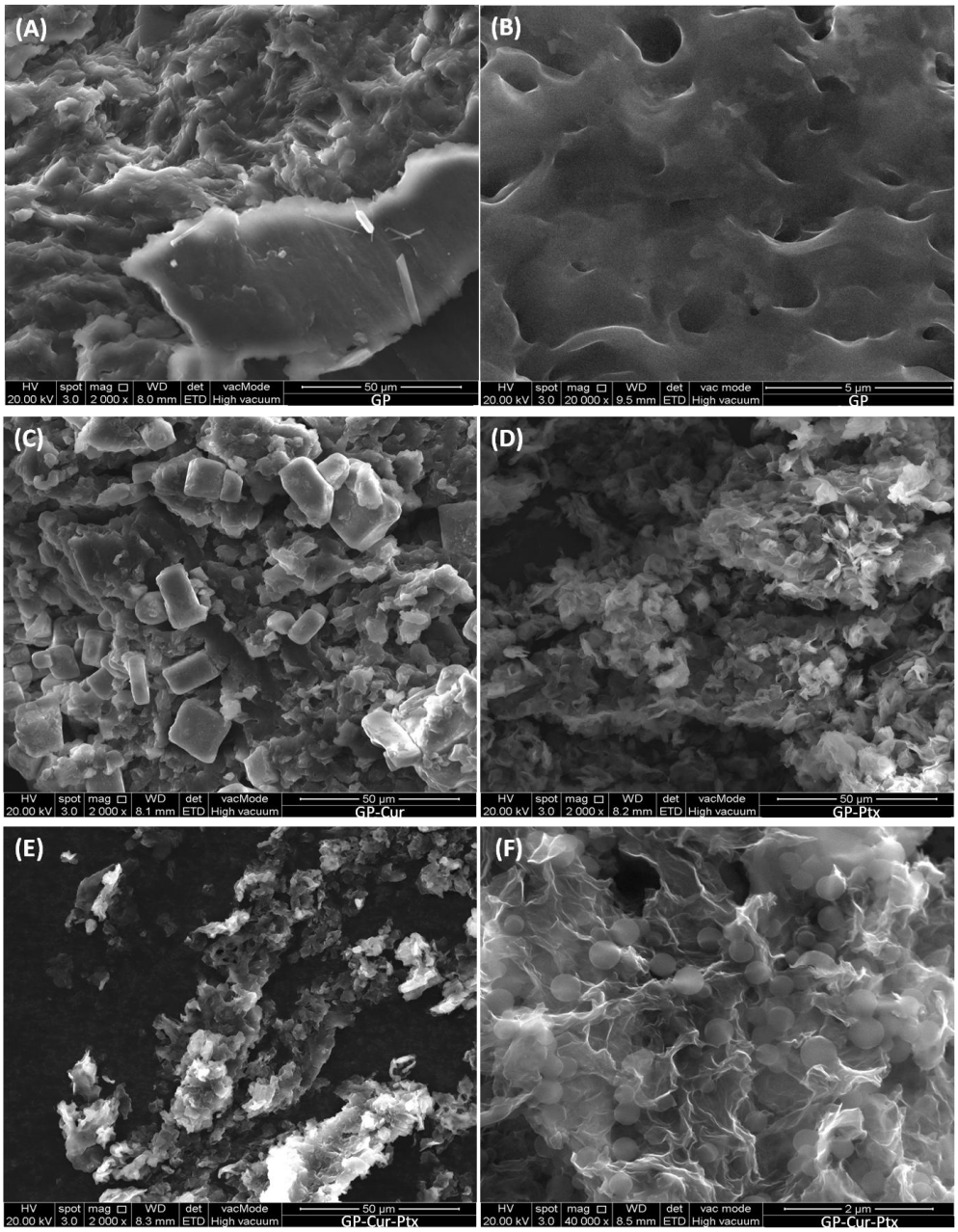

Figure 14 FESEM images of (a) GP, (b) GP in higher magnification, (c) GP-Cur, (d) GP-Ptx, (e) GP-Cur-Ptx and (f) GP-Cur-Ptx in higher magnification.
Note: GP: polymer-functionalized reduced graphene oxide; Cur: curcumin; GP-Cur: Cur loaded onto GP; Ptx: paclitaxel; GP-Ptx: Ptx loaded onto GP; GP-Cur-Ptx: Cur and Ptx co-loaded onto GP.

Table 1
The average hydrodynamic diameter of GP and drug loaded GP and its respective polydispersity index (PDI).

Sample	Average size (nm)	PDI
GP	156.3	0.111
Cur	231.6	0.019
Ptx	148.0	0.038
GP-Cur	123.5	0.245
GP-Ptx	133.1	0.078
GP-Cur-Ptx	139.9	0.063

Note: GP: polymer-functionalized reduced graphene oxide; Cur: curcumin; GP-Cur: Cur loaded onto GP; Ptx: paclitaxel; GP-Ptx: Ptx loaded onto GP; GP-Cur-Ptx: Cur and Ptx co-loaded onto GP.

3.6 Cytotoxicity assessment of GP-Cur-Ptx against A549, MDA and MRC-5 cells

Following cell viability studies, the antiproliferative effects of Cur and Cur loaded onto GP (GP-Cur) against A549 and MDA cell lines were determined. A dose-dependent cell viability was observed with cell growth inhibition evident at 0.2 µg/ml of GP-Cur in A549 and 20 µg/ml for MDA cells (Figure 15a, b). A similar dose-dependent pattern was also observed upon treatment with Ptx and GP-Ptx. Significant growth inhibition was evident at 20 ng/ml in cells treated with GP-Ptx, in contrast to 90% cell viability observed in cells treated with same concentration of Ptx alone (Figure 15c, d). As shown in Table 2, Ptx induced 50% growth inhibition in A549 and MDA cell lines with IC_{50} values of ≈0.17 and ≈0.12 µg/ml, respectively. Remarkably, an IC_{50} value of 0.0077 µg/ml of GP-Ptx was observed against A549 cells representing almost 25-fold reduction in the required potent dose as compared to Ptx. Similarly, only 0.0148 µg/ml GP-Ptx was needed to achieve IC_{50} in MDA cells, which is 8-fold lesser amount than using Ptx alone.

Since pluronic polymer has been suspected to be able to improve the cellular uptake of drugs, Cur and Ptx loaded polymer (P-Cur and P-Ptx) were also taken as controls (Figure 15A-D). Based on the observations, the cytotoxicity of P-Cur and P-Ptx appears to be the same as Cur and Ptx, respectively. This concludes that in the drug

loaded polymer solutions, the drugs present as a mixture rather than forming micelles with the pluronic polymer. If the latter was formed, higher cytotoxic effect will otherwise be observed as compared to Cur/Ptx.

Pluronic polymers alone cannot be considered as an optimal delivery vehicle for the hydrophobic drugs due to their low solubility in aqueous media and short residence time in the physiological environment [137]. Thus, alterations such as polymeric micelles, covalent modifications or polymer thermogels based synthesis are necessary to encapsulate the hydrophobic drugs (Cur/Ptx). In this work, the drugs (Cur/Ptx) were loaded via simple mixing and bath sonication for 0.5 h, which is believed to be not sufficient to form micelle or covalent bond or thermogels with the residual pluronic polymer, if any. A similar finding was also previously reported [138], whereby a non-covalent functionalized pluronic polymer-CNTs showed no enhancement in the cellular uptake by A549 cells as compared to covalent functionalized ones.

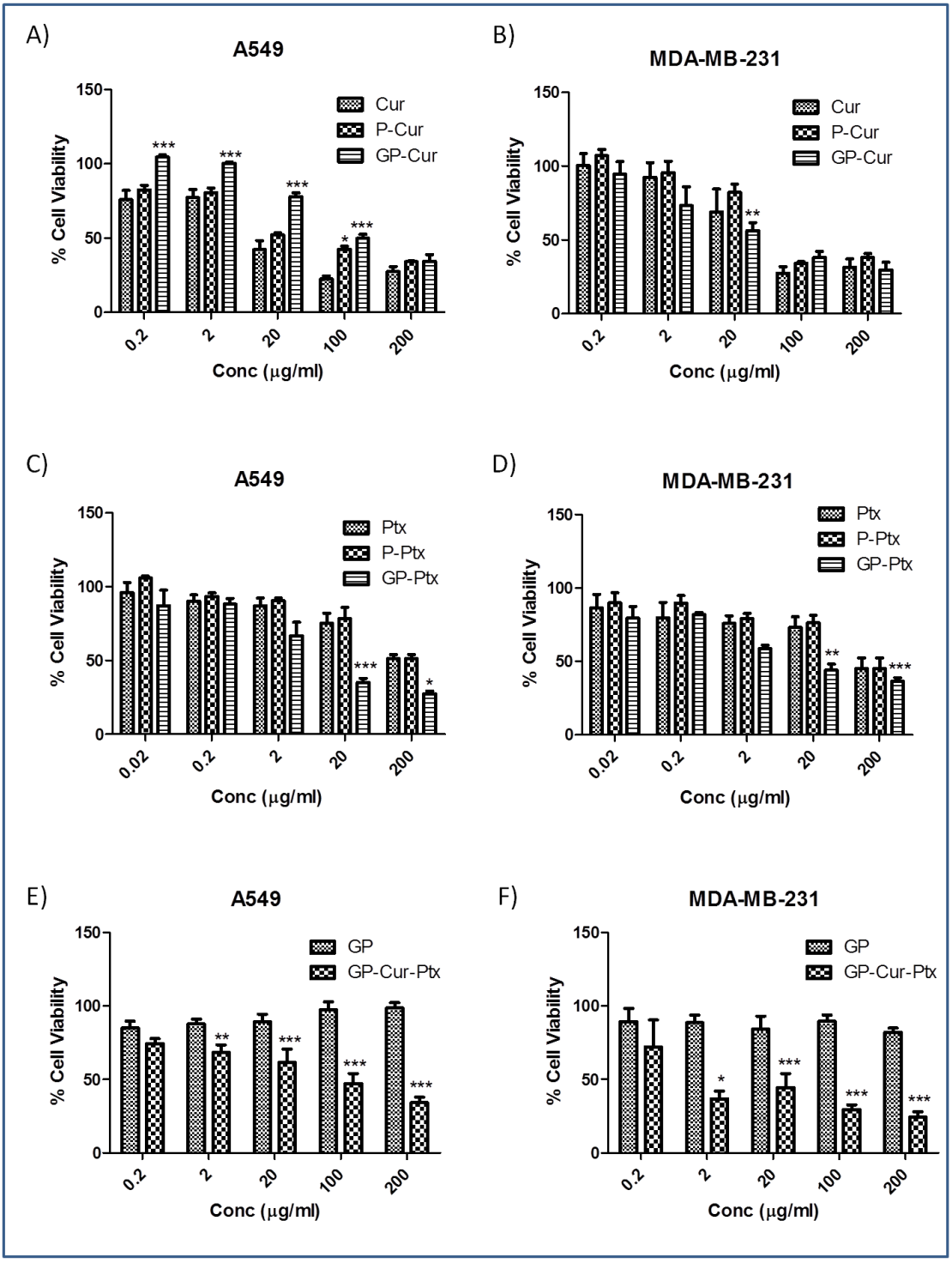

Figure 15: Representative histograms showing dose dependent growth inhibition of A) A549 cells treated with Cur, P-Cur and GP-Cur, B) MDA cells treated with Cur, P-Cur and GP-Cur, C) A549 cells treated with Ptx, P-Ptx and GP-Ptx, D) MDA cells treated with Ptx, P-Ptx and GP-Ptx, E) A549 cells treated with GP and GP-Cur-Ptx and F) MDA cells treated with GP and GP-Cur-Ptx. Following 48 h of treatment, IC_{50} was determined as described in the methods. Bars represent the mean ± SEM of triplicates from three independent experiments (n=9). *, ** and *** indicate significant difference when

compared between treatment groups, with $P<0.5$, $P<0.01$ and $P<0.001$, respectively using two-way ANOVA with Bonferroni t-test.

The enhanced cell toxicity effects seen in GP-Cur and GP-Ptx hybrid system could be due to better solubilisation of these drugs, upon loading onto the GP cargo system. The synthesized RGO [28], has good dispersion and stability in both water and physiological solution, which could have contributed to better solubilisation of the loaded drugs. In addition to this, the high surface area coverage on RGO allows more reactive sites of the drugs available for cytotoxicity reaction to take place and possibly better cell internalization. These findings raise the concern whether the markedly increased cellular toxicity of the GP-Cur and GP-Ptx hybrid system was due to toxicity from GP, instead of the drugs. Cell viability studies showed that GP did not induce toxicity to A549 and MDA cell lines, even at high concentration of 200 µg/ml (Figure 15e, f).

Based on the cell viability assay, the IC_{20} of Ptx was determined as 69.7 ng/ml for A549 cells and 46.7 ng/ml for MDA cells. With the introduction of 69.7 and 46.7 ng/ml of Ptx onto GP-Cur to the A549 and MDA cell lines, respectively, inhibition of cell growth was observed at 0.2 µg/ml (Figure 15e, f). IC_{50} values showed that the GP-Cur-Ptx system was slightly more potent towards MDA cells, needing only 1.450 µg/ml drugs, compared to 13.24 µg/ml for A549 cells (Table 3). The combination index (CI) calculated based on previously described method [139], showed synergistic growth inhibition by Ptx loaded GP-Cur (GP-Cur-Ptx) against the tested cells with slightly higher potency observed in MDA (0.43) compared to A549 (0.54) cells (Table 3).

Table 2
The 50% inhibitory concentration (IC_{50}) values of Cur and Ptx; Cur and Ptx loaded onto GP (GP-Cur and GP-Ptx) and Cur and Ptx co-loaded onto GP (GP-Cur-Ptx), tested against A549 and MDA cell lines.

Treatment (µg/ml)	A549	MDA-MB-231	MRC-5
Cur	17.83 ± 1.4	49.42 ± 1.3	> 200
GP-Cur	96.13 ± 1.1	42.98 ± 1.4	> 200
Ptx	0.1743 ± 0.0013	0.1174 ± 0.0016	0.5237 ± 0.0014
GP-Ptx	0.0077 ± 0.0015	0.0148 ± 0.0016	0.4041 ± 0.0012
GP	> 200	> 200	> 200

Note: Cur: curcumin; GP: polymer-functionalized reduced graphene oxide; GP-Cur: curcumin loaded onto GP; Ptx: paclitaxel; GP-Ptx: Ptx loaded onto GP.

Table 3
Combination index (CI) analysis of GP-Cur-Ptx against A549 and MDA cell lines and the effects of these doses on MRC-5 cells, in terms of IC_{50} values.

S/no	Cells	IC_{20} doses of Ptx (ng/ml)	Doses of GP-Cur that induced 50% growth inhibition in combination with IC_{20} dose of Ptx (µg/ml)	CI
1	A549	69.7	13.24 ± 1.8	0.54
2	MDA	46.7	1.450 ± 1.9	0.43
3	MRC-5	69.7	25.71 ± 1.2	-
4	MRC-5	46.7	37.50 ± 1.2	-

Note: Pharmacological interaction deduced the CI values of >1 as antagonistic, =1 as addictive and <1 as synergistic.

In order to ascertain that the synergistic system is not toxic towards healthy cells, cytotoxicity test was also conducted against MRC-5 cells. As shown in Table 2, GP, Cur and combined GP-Cur did not cause toxicity to non-cancerous MRC-5 cells. However, Ptx and GP-Ptx caused toxicity at 400-500 ng/ml. On the other hand, 25.71 µg/ml of GP-Cur in combination with IC_{20} (69.7 ng/ml) of Ptx was required to induce 50% growth inhibition in MRC-5 cells compared to 13.24 µg/ml required for the cancerous A549 cells (Table 3). Similarly, 37.50 µg/ml of GP-Cur was required in

combination with 46.7 ng/ml Ptx to induce 50% growth inhibition in MRC-5 cells compared to 1.450 µg/ml of GP-Cur required for MDA cells. This demonstrated that combined treatment conferred less toxicity on non-cancerous MRC-5 cells compared to A549 and MDA cell lines.

3.7 Determination of ROS generation by GP-Cur-Ptx in A549 and MDA cells

The cytotoxicity of the agents towards the cancer cells was further confirmed with determination of oxidative stress by a fluorometric assay. Upon incubation with cells, the generated ROS reacts with the fluorogenic component localized in the cytoplasm, resulting in red-fluorescent product, which is proportional to the amount of ROS present.

In both of the cancerous cells, 10-fold GP-Cur-Ptx exuberantly elevated oxidative stress in the intracellular environment in a dose-dependent manner (Figure 16a, b). In case of A549 cells, by comparing all the 10-fold IC_{50} treatment groups, 10-fold Cur demonstrated the second highest ROS elevation followed by 10-fold GP-Cur, which suggests that the presence of a higher concentration of Cur has contributed to the amplified production of ROS. In addition, by comparing the hybrid systems i.e. GP-Cur and GP-Ptx, GP-Cur showed a significantly higher generation of ROS. It was reported that Cur could either potentiate the accumulation of ROS or stimulate the generation of ROS by other anticancer drugs [140]. Although Cur possesses good ROS scavenging ability, in the GP-Cur hybrid system, Cur acts as a pro-oxidant by bringing cellular redox changes resulting in the accumulation of ROS which consequently lead to cell death [141-143]. On the contrary, Ptx, is reported to induce only a small amount of ROS due to the presence of a negative regulator of a mitochondrial ROS called UCP-2 [144]. Hence, in the synergistic GP-Cur-Ptx system, Cur acts as an antioxidant which may have an adverse effect on the anticancer drug Ptx, which then acts on tumor cells by increasing the ROS level to induce cell death [145,146]. The findings of considerably higher ROS values as observed in the GP-Cur-Ptx corroborate well with the highest cell killing in the previous cytotoxicity assay which indicates that the presence of both Cur and Ptx have effectively induced

toxicity to cancerous cells probably via a supplementary ROS-mediated mechanism. The significantly higher ROS generation as observed in MDA than in A549 cells, which substantiates with the higher potency of GP-Cur-Ptx for MDA as seen in cytotoxicity assay indicates the vulnerability of MDA to ROS assaults.

Figure 17 shows the ROS images of GP-Cur-Ptx on A549 and MDA cells. The brighter red-fluorescence shows higher ROS generation and accumulation as compared to unstained images of un-treated cells as well as lightly stained cells observed in GP-Cur and GP-Ptx (Fig. S2). The rod-like structure seen outside the cells shows the presence of GP which serves as a drug delivery vehicle and it corroborates with the hypothesis that only drugs were internalized by cells, leaving behind the GP cargo.

The shape of the drug carrier which is rod-like is also advantageous for drug delivery as rod-like drug carriers are found to exhibit 4-times more rapid transvascular penetration [147]. This was observed mainly due to reduced steric hindrance with high aspect ratios and minimal regions of curvature with its worm-like particle or structure [148]. In addition, these rod-like structure of drug carriers is also reported to posses optimal transport properties as the rod-like drug carrier has long-circulating lifetimes compared with the spherical ones due to their tendency to align with blood flow [149-151].

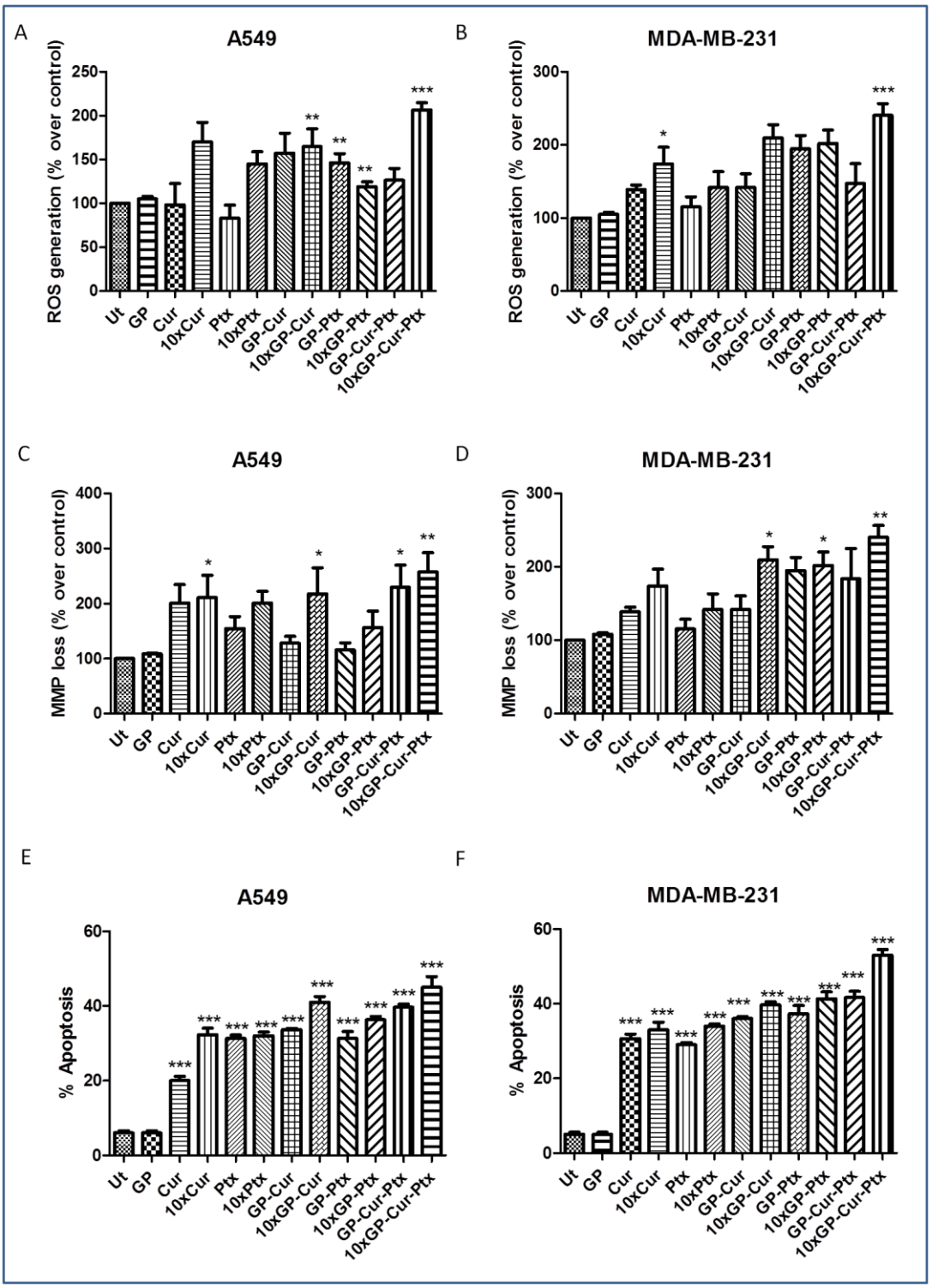

Figure 16 Percentages of ROS generation, loss of MMP and apoptosis. (A) Activity of ROS generation by the treatment groups on A549 and (B) MDA cell lines. (C) The loss of mitochondrial membrane potential (MMP) induced by treatment groups on A549 and (D) MDA cell lines. (E) Percentage of apoptosis induced by the treatment groups on A549 and (F) MDA cell lines. Plain media and GP served as untreated control (Ut) and negative control, respectively. Concentrations of the treatment groups are based on the respective IC_{50} and 10-fold IC_{50} values. Bars represent mean ± SEM,

with n=3. *, ** and *** indicate significant difference when treated groups were compared with un-treated with P<0.5, P<0.01 and P<0.001, respectively using one-way ANOVA with Dunnett's t-test.

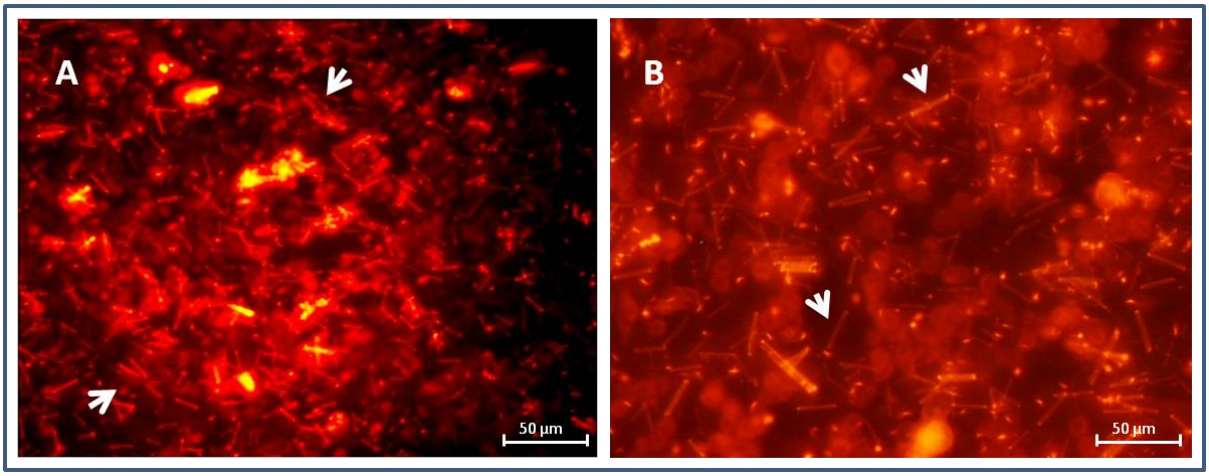

Figure 17 Representative images of ROS generation in (A) A549 and (B) MDA cell lines after treatment with GP-Cur-Ptx for 120 min. Arrows indicate the rod-like structure as seen outside the cells, which are the GP cargo. **Note:** GP-Cur-Ptx: curcumin and paclitaxel co-loaded onto GP.

3.8 Determination on the degree of MMP loss in A549 and MDA cells

ROS assault on cells is often accompanied by mitochondrial malfunction, or sometimes both happening concurrently. Thus MMP was investigated on both A549 and MDA cancer cells at the concentrations of IC_{50} and 10-fold IC_{50}. JC-10, a cationic, lipophilic dye was used to monitor the MMP in term of permeability to JC-10 quantitatively. JC-10 forms reversible red-fluorescent aggregates in healthy cells with polarized mitochondrial membrane, however upon the collapse of MMP, JC-10 will return to its monomeric green-fluorescent form [146].

For both cancer cells, the highest dye permeability was observed in GP-Cur-Ptx (Figure 16c, d), corroborating with the findings in ROS, which also scored the highest. Loss of MMP was dose-dependent for GP-Cur-Ptx in A549 cells and followed by 10-fold GP-Cur and 10-fold Cur. This indicates that the presence of Cur in these treatment groups has played a major role in disrupting the cells' mitochondria. In comparison, the current GP-Cur-Ptx combined treatments induced

significantly higher depolarization of MMP than other reports, such as cocktail drug containing an antioxidant apigenin and paclitaxel [152]. As for MDA cells, GP-Ptx was equally effective as 10-fold Ptx in causing MMP loss. Additionally, it was also observed that GP-Cur-Ptx is as effective as 10-fold GP-Ptx in causing perturbation to the mitochondria of MDA cells, proving that the integrated combination treatment allows the usage of reduced dosages to attain the same therapeutic effects.

3.9 Determination on the induction of apoptosis by GP-Cur-Ptx on A549 and MDA cells

In order to quantify living cells from apoptotic and necrotic cells, double staining method was employed using Annexin Cy3 and 6-CFDA. Annexin Cy3 stains red on necrotic cells, by binding to phosphatidylserine which is present outside of plasma membrane of cells undergoing apoptosis. On the other hand, upon entering living cells, the non-fluorescent 6-CFDA is hydrolyzed by esters producing a green fluorescent product. Cells in the early stages of apoptosis, however, will be stained yellowish-green [153].

A549 and MDA cells treated with GP-Cur-Ptx showed the highest apoptosis percentage (Figure 16e, f), which was in accordance with the highest ROS and highest loss of MMP observed. The induction of apoptosis was also dose-dependent as the 10-fold treatment groups showed higher cell death compared to their respective IC_{50} values. The hybrid treatment agents, GP-Cur and GP-Ptx were more potent in inducing apoptosis compared to single treatment of Cur and Ptx, even at 10-fold the concentration of the IC_{50} values. In order to further comprehend the apoptotic trend, the cellular morphology of the cells upon treatment was also investigated under the microscope.

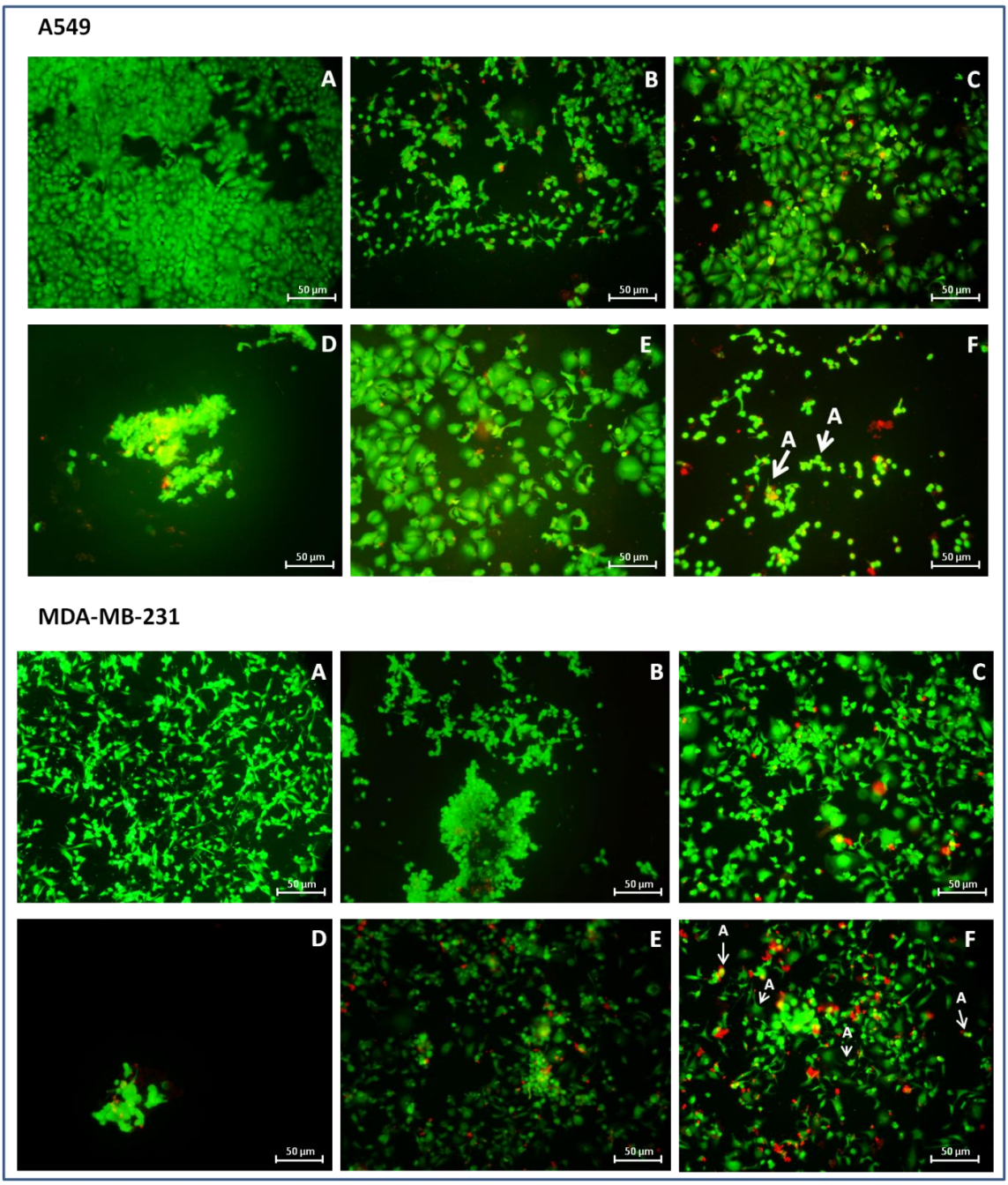

Figure 18 Merged images of A549 (upper panel) and MDA (lower panel) cells after staining with Annexin-Cy3 and 6-CFDA with (a) un-treated cells, and cells treated with: (b) Cur; (c) Ptx; (d) GP-Cur; (e) GP-Ptx and (f) GP-Cur-Ptx. Arrows labelled 'A' are representation of typical features of cells undergoing apoptosis. Cells that are green but show blebbing, cell-rupture or condensed and fragmented are taken as early stages of apoptosis, along with cells stained yellow in the merged images. Comparatively, cells stained red are regarded as necrotic [97]. **Note:** Cur: curcumin; GP: polymer-functionalized reduced graphene oxide; GP-Cur: Cur loaded onto GP; Ptx: paclitaxel; GP-Ptx: Ptx loaded onto GP; GP-Cur-Ptx: Cur and Ptx co-loaded onto GP.

For the untreated A549 and MDA cell lines, healthy cellular morphology without any abnormalities was observed and the cells were growing in close proximity (Fig. S3, S4). Upon treatment, obvious separation from the neighbouring cells was seen with a higher separation constituting to higher apoptotic cell death. Both cancer cell lines that received treatment with Cur showed obvious signs of cell shrinkage (Figure 18) [154, 97]. A similar finding was also observed for treatment with GP-Cur, along with the presence of yellowish-green in the merged images showing cells underwent early stages of apoptosis. In addition, treatment with GP-Cur severed the attachment of apoptotic cells from the surroundings cells.

On the other hand, treatment with Ptx induced the cells to undergo necrosis as more rampant red-stain was observed [153,155]. Similarly, GP-Ptx showed the presence of necrosis, with treatment in MDA showing more rounded-up cells compared to in A549 cells. This is in accordance with the higher loss of MMP seen in GP-Ptx for MDA cells. On the contrary, GP-Ptx treatment on A549 cells induced obvious cell swelling. A549 and MDA cell lines treated with Ptx and GP-Ptx showed extensive plasma membrane blebbing, which is one of the late apoptotic characteristics. However, this was not found in cells treated with Cur and GP-Cur.

Prominent features of cell apoptosis (shown by arrow) can be clearly seen in the GP-Cur-Ptx treatments (Figure 18f). Cellular shrinkage and pyknosis, which are the results of nuclear membrane condensation into more densely packed material, were observed in both treated cancer cells. Additionally, separation from the surrounding cells took place and protrusions from plasma membrane or blebs, appeared more prominently in MDA cells. It was reported that blebbing shows the presence of caspase activation involving a group of proteins which are crucial for programmed cell death [156,157]. Following this, disintegration of the nucleus into similarly dense and smaller particles takes place, forming apoptotic bodies or karyorrhexis [158,159]. This observation was found more obviously in A549 cells**.** GP-Cur-Ptx treatment on MDA cells caused late stages of apoptosis and necrosis, whereas A549 cells showed the characteristics of early stages of apoptosis. This finding could be translated to the higher level of ROS observed in MDA compared to A549 cell lines.

Based on these findings, it can be deduced that Ptx and GP-Ptx induced cell necrosis in A549 and MDA cells, which is unfavourable as the cells are passive victims due to the toxic process [159]. On the other hand, Cur and GP-Cur promotes cell apoptosis or programmed cell-death and with the introduction of Cur in the synergistic treatment, GP-Cur-Ptx, necrosis by Ptx has been completely suppressed, while promoting signal-dependent cell suicide, i.e. apoptosis.

Based on the above findings, there is a consistent relationship between increased generations of ROS and increased loss of MMP that eventually lead to cell apoptosis and thus inhibition of cell proliferation. The sequence of these events is however, in need of further elucidation. Conceivably, it was reported that Cur and Ptx works synergistically in activating caspases, cleavage of Bid to tBid and mitochondrial release of cytochrome c, which consequently induce apoptosis by extrinsic and intrinsic pathways [160]. In addition, Cur promotes the down-regulation of Ptx activated-NFkB, which eventually contributes to Ptx-induced apoptosis on A549 and MDA cells [161].

4.0 Conclusion and Recommendations

An over the counter, commercial-grade mushroom powder was used to effectively reduce GO to RGO with a reaction time of approximately 1 h. This environmentally friendly method evades the use of chemicals and significantly reduces waste with the advantage of reusability of the extract as a reducing agent. The obtained RGO was readily dispersible in water and was reasonably small with the thickness of 1-2 nm and 181-500 nm in lateral dimension. The RGO obtained through this strategy is small as compared to other reported green-synthesis methods. In addition, solubility tests using various solvents showed that RGO is stable up one year. The synthesized RGO if highly biocompatible and has not shown any anti-proliferative effects towards colon and brain cancer as well as healthy cell lines. This makes the RGO suitable as a drug delivery carrier, especially for hydrophobic anticancer drugs. Polymer-functionalization of RGO resulted in a GP cargo that further contributed to higher solubility and stability. Co-loading of Cur and Ptx onto the GP cargo has significantly increased the solubility of these 2 drugs and a remarkably high drug loading was also achieved, 678 wt.%, which to the best of our knowledge is the highest reported thus far for Cur.

The synergistic system, GP-Cur-Ptx shows a dose dependent cytotoxicity against A549 and MDA cancer cells. For comparison, GP-Cur and GP-Ptx were also tested. GP-Cur and GP-Ptx were highly effective towards the inhibition of cancer cell growth, especially GP-Ptx, needing 8-23 fold lesser dose compared to Ptx alone. Upon introduction of only IC_{20} dose of Ptx to the GP-Cur system, a highly potent treatment system was created for both A549 and MDA cells with CI values <1, suggesting a synergistic system. The same concentration tested on normal cells shows no toxicity, demonstrating that the GP-Cur-Ptx system is cell-specific cytotoxic, especially to these two cancer cell lines. Upon further elucidation, the highest ROS production was also observed in the GP-Cur-Ptx system, which was mainly due to the presence of Cur that acted as pro-oxidant and induced ROS accumulation in cells. ROS accumulation will eventually lead to polarization of the mitochondria and cell deaths, which is consistent to our findings. The percentage of apoptosis found after

treatment with GP-Cur, GP-Ptx and the combined GP-Cur-Ptx was significantly higher than treatments with one of the drugs, even with Cur and Ptx in 10-fold concentrations. Based on cell morphology, Ptx was found to induce late stages of apoptosis and necrosis in cells. However, in the combined treatment, cell necrosis by Ptx was significantly suppressed and the GP-Cur-Ptx majorly induced early stages of apoptosis. In addition, upon close examination, only the drugs were engulfed by cells, leaving behind the GP cargo. For future studies, further investigation is needed to determine the reaction pathways that are activated by the GP-Cur-Ptx system, other than the commonly reported for Cur and Ptx. The current findings seem promising for possibly future *in vivo* and clinical applications.

References

[1] Novoselov KS, Geim AK, Morozov SV, Jiang D, Zhang Y, Dubonos SV, Grigorieva IV, Firsov AA. Electric field effect in atomically thin carbon films. *Science*. 2004;306:666-669.

[2] **Muthoosamy K**, Bai RG, Manickam S. Graphene and graphene oxide as a docking station for modern drug delivery system. *Curr. Drug Deliv.* 2014;11:701-718.

[3] Afreen S, **Muthoosamy K**, Manickam S, Hashim U. Functionalized fullerene (C_{60}) as a potential nanomediator in the fabrication of highly sensitive biosensors. *Biosens. and Bioelectron.* 2015;63:354-364.

[4] Singh V, Joung D, Zhai L, Das S, Khondaker S, Seal S. Graphene based materials: Past, present and future. *Prog. Mat. Sci*. 2011;56(8):1178-1271.

[5] Monthioux M, Kuznetsov V. Who should be given the credit for the discovery of carbon nanotubes? *Carbon.* 2006;44(9):1621-1623.

[6] Stoller MD, Park S, Zhu Y, An J, Ruoff RS. Graphene-based ultracapacitors. *Nano Lett.* 2008;8(10):3498-3502.

[7] Balandin AA, Ghosh S, Bao W, Calizo I, Teweldebrhan D, Miao F, Lau CN. Superior thermal conductivity of single layer graphene. *Nano Lett.* 2008;8:902-907.

[8] Novoselov KS, Geim AK, Morozov SV, Jiang D, Katsnelson MI, Grigorieva IV, Dubonos SV, Firsov AA. Two-dimensional gas of massless Dirac fermions in graphene. *Nature.* 2005;438:197-200.

[9] Morozov SV, Novoselov KS, Katsnelson MI, Schedin F, Ponomarenko LA, Geim AK. Strong suppression of weak localization in graphene. *Phys. Rev. Lett.* 2006;97:016801.

[10] Georgakilas V, Otyepka M, Bourlinos AB, Chandra V, Kim N, Kemp KC, Hobza P, et al. Functionalization of graphene: covalent and non-covalent approaches, derivatives and applications. *Chem. Rev.* 2012;112(11):6156-6214.

[11] Huang X, Qi X, Boey F, Zhang H. Graphene-based composites. *Chem. Soc. Rev.* 2012;41(2):666-686.

[12] Jiang HJ. Chemical preparation of graphene-based nanomaterials and their applications in chemical and biological sensors. *Small.* 2011;7(11):2413-2427.

[13] Guo SJ, Dong SJ. Graphene nanosheets: synthesis, molecular engineering, thin film, hybrids, and energy and analytical applications. *Chem. Soc. Rev.* 2011;40(5):2644-2672.

[14] Bai RG, Ninan N, **Muthoosamy K**, Manickam S. Graphene: a versatile platform for nanotheranostics and tissue engineering. *Under review, Progress in Materials Science, Oct 2015.*

[15] Ariffin SN, Lim HN, Tumeri FA, Abdullah AH, Ahmad M, Ibrahim NA, Huang NM, Teo PS, **Muthoosamy K**, Harrison I. Modification of polypropylene filter with metal oxide and reduced graphene oxide for water treatment. *Ceramics Int.* 2014; 40(5), 6927-36.

[16] Liu C, Alwarappan S, Chen ZF, Kong X, Li CZ. Membraneless enzymatic biofuel cells based on graphene nanosheets. *Biosens. and Bioelectron.* 2010;25:1829-1833.

[17] Wang L, Lee K, Sun YY, Lucking M, Chen Z, Zhao JJ, Zhang SB. Graphene oxide as an ideal substrate for hydrogen storage. *ACS Nano.* 2009;3(10):2995-3000.

[18] Lu CH, Yang HH, Zhu CL, Chen X, Chen GN. A graphene platform sensing biomolecules. *Angew. Chem. Int. Ed.* 2009;121(26):4879-4881.

[19] Bai RG, **Muthoosamy K**, Shipton FN, Pandikumar A, Kumar PR, Huang NM, Manickam S. Biogenic synthesis of reduced graphene oxide-silver (RGO-Ag) nanocomposite and its dual applications as antibacterial agent and cancer biomarker sensor. *RSC Advances*. 2016; 6: 36576-36587.

[20] Yang Y, Asiri AM, Tang Z, Du D, Lin Y. Graphene based materials for biomedical applications. *Mat. Today.* 2013;16(10):365-373.

[21] Wang Y, Li Z, Wang J, Li J, Lin Y. Graphene and graphene oxide: biofunctionalization and applications in biotechnology. *Trends Biotechnol*. 2011;29(5):205-212.

[22] Shen H, Zhang L, Liu M, Zhang Z. Biomedical applications of graphene. *Theranostics.* 2012;2(3):283-294.

[23] Akhavan O, Ghaderi E. Toxicity of graphene and graphene oxide nanowalls against bacteria. *ACS Nano.* 2010;4:5731-5736.

[24] Hu W, Peng C, Luo W, Lv M, Li X, Li D, Huang Q, Fan C. Graphene-based antibacterial paper. *ACS Nano.* 2010;4:4317-4323.

[25] Aissa B, Memon NK, Ali A, Khraisheh MK. Recent progress in the growth and applications of graphene as a smart material: a review. *Front. Mater.* 2015, doi: 10.3389/fmats.2015.00058

[26] Higgins D, Zamani P, Yu A, Chen Z. The application of graphene and its composites in oxygen reduction electrocatalysis: a perspective and review of recent progress. *Energy Environ. Sci.* 2016; 9: 357-390.

[27] Sanchez VC, Jachak A, Hurt RH, Kane AB. Biological interactions of graphene-family nanomaterials: an interdisplinary review. *Chem. Res. Toxicol*. 2012;25:15-34.

[28] **Muthoosamy K**, Bai RG, Abubakar IB, Sudheer SM, Lim HN, Loh HS, et al. Exceedingly biocompatible and thin-layered reduced graphene oxide nanosheets using an eco-friendly mushroom extract strategy. *Int. J. Nanomed*. 2015;10:1505-1519.

[29] Liu H, Li T, Liu Y, Qin G, Wan X, Chen T. Glucose-reduced graphene oxide with excellent biocompatibility and photothermal efficiency as well as drug loading. *Nanoscale Res. Lett.* 2016; 11: 211-221.

[30] Liu KP, Zhang JJ, Cheng FF, Zheng TT, Wang CM, Zhu JJ. Green and facile synthesis of highly biocompatible graphene nanosheets and its application for cellular imaging and drug delivery. *J. Mater. Chem.* 2011;21(32):12034-12040.

[31] An J, Gou YQ, Yang CX, Hu FD, Wang CM. Synthesis of a biocompatible gelatin functionalized graphene nanosheets and its application for drug delivery. *Mat. Sci. Eng. C.* 2013;33(5):2827-2837.

[32] Xu LQ, Wang L, Zhang B, Lim CH, Chen Y, Neoh KG, et al. Functionalization of reduced graphene oxide nanosheets via stacking interactions with the fluorescent andwater-soluble perylene bisimide-containing polymers. *Polymer.* 2011;52(11):2376-2383.

[33] Berger C, Song ZM, Li TB, Li XB, Ogbazghi AY, Feng R, et al. Ultrathin epitaxial graphite: 2D electron gas properties and a route toward graphene-based nanoelectronics. *J. Phys. Chem. B.* 2004;108(52):19912-19916.

[34] Lee S, Lee K, Zhong ZH. Wafer scale homogeneous bilayer graphene films by chemical vapor deposition. *Nano Lett.* 2010;10(11):4702-4707.

[35] Kosynkin DV, Higginbotham AL, Sinitskii A, Lomeda JR, Dimiev A, Price BK, et al. Longitudinal unzipping of carbon nanotubes to form graphene nanoribbons. *Nature*. 2009;458(7240):872-876.

[36] Stankovich S, Dikin DA, Piner RD, Kohlhaas KA, Kleinhammes A, Jia Y, et al. Synthesis of graphene-based nanosheets via chemical reduction of exfoliated graphite oxide. *Carbon.* 2007;45(7):1558-1565.

[37] Zhu PY, Shen M, Xiao SH, Zhang D. Experimental study on the reducibility of graphene oxide by hydrazine hydrate. *Physica B.* 2011;406(3):498-502.

[38] Gurunathan S, Han JW, Eppakayala V, Kim JH. Microbial reduction of graphene oxide by Escherichia coli: A green chemistry approach. *Colloid Surface B.* 2013;102:772-777.

[39] Furst A, Berlo RC, Hooton S. Hydrazine as a reducing agent for organic compounds (catalytic hydrazine reductions). *Chem. Rev*. 1965;65(1):51-68.

[40] Tung VC, Allen MJ, Yang Y, Kaner RB. High-throughput solution processing of large-scale graphene. *Nat. Nanotechnol.* 2009;4(1):25-29.

[41] Fernandez-Merino MJ, Guardia L, Paredes JI, Villar-Rodil S, Solis-Fernandez P, Martinez-Alonso A, et al. Vitamin C is an ideal substitute for hydrazine in the reduction of graphene oxide suspensions. *J. Phys. Chem. C.* 2010;114(14):6426-6432.

[42] Wang GX, Yang J, Park J, Gou XL, Wang B, Liu H, et al. Facile synthesis and characterization of graphene nanosheets. *J. Phys. Chem. C*. 2008;112(22):8192-8195.

[43] Perera SD, Mariano RG, Nijem N, Chabal Y, Ferraris JP, Balkus KJ. Alkaline deoxygenated graphene oxide for supercapacitor applications: An effective green alternative for chemically reduced graphene. *J. Power Sources.* 2012;215:1-10.

[44] Park JH, Mitchel WC, Smith HE, Grazulis L, Eyink KG. Studies of interfacial layers between 4H-SiC (0001) and graphene. *Carbon.* 2010;48(5):1670-1673.

[45] Fan ZJ, Kai W, Yan J, Wei T, Zhi LJ, Feng J, et al. Facile synthesis of graphene nanosheets via Fe reduction of exfoliated graphite oxide. *ACS Nano.* 2011;5(1):191-198.

[46] Zhang JL, Yang HJ, Shen GX, Cheng P, Zhang JY, Guo SW. Reduction of graphene oxide via L-ascorbic acid. *Chem. Commun*. 2010;46(7):1112-1114.

[47] Liu Z, Robinson JT, Sun XM, Dai HJ. PEGylated nanographene oxide for delivery of water-insoluble cancer drugs. *J. Am. Chem. Soc*. 2008;130(33):10876-10877.

[48] Zhu CZ, Guo SJ, Fang YX, Dong SJ. Reducing sugar: new functional molecules for the green synthesis of graphene nanosheets. *ACS Nano*. 2010;4(4):2429-2437.

[49] Liu J, Fu S, Yuan B, Li Y, Deng Z. Toward a universal "adhesive nanosheet" for the assembly of multiple nanoparticles based on a protein-induced reduction/decoration of graphene oxide. *J. Am. Chem. Soc.* 2010;132(21):7279-7281.

[50] Khan M, Al-Marri AH, Khan M, Shaik MR, Mohri N, Adil SF, et al. Green approach for the effective reduction of graphene oxide using *Salvadora persica* L. root (Miswak) extract. *Nanoscale Res. Lett*. 2015, doi: 10.1186/s11671-015-0987-z

[51] Wang Y, Shi Z, Yin J. Facile synthesis of soluble graphene via a green reduction of graphene oxide in tea solution and its biocomposites. *ACS App. Mater. Interfaces.* 2011;3(4):1127-1133.

[52] Akhavan O, Kalaee M, Alavi ZS, Ghiasi SMA, Esfandiar A. Increasing the antioxidant activity of green tea polyphenols in the presence of iron for the reduction of graphene oxide. *Carbon.* 2012;50(8):3015-3025.

[53] Kim YK, Kim MH, Min DH. Biocompatible reduced graphene oxide prepared by using dextran as a multifunctional reducing agent. *Chem. Commun.* 2011;47(11):3195-3197.

[54] Salas EC, Sun ZZ, Luttge A, Tour JM. Reduction of graphene oxide via bacterial respiration. *ACS Nano.* 2010;4(8):4852-4856.

[55] Chen TQ, Pan LK, Yu K, Sun Z. Microwave-assisted synthesis of reduced graphene oxide-carbon nanotube composites as negative electrode materials for lithium ion batteries. *Solid State Ionics.* 2012;229:9-13.

[56] Delzenne NM, Bindels LB. Gut microbiota: *Ganoderma lucidum*, a new prebiotic agent to treat obesity? *Nat. Rev. Gastroenterol. Hepatol*. 2015;12;553-554.

[57] Paterson RRM. Ganoderma - A therapeutic fungal biofactory. *Phytochemistry.* 2006; 67(18):1985-2001.

[58] Saltarelli R, Ceccaroli P, Iotti M, Zambonelli A, Buffalini M, Casadei L, et al. Biochemical characterisation and antioxidant activity of mycelium of *Ganoderma lucidum* from Central Italy. *Food Chem*. 2009;116(1):143-151.

[59] Kozarski M, Klaus A, Niksic M, Vrvic MM, Todorovic N, Jakovljevic D, Leo JLD, Griensven V. Antioxidative activities and chemical characterization of polysaccharide extracts from the widely used mushroom. *J. Food Comp. Analysis.* 2012;26(1-2):144-153.

[60] Shi M, Zhang Z, Yang Y. Antioxidant and immunoregulatory activity of *Ganoderma lucidum* polysaccharide (GLP). *Carbohydr. Polym*. 2013;95(1):200-206.

[61] Kozarski M, Klaus A, Niksic M, Jakovljevic D, Helsper PFG. Antioxidative and immunomudulating activities of polysaccharide extracts of the medicinal mushroom. *Food Chem.* 2011;129(4):1667-1675.

[62] Boztas AO, Karakuzu O, Galante G, Ugur Z, Kocabas F, Altuntas CZ, et al. Synergistic interaction of paclitaxel and curcumin with cyclodextrin polymer complexation in human cancer cells. *Mol. Pharm.* 2013;10(7):2676-2683.

[63] Szakacs G, Paterson JK, Ludwig JA, Booth-Genthe C, Gottesman MM. Targeting multidrug resistance in cancer. *Nat. Rev. Drug Discov*. 2006;5:219-234.

[64] Naksuriya O, Okonogi S, Schiffelers RM, Hennink WE. Curcumin nanoformulations: a review of pharmaceutical properties and preclinical studies and clinical data related to cancer treatment. *Biomaterials.* 2014;35:3365-3383.

[65] Anand P, Sundaram C, Jhurani S, Kunnumakkara AB, Aggarwal BB. Curcumin and cancer: an "old-age" disease with an "age-old" solution. *Cancer Lett.* 2008;267:133-136.

[66] Bar-Sela G, Epelbaum R, Schaffer M. Curcumin as an anti-cancer agent: review of the gap between basic and clinical applications. *Curr. Med. Chem.* 2010:17:190-197.

[67] Kaura N, Kumara M, Dhimana S, Kaura J, Devia M, Singha R, et al. Curcumin and its derivatives as chemotherapeutic agents. *J. Chem. Pharm. Res.* 2016; 8(2):301-318

[68] Sarkar A, De R, Mukhopadhyay AK. Curcumin as a potential therapeutic candidate for Helicobacter pylori associated diseases. World J Gastroenterol. 2016;22(9):2736-2748.

[69] Esatbeyoglu T, Huebbe P, Ernst IM, Chin D, Wagner AE, Rimbach G. Curcumin--from molecule to biological function. *Angew Chem. Int. Ed.* 2012;51:5308-5332.

[70] Khanna C, Rosenberg M, Vail DM. A review of paclitaxel and novel formulations including those suitable for use in dogs. *J. Vet. Intern. Med*. 2015;29(4):10006-10012.

[71] Sidaway P. Weekly or 3-weekly paclitaxel are equally effective. *Nat. Rev. Clin. Oncol*. 2016;13:264.

[72] Zeichner SB, Terawaki H, Gogineni K. A review of systemic treatment in metastatic triple-negative breast cancer. *Breast Cancer.* 2016;10:25-36.

[73] Priyadarshini K, Keerthi AU. Paclitaxel against cancer: a short review. *Med. Chem*. 2012;2:139-141.

[74] Marupudi NI, Han JE, Li KW, Renard VM, Tyler BM, Brem H. Paclitaxel: a review of adverse toxicities and novel delivery strategies. *Expert Opin. on Drug. Saf.* 2007;6:609-621.

[75] Spencer CM, Faulds D. Paclitaxel. A review of its pharmacodynamic and pharmacokinetic properties and therapeutic potential in the treatment of cancer. *Drugs.* 1994;48:794-847.

[76] Kim B, Lee C, Lee ES, Shin BS, Youn YS. Paclitaxel and curcumin co-bound albumin nanoparticles having antitumor potential to pancreatic cancer. *Asian J. Pharm. Sci*. 2016, doi:10.1016/j.ajps.2016.05.005

[77] Nguyen HN, Ha PT, Nguyen AS, Nyugen DT, Do HD, Thi QY, et al. Curcumin as fluorescent probe for directly monitoring in vitro uptake of curcumin combined paclitaxel loaded PLA-TPGS nanoparticles. *Adv. Nat. Sci. Nanosci. Nanotechnol.* 2016:7: doi:10.1088/2043-6262/7/2/025001

[78] Altmann KH, Gertsch J. Anticancer drugs from nature - natural products as a unique source of new microtubule-stabilizing agents. *Nat. Prod. Rep.* 2007;24:327-57.

[79] Aggarwal BB, Shishodia S, Takada Y, Banerjee S, Newman RA, Bueso-Ramos CE, Price JE. Curcumin suppresses the paclitaxel-induced nuclear factor-kB pathway in breast cancer cells and inhibits lung metastasis of human breast cancer in nude mice. *Clin. Cancer Res.* 2005;11:7490-7498.

[80] Shehzad A, Wahid F, Lee YS. Curcumin in cancer chemoprevention: molecular targets, pharmacokinetics, bioavailability and clinical trials. *Arch. Pharm.* 2010;343:489-499.

[81] Ruttala HB, Ko YT. Liposomal co-delivery of curcumin and albumin/paclitaxel nanoparticle for enhanced synergistic antitumor efficacy. *Colloids Surf. B Biointerfaces*. 2015;128:419-426.

[82] Chearwae W, Wu CP, Chu HY, Lee TR, Ambudkar SV, Limtrakul P. Curcuminoids purified from turmeric powder modulate the function of human multidrug resistance protein 1 (ABCC1). *Cancer Chemother. Pharmacol*. 2006;57:376-388.

[83] Ganta S and Amiji M. Coadministration of paclitaxel and curcumin in nanoemulsion formulations to overcome multidrug resistance in tumor cells. *Mol. Pharm.* 2009;6:928-939.

[84] Hu H, Yu J, Li Y, Zhao J, Dong H. Engineering of a novel pluronic F127/graphene nanohybrid for pH responsive drug delivery. *J. Biomed. Mater. Res. A* 2012;100:141-148.

[85] Lee KL, Shukla S, Wu M, Ayat NR, El Sanadi CE, Wen AM, *et. al*. Stealth filaments: polymer chain length and conformation affect the *in vivo* fate of PEGylated potato virus X. *Acta Biomat.* 2015;19:166-179.

[86] Amoozgar Z, Yeo Y. Recent advances in stealth coating of nanoparticle drug delivery systems. *Interdiscip. Rev. Nanomed. Nanobiotechnol*. 2012; 4(2):219-233.

[87] Thomas HR, Phillips DJ, Wilson NR, Gibson MI, Rourke JP. One-step grafting of polymers to graphene oxide. *Polym. Chem.* 2015; 6:8270-8274.

[88] Dreaden EC, Austin LA, Mackey MA, El-Sayed MA. Size matters: gold nanoparticles in targeted cancer drug delivery. *Ther. Deliv.* 2012; 3(4):547-78.

[89] Shenoy DB, Amiji MM. Poly(ethylene oxide)-modified poly(ε-caprolactone) nanoparticles for targeted delivery of tamoxifen in breast cancer, Int. J. Pharm. 2005;293(1-2):261-270.

[90] **Muthoosamy K**, Abubakar IB, Bai RG, Loh HS, Manickam S. Engineered design for the exceedingly higher Co-loading of Curcumin and Paclitaxel onto polymer-functionalized reduced graphene oxide cargo shows highly potent synergistic anticancer effects in lung and breast cancer cells. *Under review @ Scientific Reports, Mar 2016.*

[91] Huang NM, Lim HN, Chia CH, Yarmo MA, Muhamad MR. Simple room-temperature preparation of high-yield large-area graphene oxide. *Int J Nanomedicine.* 2011;6:3443-3448.

[92] Dubois M, Gilles KA, Hamilton JK, Rebers PA, Smith F. Colorimetric method for determination of sugars and related substances. *Anal Chem*. 1956;28(3):350-356.

[93] Lim SW, Ting KN, Bradshaw TD, Zeenathul NA, Wiart C, Khoo TJ, Lim KH, Loh HS. *Acalypha wilkesiana* extracts induce apoptosis by causing single strand and double strand DNA breaks. *J. Ethnopharmacol.* 2011;138(2):616–623.

[94] Lim SW, Loh HS, Ting KN, Bradshaw TD, Zeenathul NA. *Acalypha wilkesiana* ethyl acetate extract enhances the *in vitro* cytotoxic effects of α-tocopherol in human brain and lung cancer cells. *Int J Biosci Biochem Bioinforma*. 2013;3(4):335-340.

[95] Lim SW, Loh HS, Ting KN, Bradshaw TD, Zeenathul NA. Antiproliferation and induction of caspase-8-dependent mitochondria-mediated apoptosis by beta-tocotrienol in human lung and brain cancer cell lines. *Biomed. Pharmacother.* 2014;68:1105-1115.

[96] Chatterjee A, Chattopadhyay D, Chakrabarti G. miR-17-5p downregulation contributes to paclitaxel resistance of lung cancer cells through altering beclin1 expression. *PloS One. 2014*, 9, doi: 10.1371/journal.pone.0095716

[97] Koopman G, Reutelingsperger CP, Kujiten GA, Keehnen RM, Pals ST, et al. Annexin V for flow cytometric detection of phosphatidylserine expression on B cells undergoing apoptosis. *Blood*. 1994;84:1415-1420.

[98] Han YJ, Luo ZM, Yuwen LH, Tian J, Zhu XR, Wang LH. Synthesis of silver nanoparticles on reduced graphene oxide under microwave irradiation with starch as an ideal reductant and stabilizer. *Appl. Surf. Sci.* 2013;266:188-193.

[99] Zhou Y, Bao QL, Tang LAL, Zhong YL, Loh KP. Hydrothermal dehydration for the "Green" reduction of exfoliated graphene oxide to graphene and demonstration of tunable optical limiting properties. *Chem. Mater.* 2009;21(13):2950-2956.

[100] Wojtoniszak M, Chen XC, Kalenczuk RJ, Wajda A, Lapczuk J, Kurzewski M, et al. Synthesis, dispersion, and cytocompatibility of graphene oxide and reduced graphene oxide. *Colloid Surface B.* 2012;89:79-85.

[101] Acik M, Lee G, Mattevi C, Chhowalla M, Cho K, Chabal YJ. Unusual infrared-absorption mechanism in thermally reduced graphene oxide. *Nat. Mater.* 2010;9(10):840-845.

[102] Wang X, Chen XL, Qi ZM, Liu XC, Li WZ, Wang SY. A study of *Ganoderma lucidum* spores by FTIR microspectroscopy. *Spectrochim. Acta A.* 2012;91:285-289.

[103] Chen X, Liu X, Sheng D, Huang D, Li W, Wang X. Disctinction of broken cellular wall *Ganoderma lucidum* spores and *G.lucidum* spores using FTIR microspectroscopy. *Spectrochim. Acta A.* 2012;9;667-672.

[104] Gurunathan S, Han JW, Dayem AA, Eppakayala V, Park MR, Kwon DN, et al. Antibacterial activity of dithiothreitol reduced graphene oxide. *J. Ind. Eng. Chem.* 2013;19(4):1280-1288.

[105] Zhang HB, Zheng WG, Yan Q, Yang Y, Wang JW, Lu ZH, et al. Electrically conductive polyethylene terephthalate/graphene nanocomposites prepared by melt compounding. *Polymer.* 2010;51(5):1191-1196.

[106] Jin YH, Huang S, Zhang M, Jia MQ, Hu D. A green and efficient method to produce graphene for electrochemical capacitors from graphene oxide using sodium carbonate as a reducing agent. *Appl. Surf. Sci.* 2013;268:541-546.

[107] Liu PB, Huang Y, Wang L. A facile synthesis of reduced graphene oxide with Zn powder under acidic condition. *Mater. Lett.* 2013;91:125-128.

[108] Si W, Wu X, Zhou J, Guo F, Zhuo S, Cui H, et al. Reduced graphene oxide aerogel with high-rate supercapacitive performance in aqueous electrolytes. *Nanoscale Research Lett*. 2013;8(1):247.

[109] Zhang W, He W, Jing X. Preparation of a stable graphene dispersion with high concentration by ultrasound. *J. Phys. Chem. B*. 2010;114(32):10368-10373.

[110] Roy I, Sarkar G, Mondal S, Rana D, Bhattacharyya A, Ranian N, et al. Synthesis and characterization of graphene from waste dry cell battery for electronic applications. *RSC Adv.* 2016; 6:10557-10564.

[111] Guo DJ, Wei ZY, Shi B, Wang SW, Wang LZ, Tan W, et al. Copper nanoparticles spaced 3D graphene films for binder-free lithium-storing electrodes. *J. Mater. Chem. A*. 2016; 4: 8466-8847.

[112] Lotya M, Hernandez Y, King PJ, Smith RJ, Nicolosi V, Karlsson LS, et al. Liquid phase production of graphene by exfoliation of graphite in surfactant/water solutions. *J. Am. Chem. Soc*. 2009;131(10):3611-3620.

[113] Dreyer DR, Park S, Bielawski CW, Ruoff RS. The chemistry of graphene oxide. *Chem. Soc. Rev.* 2010;39;228-240.

[114] Schniepp HC, Li JL, McAllister MJ, Sai H, Herrera-Alonso M, Adamson DH, et al. Functionalized single graphene sheets derived from splitting graphite oxide. *J. Phys. Chem. B.* 2006;110(17):8535-8539.

[115] Kudin KN, Ozbas B, Schniepp HC, Prud'homme RK, Aksay IA, Car R. Raman spectra of graphite oxide and functionalized graphene sheets. *Nano Lett.* 2008;8(1):36-41.

[116] Shen J, Li T, Shi M, Li N, Ye M. Polyelectrolyte-assisted one-step hydrothermal synthesis of Ag-reduced graphene oxide composite and its antibacterials properties. *Mater. Sci. Eng. C.* 2012;32(7):2042-2047.

[117] Alanyalioglu M, Segura JJ, Oro-Sole J, Casan-Pastor N. The synthesis of graphene sheets with controlled thickness and order using surfactant-assisted electrochemical processes. *Carbon.* 2012;50(1):142-152.

[118] Wang F, Zhang K. Reduced graphene oxide-TiO_2 nanocomposite with high photocatalystic activity for the degradation of rhodamine B. *J. Mol. Catal. A-Chem.* 2011;345(1-2):101-107.

[119] Ferrari AC, Meyer JC, Scardaci V, Casiraghi C, Lazzeri M, Mauri F, et al. Raman spectrum of graphene and graphene layers. *Phys. Rev. Lett.* 2006;97(18).

[120] Li D, Muller MB, Gilje S, Kaner RB, Wallace GG. Processable aqueous dispersions of graphene nanosheets. *Nat. Nanotechnol*. 2008;3(2):101-105.

[121] Stankovich S, Dikin DA, Dommett GHB, Kohlhaas KM, Zimney EJ, Stach EA, et al. Graphene-based composite materials. *Nature.* 2006;442(7100):282-286.

[122] Compton OC, An Z, Putz KW, Hong BJ, Hauser BG, Brinson LC, et al. Additive-free hydrogelation of graphene oxide by ultrasonication. *Carbon.* 2012;50(10):3399-3406.

[123] Repetto G, del Peso A, Zurita JL. Neutral red uptake assay for the estimation of cell viability/cytotoxicity. *Nat. Protoc*. 2008;3(7):1125-1131.

[124] Guo X, Mei N. Assessment of the toxic potential of graphene family nanomaterials. *J. Food Drug Anal.* 2014;22;105-115.

[125] Sasidharan A, Panchakarla LS, Chandran P, Menon D, Nair S, Rao CN, et al. Differential nano-bio interactions and toxicity effects of pristine versus functionalized graphene. *Nanoscale.* 2011;3(6):2461-2464.

[126] Mohan PRK, Sreelakshmi G, Muraleedharan CV, Joseph R. Water soluble complexes of curcumin with cyclodextrins: characterization by FT-Raman spectroscopy. *Vib. Spectrosc*. 2012;62:77-84.

[127] Hiremath JG, Khamar NS, Palavalli SG, Rudani CG, Aitha R, Mura P. Paclitaxel loaded carrier based biodegradable polymeric implants: preparation and in vitro characterization. *Saudi Pharm. J.* 2013;21:85-91.

[128] Qian F, Tao J, Desikan S, Hussain M, Smith RL. Mechanistic investigation of Pluronic based nano-crystalline drug-polymer solid dispersions. *Pharm. Res.* 2007;24:1551-1560.

[129] Yallapu MM, Jaggi M, Chauhan SC. Poly(beta-cyclodextrin)/curcumin self-assembly: a novel approach to improve curcumin delivery and its therapeutic efficacy in prostate cancer cells. *Macromol. Biosci.* 2010;10:1141-1151.

[130] Huang J, Zong C, Shen H, Cao YH, Ren B, Zhang ZJ. Tracking the intracellular drug release from graphene oxide using surface-enhanced Raman spectroscopy. *Nanoscale*. 2013;5:10591-10598.

[131] Nardecchia S, Carriazo D, Ferrer ML, Gutierrez MC, del Monte F. Three dimensional macroporous architectures and aerogels built of carbon nanotubes and/or graphene: synthesis and applications. *Chem. Soc. Rev.* 2013;42:794-830.

[132] Zheng Z, Zhang X, Carbo D, Clark C, Nathan C, Lvov Y. Sonication-assisted synthesis of polyelectrolyte-coated curcumin nanoparticles. *Langmuir* 2010;26:7679-7681.

[133] Blanco E, Shen H, Ferrari M. Box 2: Nanoparticle rational design implementation for overcoming delivery barriers. *Nat. Biotech.* 2015; 33:941-951.

[134] Hobbs SK, Monsky WL, Yuan F, Roberts WG, Griffith L, Torchilin VP, Jain RK. Regulation of transport pathways in tumor vessels: Role of tumor type and microenvironment. *Proc. Natl. Acad. Sci*. 1998;95:4607–4612.

[135] Leu AJ, Berk DA, Lymboussaki A, Alitalo K, Jain RK. Absence of functional lymphatics within a murine sarcoma: a molecular and functional evaluation. *Cancer Res.* 2000;60:4324–4327.

[136] Maeda H, Bharate GY, Daruwalla J. Polymeric drugs for efficient tumor-targeted drug delivery based on EPR-effect. Eur. J. Pharm. Biopharm. 2009;71:409–419

[137] Akash MSH, Rehman K. Recent progress in biomedical applications of Pluronic (PF127): Pharmaceutical perspectives. *J. Control. Release* 2015;209:120-138.

[138] Ali-Boucetta H, Al-Jamal KT, Muller KH, Li S, Porter AE, Eddaoudi A, et al. Cellular uptake and cytotoxic impact of chemically functionalized and polymer-coated carbon nanotubes. *Small* 2011;7:3230-3238.

[139] Yang MY, Wang CJ, Chen NF, Ho WH, Lu FJ, Tseng TH. Luteolin enhances paclitaxel-indeuced apoptosis in human breast cancer MDA-MB-231 cells by blocking STAT3. *Chem. Biol. Interact.* 2014;213;60-68.

[140] Sanchez Y, Simon GP, Calvino E, de Blas E, Aller P. Curcumin stimulates reactive oxygen species production and potentiates apoptosis induction by the antitumor drugs arsenic trioxide and lonidamine in human myeloid leukemia cell lines. *J. Pharmacol. Exp. Ther*. 2010;335:114-123.

[141] Atsumi T, Tonosaki K, Fujisawa S. Comparative cytotoxicity and ROS generation by curcumin and tetrahydrocurcumin following visible-light irradiation or treatment with horseradish peroxidase. *Anticancer Res.* 2007;27:363-371.

[142] Javvadi P, Segan AT, Tuttle SW, Koumenis C. The chemopreventive agent curcumin is a potent radiosensitizer of human cervical tumor cells via increased reactive oxygen species production and overactivation of the mitogen-activated protein kinase pathway. *Mol. Pharmacol.* 2008;73:1491-1501.

[143] Woo JH, Kim YH, Choi YJ, Kim DG, Lee KS, Bae JH, et al. Molecular mechanisms of curcumin-induced cytotoxicity: induction of apoptosis through generation of reactive oxygen species, down-regulation of Bcl-XL and IAP, the release of cytochrome c and inhibition of Akt. *Carcinogenesis* 2003;24:1199-1208.

[144] Su WP, Lo YC, Yan JJ, Liao IC, Tsai PJ, Wang HC, et al. Mitochondrial uncoupling protein 2 regulates the effects of paclitaxel on Stat3 activation and cellular survival in lung cancer cells. *Carcinogenesis* 2012;33:2065-2075.

[145] Liou GY, Storz P. Reactive oxygen species in cancer. *Free Radic. Res.* 2010;44:479-496.

[146] Kikuchi H, Kuribayashi F, Kiwaki N, Nakayama T. Curcumin dramatically enhances retinoic acid-induced superoxide generating activity via accumulation of p47-phox and p67-phox proteins in U937 cells. *Biochem. Biophys. Res. Commun.* 2010;395:61-65.

[147] Chauhan VP, Popović Z, Chen O, et al. Fluorescent nanorods and nanospheres for real-time *in vivo* probing of nanoparticle shape-dependent tumor penetration. *Angew. Chem. Int. Ed. Engl.* 2011;50(48):11417–11420.

[148] Champion JA, Mitragotri, S. Shape induced inhibition of phagocytosis of polymer particles. *Pharm. Res.* 2009**;**26:244–249.

[149] Longmire MR, Ogawa M, Choyke PL, Kobayashi H. Biologically optimized nanosized molecules and particles: more than just size. *Bioconjug. Chem.* 2011;22(6):993-1000.

[150] Gen Y, Dalhaimer P, Cai S, Tsai R, Tewari M, Minko T, et al. Shape effects of filaments versus spherical particles in flow and drug delivery. *Nat. Nanotechnol.* 2007**;2:**249–255.

[151] Christian DA, Cai S, Garbuzenko OB, Harada T, Zajac AL, et al. Flexible filaments for in vivo imaging and delivery: persistent circulation of filomicelles opens the dosage window for sustained tumor shrinkage. *Mol. Pharm.* 2009;**6**:1343–1352.

[152] Chatterjee A, Chattopadhyay D, Chakrabarti G. miR-17-5p downregulation contributes to paclitaxel resistance of lung cancer cells through altering beclin1 expression. *PloS One* 2014;9.

[153] Lin SS, Huang HP, Yang JS, Wu JY, Hsai TC, Lin CC, et al. DNA damage and endoplasmic reticulum stress mediated curcumin-induced cell cycle arrest and apoptosis in human lung carcinoma A-549 cells through the activation caspases cascade- and mitochondrial-dependent pathway. *Cancer Lett*. 2008;272:77-90.

[154] Wlodkowic D, Telford W, Skommer J, Darzynkiewicz Z. Apoptosis and beyond: cytometry in studies of programmed cell death. *Method Cell Biol.* 2011;103:55-98.

[155] Lv ZD, Liu XP, Zhao WJ, Dong Q, Li FN, Wang HB, et al. Curcumin induces apoptosis in breast cancer cells and inhibits tumor growth in vitro and in vivo. *Int. J. Clin. Exp. Pathol.* 2014;7:2818-2824.

[156] Ribble D, Goldstein NB, Norris DA, Shellman YG. A simple technique for quantifying apoptosis in 96-well plates. *Bmc Biotechnol*. 2005;5.

[157] Hacker G. The morphology of apoptosis. *Cell Tissue Res.* 2000;301:5-17.

[158] Reddy CA, Somepalli V, Golakoti T, Kanugula AK, Karnewar S, Rajendiran K, et al. Mitochondrial-targeted curcuminoids: a strategy to enhance bioavailability and anticancer efficacy of curcumin. *PloS One* 2014;9.

[159] Coleman ML, Sahai EA, Yeo M, Bosch M, Dewar A, Olson MF. Membrane blebbing during apoptosis results from caspase-mediated activation of ROCK I. *Nat. Cell Biol*. 2001;3:339-345.

[160] Elmore S. Apoptosis: A review of programmed cell death. *Toxicol. Pathol.* 2007;35:495-516.

[161] Hossain MM, Banik NL, Ray SK. Synergistic anti-cancer mechanisms of curcumin and paclitaxel for growth inhibition of human brain tumor stem cells and LN18 and U138MG cells. *Neurochem. Int.* 2012;61:1102-1113.

Supplementary Information

Characterizations of Cur and Ptx loaded onto GP

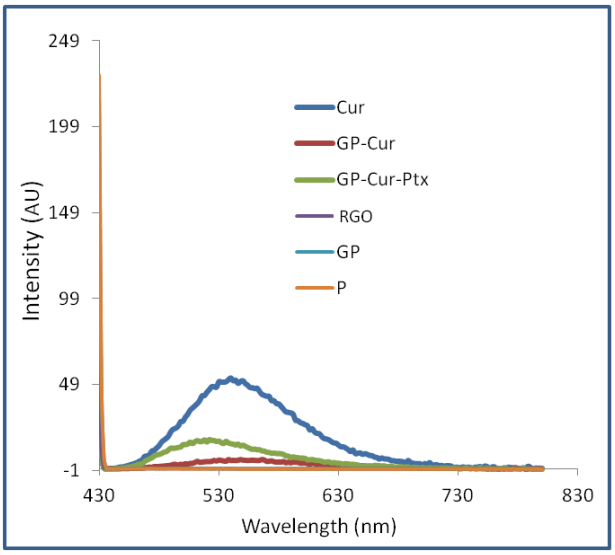

Fig. S1 Fluorescence spectra of Cur and Ptx loaded onto GP.
Note: GP: polymer-functionalized RGO

Determination of ROS generation by treatment groups in A549 and MDA cells

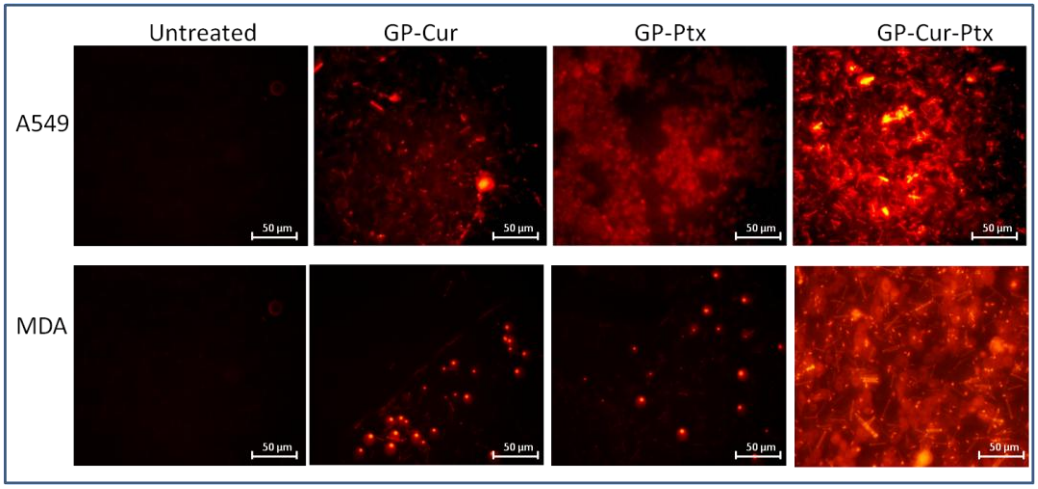

Fig. S2: ROS generation images of A549 (upper) and MDA-MB-231 (lower) of cells treated with media alone (Un-treated) and cells after treatment with GP-Cur, GP-Ptx and GP-Cur-Ptx for 120 min.

Note: Cur: curcumin; GP: polymer-functionalized reduced graphene oxide; GP-Cur: Cur loaded onto GP; Ptx: paclitaxel; GP-Ptx: Ptx loaded onto GP; GP-Cur-Ptx: Cur and Ptx loaded onto GP.

Morphology of cells undergoing apoptosis in A549 cancer cells

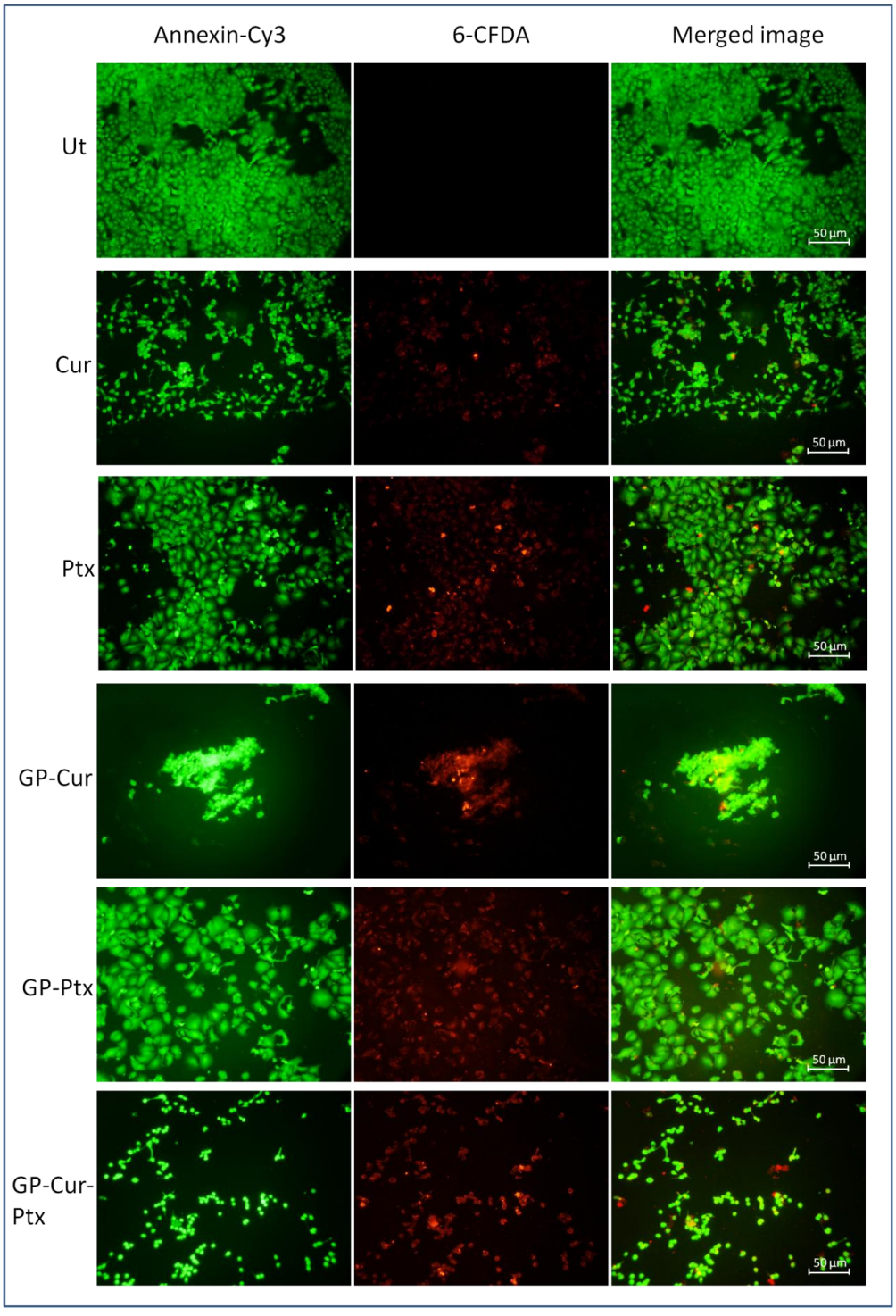

Fig. S3: Images of un-treated (Ut) A549 cells and A549 cells treated with Cur, Ptx, GP-Cur, GP-Ptx and GP-Cur-Ptx. The green fluorescent (left panel) represents the non-apoptotic cells. The red fluorescent (middle panel) represents necrotic cells and the yellowish-green fluorescent seen in the overlay images (right panel) represents early stages of apoptosis. **Note:** Cur: curcumin; GP: polymer-functionalized reduced graphene oxide; GP-Cur: Cur loaded onto GP; Ptx: paclitaxel; GP-Ptx: Ptx loaded onto GP; GP-Cur-Ptx: Cur and Ptx loaded onto GP.

Morphology of cells undergoing apoptosis in MDA cancer cells

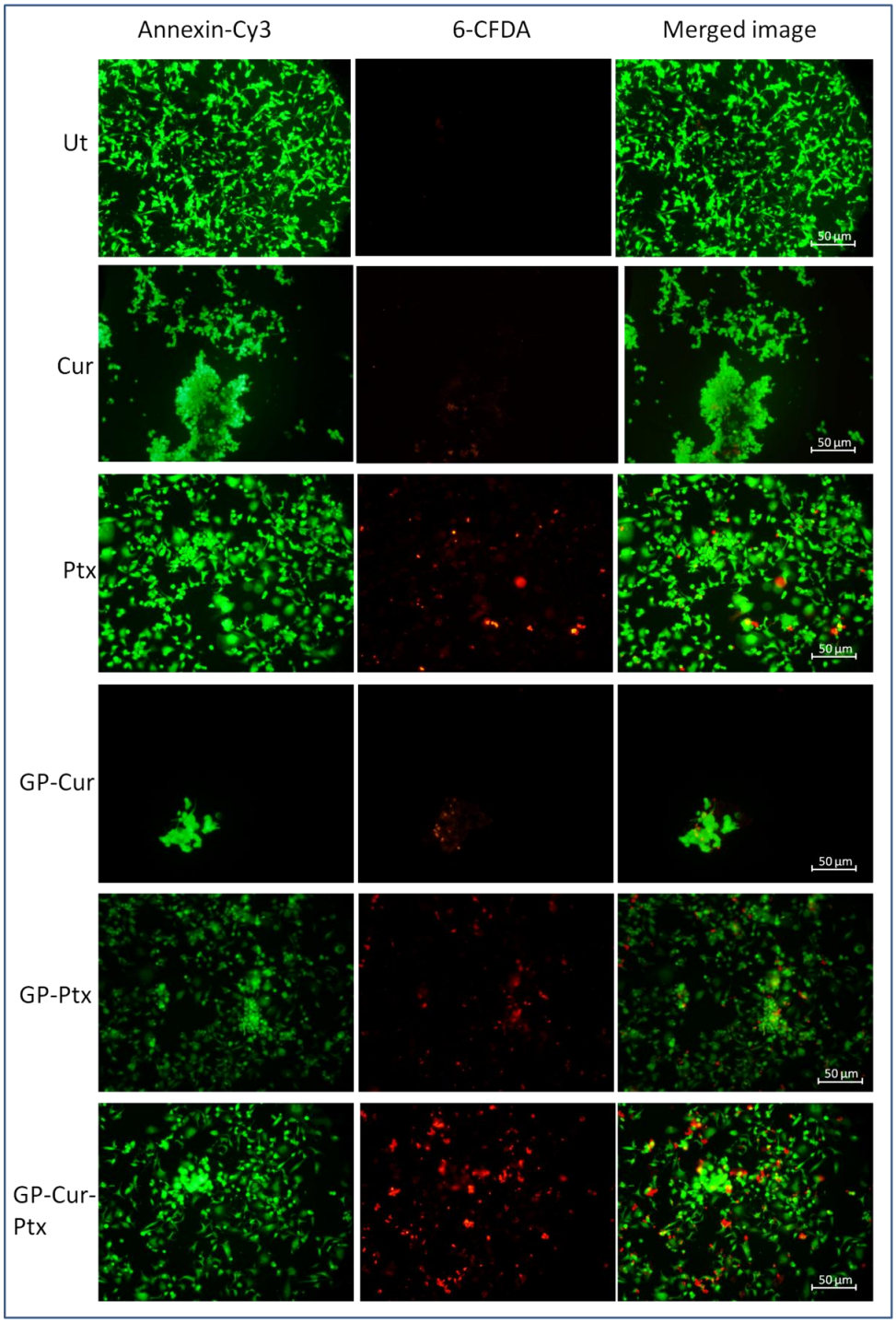

Fig. S4: Images of un-treated (Ut) MDA-MB-231 cells and MDA-MB-231 cells treated with Cur, Ptx, GP-Cur, GP-Ptx and GP-Cur-Ptx. The green fluorescent (left panel) represents the non-apoptotic cells. The red fluorescent (middle panel) represents necrotic cells and the yellowish-green fluorescent seen in the overlay images (right panel) represents early stages of apoptosis. **Note:** Cur: curcumin; GP: polymer-functionalized reduced graphene oxide; GP-Cur: Cur loaded onto GP; Ptx: paclitaxel; GP-Ptx: Ptx loaded onto GP; GP-Cur-Ptx: Cur and Ptx loaded onto GP.

The University of Nottingham
UNITED KINGDOM · CHINA · MALAYSIA

Declaration of Contribution for Published Papers

Paper 1:

Muthoosamy K, Bai RG, Manickam S. Graphene and graphene oxide as a docking station for modern drug delivery system. *Curr. Drug Deliv.* **2014**;11;1-18.

Description of contribution: Main contributor which includes complete lab works, characterizations and analysis as well as write-up of the whole paper.

I hereby declare that the first author Kasturi Muthoosamy has the major contribution towards the above published paper.

Name of Corresponding author: Prof. Dr Sivakumar Manickam

Email: Sivakumar.Manickam@nottingham.edu.my

Signature: 

The University of Nottingham
UNITED KINGDOM · CHINA · MALAYSIA

Declaration of Contribution for Published Papers

Paper 2:

Muthoosamy K, Bai RG, Abubakar IB, Sudheer SM, Lim HN, Loh HS, Huang NM, Chia CH, Manickam S. Exceedingly biocompatible and thin-layered reduced graphene oxide nanosheets using an eco-friendly mushroom extract strategy. *Int. Journal of Nanomedicine*. **2015**;10:1505-1519.

Description of contribution: Main contributor which includes complete lab works, characterizations and analysis as well as write-up of the whole paper.

I hereby declare that the first author Kasturi Muthoosamy has the major contribution towards the above published paper.

Name of Corresponding author: Prof. Dr Sivakumar Manickam

Email: Sivakumar.Manickam@nottingham.edu.my

Signature:

The University of Nottingham
UNITED KINGDOM · CHINA · MALAYSIA

Declaration of Contribution for Published Papers

Paper 3:

Muthoosamy K, Abubakar IB, Bai RG, Loh HS, Manickam S. Engineered design for the exceedingly higher co-loading of Curcumin and Paclitaxel onto polymer-functionalized reduced graphene oxide cargo shows highly potent synergistic anticancer effects in lung and breast cancer cells. *Under review Scientif Reports, Mar 2016.*

Description of contribution: Main contributor which includes complete lab works, characterizations and analysis as well as write-up of the whole paper.

I hereby declare that the first author Kasturi Muthoosamy has the major contribution towards the above published paper.

Name of Corresponding author: Prof. Dr Sivakumar Manickam

Email: Sivakumar.Manickam@nottingham.edu.my

Signature: 

The University of Nottingham
UNITED KINGDOM · CHINA · MALAYSIA

Declaration of Contribution for Published Papers

Paper 4:

Bai RG, Ninan N, **Muthoosamy K**, Manickam S. Graphene: a versatile platform for nanotheranostics and tissue engineering. *Under review, Progress in Materials Sciences, Sept 2015.*

Description of contribution: Overall technicality of the contents of the paper, developed the skeletal information and scope of the paper, cross-checking the facts and references, literature review contribution and proof-reading.

I hereby declare that the co-author Kasturi Muthoosamy has **30%** contribution towards the above published paper.

Name of Corresponding author: Prof. Dr Sivakumar Manickam

Email: Sivakumar.Manickam@nottingham.edu.my

Signature: 

Declaration of Contribution for Published Papers

Paper 5:

Afreen S, **Muthoosamy K**, Manickam S, Hashim U. Functionalized fullerene (C60) as a potential nanomediator in the fabrication of highly sensitive biosensors. Biosensors & Bioelectronics. **2015**; 63; 354-64.

Description of contribution: Overall technicality of the contents of the paper, developed the skeletal information, cross-checking the facts and references, literature review contribution and proof-reading.

I hereby declare that the co-author Kasturi Muthoosamy has **40%** contribution towards the above published paper.

Name of Corresponding author: Prof. Dr Sivakumar Manickam

Email: Sivakumar.Manickam@nottingham.edu.my

Signature: 

Declaration of Contribution for Published Papers

Paper 6:

Ng CM, **Muthoosamy K**, Loh HS, Manickam S, Sridewi N. Conjugation of insulin onto the sidewalls of single-walled carbon nanotubes (SWCNTs) through functionalization and diimide-activated amidation. *Int. Journal of Nanomedicine.* 2016; 11: 1607-14.

Description of contribution: Design of the functionalization of SWCNTs, optimization of the insulin conjugation and development of protein assay for insulin concentration determination.

I hereby declare that the co-author Kasturi Muthoosamy has **40%** contribution towards the above published paper.

Name of Corresponding author: Prof. Dr Sivakumar Manickam

Email: Sivakumar.Manickam@nottingham.edu.my

Signature: 

Declaration of Contribution for Published Papers

Paper 7:

Afreen S, **Muthoosamy K**, Kokubo K, Manickam S. Hydration or hydroxylation: A quantitative study towards a facile approach of producing Fullerenol by introducing hydroxyl groups onto C60 cage via acoustic cavitation in presence of hydrogen peroxide. *Under review, RSC Advances, Dec 2015.*

Description of contribution: Design of the functionalization of fullerene, optimization with the acoustic system, characterizations and intensive data analysis, specifically on AFM and DLS.

I hereby declare that the co-author Kasturi Muthoosamy has **40%** contribution towards the above published paper.

Name of Corresponding author: Prof. Dr Sivakumar Manickam

Email: Sivakumar.Manickam@nottingham.edu.my

Signature: 

The University of Nottingham
UNITED KINGDOM · CHINA · MALAYSIA

Declaration of Contribution for Published Papers

Paper 8:

Bai RG, **Muthoosamy K**, Shipton FN, Pandikumar A, Kumar PR, Huang NM, Manickam S. Biogenic synthesis of reduced graphene oxide-silver (RGO-Ag) nanocomposite and its dual applications as antibacterial agent and cancer biomarker sensor. *RSC Advances*. 2016; 6: 36576-87.

Description of contribution: Design of the synthesis route for the preparation of RGO-Ag nanocomposite. Design and optimization of the antibacterial and electrochemical studies.

I hereby declare that the co-author Kasturi Muthoosamy has **40%** contribution towards the above published paper.

Name of Corresponding author: Prof. Dr Sivakumar Manickam

Email: Sivakumar.Manickam@nottingham.edu.my

Signature: 

The University of Nottingham
UNITED KINGDOM · CHINA · MALAYSIA

Declaration of Contribution for Published Papers

Paper 9:

Ariffin SN, Lim HN, Tumeri FA, Abdullah AH, Ahmad M, Ibrahim NA, Huang NM, Teo PS, **Muthoosamy K**, Harrison I. Modification of polypropylene filter with metal oxide and reduced graphene oxide for water treatment. *Ceramics Int*. **2014**;40(5), 6927-36.

Description of contribution: Chemical characterization specifically on thermogravimetric analysis (TGA) and proof-reading.

I hereby declare that the co-author Kasturi Muthoosamy has **15%** contribution towards the above published paper.

Name of Corresponding author: Dr Lim Hong Ngee

Email: janet_limhn@science.upm.edu.my

Signature: 

Declaration of Contribution for Published Papers

Book Chapter:

Bai RG, **Muthoosamy K**, Manickam S. *Nanomedicine in Theranostics. Nanotechnology Applications in Tissue Engineering. Publisher: Elsevier* http://store.elsevier.com/Nanotechnology-Applications-for-Tissue-Engineering/isbn-9780323328890/, Editors: Neethu Ninan, Sabu Thomas, Yves Grohens, **2015**. pp.195-213.

Description of contribution: Overall technicality of the contents of the paper, developed the skeletal information and scope of the paper, cross-checking the facts and references, literature review contribution and proof-reading.

I hereby declare that the co-author Kasturi Muthoosamy has **40%** contribution towards the above published paper.

Name of Corresponding author: Prof. Dr Sivakumar Manickam

Email: Sivakumar.Manickam@nottingham.edu.my

Signature: 

Appendix

Published papers

-This page has been intentionally left blank-

Send Orders for Reprints to reprints@benthamscience.net
Current Drug Delivery, 2014, *11*, 000-000

Graphene and Graphene Oxide as a Docking Station for Modern Drug Delivery System

Kasturi Muthoosamy, Renu Geetha Bai and Sivakumar Manickam*

Manufacturing and Industrial Processes Research Division, University of Nottingham Malaysia Campus, Malaysia

Abstract: Motivated by the success and exhaustive research on carbon nanotubes (CNTs) based drug delivery, graphene, a two-dimensional; honey-comb crystal lattice has emerged as the rising star in recent years. Graphene is a flat monolayer of carbon atoms that holds many promising properties such as unparalleled thermal conductivity, remarkable electronic properties, and most intriguingly higher planar surface and superlative mechanical strength, which are attractive in bio-technological applications. Delivery of anti-cancer drugs using graphene and its derivatives has sparked major interest in this emerging field. The anti-cancer therapies often pose a limitation of insolubility, administration problems and cell-penetration ability. In addition, systemic toxicity caused by lack of selective targeting towards cancer cells and inefficient distribution limits its clinical applications. Graphene nanocomposite is a promising tool to address these drawbacks. This review will focus on various synthesis and functionalization of graphene and graphene oxide for providing better solubility and targeted drug delivery at cancer cells. A more advanced and 'smart' graphene hybrid nanostructures that have several functionalities such as stimulus-response mediated delivery, imaging at release sites as well as transfection into cancer cells are also presented. A brief description on the challenges and perspectives for future research in this field is also discussed.

Keywords: Cancer, Drug delivery, Graphene, Graphene oxide, Smart delivery, Graphene hybrids.

1. INTRODUCTION

Graphene, a 'wonder material' of this decade has gained tremendous interest from researchers across the globe since its discovery in 2004, using a sticky tape and a pencil [1]. Graphene is a two-dimensional (2D) sheet with one atom thickness and consists of sp^2 hybridized carbon atoms, arranged in a honeycomb network. It is also the building block of other carbon allotropes, whereby wrapping of graphene forms 0D fullerene, rolling forms 1D carbon nanotubes (CNTs), and stacking produces 3D graphite [2]. In this short period of time, extensive research has been carried out on graphene and its derivatives, with the number of publications exceeding 23,000 (ScienceDirect), closely catching up on CNTs' 33,000 publications, which was discovered back in 1991 [3]. The explosion of interest in this new nanomaterial is due to its astounding properties such as superlative mechanical strength (Young's modulus of 1100 GPa) [4], unparalleled thermal conductivity (5000 W/m/K) [5], exceptional electrical conductivity (mobility of charge carriers of 200,000 $cm^2V^{-1}s^{-1}$) [6, 7], higher planar surface area (2630 m^2/g) [4], ease of functionalization [8, 9], low cost and easy scalability on its production [10, 11]. As graphene research has expanded, many potential applications were discovered such as energy storage devices, sensors, transparent electrodes, photodetectors [4, 12-14], as well as recent advances in medical applications such as drug or gene delivery, biosensor, medical imaging, tissue engineering, photothermal therapy and antibacterial applications [15-19].

Graphene oxide (GO) and reduced graphene oxide (RGO) are parts of the graphene family, besides other derivatives such as graphene nanosheets (GNS), few-layer graphene (FLG) and ultrathin graphite [20]. GO, in particular is the most researched material in the graphene family due to its ease of functionalization. GO is the oxidized form of graphene that consists of carboxylate groups on the periphery, and epoxide and hydroxyl groups on the basal plane. The carboxylate groups provide colloidal stability and pH dependent negative surface charge, whereas the hydroxyl and epoxide functional groups are uncharged, allowing hydrogen bonding and surface reactions with other materials. Besides hydroxyl and epoxide groups, there are also unmodified graphenic domains on the basal plane, which exhibit hydrophobicity and displays π-π interactions with other aromatic molecules. Therefore, GO demonstrates amphiphilic properties, which can be used to stabilize hydrophobic molecules, such as water-insoluble drugs [21-23]. On the other hand, RGO is commonly produced by chemical reduction of GO using hydrazine or other milder reducing agents. The reduction of GO increases electrical conductivity, however it reduces water dispersibility as hydrophobicity is increased due to the removal of oxygen groups. Functionalization can still be carried out on RGO by using hydrophobic and π-π interactions [24, 25].

Due to the larger surface area of GO and RGO, which is at least an order of magnitude larger than any other biomaterials, it is an ideal material for drug loading and drug deliv-

*Address correspondence to this author at the Manufacturing and Industrial Processes Research Division, University of Nottingham Malaysia Campus, Jalan Broga, Semenyih 43500, Malaysia; Tel: +60389248156; Fax: +60389248017; E-mail: Sivakumar.Manickam@nottingham.edu.my

1567-2018/14 $58.00+.00

International Journal of Nanomedicine

Dovepress
open access to scientific and medical research

Open Access Full Text Article

ORIGINAL RESEARCH

Exceedingly biocompatible and thin-layered reduced graphene oxide nanosheets using an eco-friendly mushroom extract strategy

This article was published in the following Dove Press journal:
International Journal of Nanomedicine
20 February 2015
Number of times this article has been viewed

Kasturi Muthoosamy[1]
Renu Geetha Bai[1]
Ibrahim Babangida Abubakar[2]
Surya Mudavasseril Sudheer[1]
Hong Ngee Lim[3]
Hwei-San Loh[2,4]
Nay Ming Huang[5]
Chin Hua Chia[6]
Sivakumar Manickam[1]

[1]Manufacturing and Industrial Processes Research Division, Faculty of Engineering, [2]School of Biosciences, Faculty of Science, University of Nottingham Malaysia Campus, Semenyih, Selangor, Malaysia; [3]Department of Chemistry, Faculty of Science, Universiti Putra Malaysia, Serdang, Selangor, Malaysia; [4]Biotechnology Research Centre, University of Nottingham Malaysia Campus, Semenyih, Selangor, Malaysia; [5]Low Dimension Materials Research Centre, Department of Physics, Faculty of Science, University of Malaya, Kuala Lumpur, Malaysia; [6]School of Applied Physics, Faculty of Science and Technology, Universiti Kebangsaan Malaysia, Bangi, Selangor, Malaysia

Correspondence: Sivakumar Manickam
Manufacturing and Industrial Processes Research Division, Faculty of Engineering, University of Nottingham Malaysia Campus, Jalan Broga, 43500 Semenyih, Selangor, Malaysia
Tel +60 3 8924 8156
Fax +60 3 8924 8017
Email sivakumar.manickam@nottingham.edu.my

Purpose: A simple, one-pot strategy was used to synthesize reduced graphene oxide (RGO) nanosheets by utilizing an easily available over-the-counter medicinal and edible mushroom, *Ganoderma lucidum*.

Methods: The mushroom was boiled in hot water to liberate the polysaccharides, the extract of which was then used directly for the reduction of graphene oxide. The abundance of polysaccharides present in the mushroom serves as a good reducing agent. The proposed strategy evades the use of harmful and expensive chemicals and avoids the typical tedious reaction methods.

Results: More importantly, the mushroom extract can be easily separated from the product without generating any residual byproducts and can be reused at least three times with good conversion efficiency (75%). It was readily dispersible in water without the need of ultrasonication or any surfactants; whereas 5 minutes of ultrasonication with various solvents produced RGO which was stable for the tested period of 1 year. Based on electrochemical measurements, the followed method did not jeopardize RGO's electrical conductivity. Moreover, the obtained RGO was highly biocompatible to not only colon (HT-29) and brain (U87MG) cancer cells, but was also viable towards normal cells (MRC-5).

Conclusion: Besides being eco-friendly, this mushroom based approach is easily scalable and demonstrates remarkable RGO stability and biocompatibility, even without any form of functionalization.

Keywords: extraction, Ganoderma, RGO, ultrasound

Introduction

Graphene, a monolayer of sp^2 hybridized carbon atoms arranged in a honeycomb lattice, has gained tremendous attention among researchers due to its unique mechanical, electrical, and thermal properties, as well as due to its high surface to volume ratio. Various technological applications have been reported for graphene such as in nanoelectronics, supercapacitors, polymer nanocomposites, drug delivery systems, biosensing, solar cells, memory electronics, optoelectronics, transistor devices, etc.[1,2] However, graphene sheet, also known as reduced graphene oxide (RGO), is hydrophobic and tends to agglomerate irreversibly or even transforms back to graphite due to its van der Waals' interaction and its stronger π–π stacking, which limits its further applications. Therefore, the route of synthesis of RGO is of vital importance to impart stability as most of its unique electrical and mechanical properties are associated only with the individualized graphene sheets.[3–5] In addition, imparting solubility in water is also crucial as a well-dispersed RGO would allow further functionalization and open opportunities for various technological applications.

submit your manuscript | www.dovepress.com
Dovepress
http://dx.doi.org/10.2147/IJN.S75213

Biosensors and Bioelectronics 63 (2015) 354–364

Contents lists available at ScienceDirect

Biosensors and Bioelectronics

journal homepage: www.elsevier.com/locate/bios

Functionalized fullerene (C_{60}) as a potential nanomediator in the fabrication of highly sensitive biosensors

Sadia Afreen [a], Kasturi Muthoosamy [a], Sivakumar Manickam [a,*], Uda Hashim [b]

[a] Manufacturing and Industrial Processes Research Division, The University of Nottingham Malaysia Campus, Jalan Broga, Semenyih, Selangor D.E. 43500, Malaysia
[b] Institute of Nano Electronic Engineering, Universiti Malaysia Perlis, Perlis 01000, Malaysia

ARTICLE INFO

Article history:
Received 25 April 2014
Received in revised form
14 July 2014
Accepted 14 July 2014
Available online 25 July 2014

Keywords:
Fullerene
Functionalization
Derivatives
Biosensor
Nano
Biomolecules

ABSTRACT

Designing a biosensor for versatile biomedical applications is a sophisticated task and how dedicatedly functionalized fullerene (C_{60}) can perform on this stage is a challenge for today and tomorrow's nanoscience and nanotechnology. Since the invention of biosensor, many ideas and methods have been invested to upgrade the functionality of biosensors. Due to special physicochemical characteristics, the novel carbon material "fullerene" adds a new dimension to the construction of highly sensitive biosensors. The prominent aspects of fullerene explain its outstanding performance in biosensing devices as a mediator, e.g. fullerene in organic solvents exhibits five stages of reversible oxidation/reduction, and hence fullerene can work either as an electrophile or nucleophile. Fullerene is stable and its spherical structure produces an angle strain which allows it to undergo characteristic reactions of addition to double bonds (hybridization which turns from sp^2 to sp^3). Research activities are being conducted worldwide to invent a variety of methods of fullerene functionalization with a purpose of incorporating it effectively in biosensor devices. The different types of functionalization methods include modification of fullerene into water soluble derivatives and conjugation with enzymes and/or other biomolecules, e.g. urease, glucose oxidase, hemoglobin, myoglobin (Mb), conjugation with metals e.g. gold (Au), chitosan (CS), ferrocene (Fc), etc. to enhance the sensitivity of biosensors. The state-of-the-art research on fullerene functionalization and its application in sensor devices has proven that fullerene can be implemented successfully in preparing biosensors to detect glucose level in blood serum, urea level in urine solution, hemoglobin, immunoglobulin, glutathione in real sample for pathological purpose, to identify doping abuse, to analyze pharmaceutical preparation and even to detect cancer and tumor cells at an earlier stage. Employing fullerene-metal matrix for the detection of tumor and cancer cells is also possible by the inclusion of fullerene in single-walled carbon nanotubes (SWCNTs) known as peapods as well as in double-walled carbon nanotubes (DWCNTs), to augment the effectiveness of biosensors. This review discusses various approaches that have been reported for functionalizing fullerene (C_{60}) derivatives and their application in different types of biosensor fabrication.

Contents

Abbreviations: Au, gold; $C_{60}[C(COOH)_2]_2$, carboxyl-modified fullerene; C_{60}-NCNTs/CHIT, fullerene-nitrogen doped carbon nanotubes and chitosan; ChO, choline oxidase; CNO, carbon nano-onions; CNT, carbon nanotube; CS, chitosan; Cys, L-Cysteine; DWCNT, double walled carbon nanotube; ECL, electrochemiluminescence; *E. coli*, *Escherichia coli*; Fc, ferrocene; GCE, glassy carbon electrode; GOx, glucose oxidase; Hb, hemoglobin; H_2O_2, hydrogen peroxide; IgG, immunoglobulin G; IL, ionic liquid; ITO, Indium tin oxide; K_m, Michaelis–Menten Constant; Mb, myoglobin; MWCNT, multi-walled carbon nanotube; OMC, ordered mesoporous carbon; Pd, palladium; PDDA, poly (diallyldimethylammonium) chloride; PDGF-BB, platelet-derived growth factor B-chain; PdNCs, palladium nanocages; PGE, pyrolytic graphite electrode; Pt, platinum; PTC-NH_2, amino functionalized 3.4.9.10-perylenetetracarboxylic dianhydride; PZ, piezoelectric; QCM, quartz crystal microbalance; R.S.D, relative standard deviation; SAW, surface acoustic wave; s-BLM, self-assembled bilayer lipid membrane; SS2, Streptococcus suis Serotype 2; SWCNT, single walled carbon nanotube; SWNT, single walled nanotube; TMB, 3.3′,5.5′-tetramethylbenzidine

* Corresponding author. Tel.: +60 3 8924 8156; fax: +60 3 8924 8017.
E-mail address: Sivakumar.Manickam@nottingham.edu.my (S. Manickam).

http://dx.doi.org/10.1016/j.bios.2014.07.044
0956-5663/

Available online at www.sciencedirect.com
ScienceDirect
Ceramics International 40 (2014) 6927–6936
CERAMICS INTERNATIONAL
www.elsevier.com/locate/ceramint

Modification of polypropylene filter with metal oxide and reduced graphene oxide for water treatment

Ariffin S.N.[a], Lim H.N.[a,b,*], Jumeri F.A.[a], Zobir M.[a], Abdullah A.H.[a], Ahmad M.[a], Ibrahim N.A.[a], Huang N.M.[c], Teo P.S.[c], Muthoosamy K.[d], Harrison I.[d]

[a]*Department of Chemistry, Faculty of Science, University Putra Malaysia, UPM Serdang, 43400 Selangor, Malaysia*
[b]*Functional Device Laboratory, Institute of Advanced Technology, Universiti Putra Malaysia, UPM Serdang, 43400 Selangor, Malaysia*
[c]*Low Dimension Materials Research Centre, Department of Physics, Faculty of Science, University of Malaya, Kuala Lumpur 50603, Malaysia*
[d]*Faculty of Engineering, The University of Nottingham Malaysia Campus, JalanBroga, 43500 Semenyih, Selangor, Malaysia*

Received 26 November 2013; received in revised form 3 December 2013; accepted 3 December 2013
Available online 12 December 2013

Abstract

A hydrothermal method for the synthesis of reduced graphene oxide/titanium dioxide filter (RGO/TiO_2) and reduced graphene oxide/zinc oxide filter (RGO/ZnO) by using polypropylene (PP) porous filter is reported. Field emission scanning electron microscopy illustrated that the nanoparticles were uniformly distributed on the reduced graphene oxide nanosheets. Flexural tests showed that the physical properties of the modified filters have greater strength than the original filter. Thermogravimetric analysis revealed that the thermal property of the modified filters is the same as that of the original filter. Under a halogen lamp, the modified filter exhibited excellent photocatalytic degradation of methylene blue. The RGO/TiO_2 filter maintained its ability to degrade MB efficiently, even after five cycles of photocatalysis.

Keywords: Adsorption; Graphene; Photocatalysis; Titanium oxide; Water filter; Zinc oxide

1. Introduction

Impeccable hygiene is needed to maintain the high quality and shelf life of end-products. Purification of water is required to ensure safety and to achieve hygienic conditions. During the preparation, processing, manufacturing, and packaging of pharmaceutical and cosmetic products, foods and beverages, there is a need to maintain a high level of cleanliness and the purity of ingredients/raw materials to guarantee high standards and shelf life. Water is used in many of the requisite processes and so controlling its purity and removing pathogenic organisms responsible for waterborne diseases such as cholera, typhoid fever, and dysentery (disinfection) is absolutely essential [1]. Most municipal water supply systems achieve disinfection by chlorinating the water because this is a highly efficient and cost-effective method. Filtration methods such as ultrafiltration, nanofiltration, microfiltration, and reverse osmosis can also be used when there is a need to remove organic contaminants like proteins, gelatins, and colour pigments, but in general this requires the use of state-of-the-art technologies and makes the process more expensive. There are other disinfectant methods of microbiological impurities such as ultraviolet (UV) and ozone plants. They have the advantage of not adding any other compound to the water but are not so effective in terms of purifying the water.

The current water purification strategies mentioned above have several drawbacks. In chlorination, chlorine, chlorine oxide, or orhydrochlorous acid is added to the water to kill micro-organisms. These chlorine compounds can also react with naturally occurring organics, however, resulting in the formation of carcinogenic halo-organic compounds [2]. As a consequence, the quality of the water needs to be monitored [3]. In filtered systems, it is necessary to replace the filters frequently in order to meet the demand for high-quality water. Scheduled replacement of the filters increases the system's downtime and hence the operating costs. Conventional

*Corresponding author at: Department of Chemistry, Faculty of Science, University Putra Malaysia, UPM Serdang, 43400 Selangor, Malaysia.
E-mail address: janet_limhn@yahoo.com (H.N. Lim).

0272-8842/$ - see front matter © 2013 Elsevier Ltd and Techna Group S.r.l. All rights reserved.
http://dx.doi.org/10.1016/j.ceramint.2013.12.016

CHAPTER

NANOMEDICINE IN THERANOSTICS

12

Renu Geetha Bai, Kasturi Muthoosamy and Sivakumar Manickam
Faculty of Engineering, Manufacturing and Industrial Processes Research Division,
The University of Nottingham Malaysia Campus, Jalan Broga, Semenyih, Selangor D.E., Malaysia

12.1 INTRODUCTION

Nanotechnology has carved its own niche in the medical field. Owing to unique physical and chemical characteristics, nanomaterials show improvement in the properties, such as high surface area, easy functionalization, and good loading capacity. This leads to utilizing them for a diverse technological application. Theranostics is the combination of diagnosis and therapy. The concept of personalized nanomedicine is the backbone of nanotheranostics. Personalized medicine has been introduced by Hood in 2004, when he presented the Predictive, Personalized, Preventive, and Participatory (P4) medicine approach [1]. The core of personalized medicine emphasizes on the collection of specific data about the disease, health condition, and drug response of individuals from their cells or biomolecules. Personalized medicine has gained more attention due to its individual specific approach. Molecular level data of each individual can be decoded and collected by various methods like genomics, proteomics, metabolomics, etc. In the last few decades, the traditional Evidence-Based Medicine (EBM) perception is gradually shifting toward individualized or personalized medicine system. The conventional treatments are focused toward optimized therapies catered for a population, whereas the new approach is based on the individual's genetic variations, therefore, the chance of side effects due to therapy can be minimized and the effect of treatment can be improved.

Nanotechnology is the arena of science that deals with the manipulation of atoms and molecules to construct materials in the nanometer range, preferably below 100 nm. It includes the production and applications of physical, chemical, and biological systems, where the properties of the system change based on the change in size. In today's scenario, the prominent field of nanotechnology is nanomedicine, where nanomaterials are used for detection, treatment, diagnosis, monitoring, and control of biological systems. Nanomedicine mainly deals with the delivery of therapeutic and diagnostic agents and their efficacy in targeting and curing diseases. Cancer nanotechnology is one of the major disciplines of nanomedicine, which has been improved tremendously over the years, with the advancements in the area of nanomedicine. Early detection, better treatment options, and fewer side effects are the advantages of nanotechnology-mediated innovations in the cancer therapy [2].

Diagnosis is the preliminary step for the confirmation of a disease. Detection of an abnormality in the body in its early stage is the best way to prevent it from progression and treat it from its

S. Thomas, Y. Grohens, N. Ninan: Nanotechnology Applications for Tissue Engineering. ISBN: 978-0-323-32889-0
 DOI: http://dx.doi.org/10.1016/B978-0-323-32889-0.00012-1

RSC Advances

PAPER

Cite this: *RSC Adv.*, 2016, 6, 36576

The biogenic synthesis of a reduced graphene oxide–silver (RGO–Ag) nanocomposite and its dual applications as an antibacterial agent and cancer biomarker sensor†

Renu Geetha Bai,[a] Kasturi Muthoosamy,[a] Fiona Natalia Shipton,[b] Alagarsamy Pandikumar,[c] Perumal Rameshkumar,[c] Nay Ming Huang[c] and Sivakumar Manickam*[a]

Cancer nanotechnology encourages cutting edge research utilizing nanomaterials for the diagnosis, therapy and prevention of cancer. Recognition of cancer-related biomarkers in the body has made early detection possible and thus, paves the way towards devising methods to control it from progressing to advanced stages. Hydrogen peroxide (H_2O_2) is a critical biomolecule, which plays an important dual role in cancer progression. Herein, we have developed a sensitive method for the detection of H_2O_2 utilizing a reduced graphene oxide–silver (RGO–Ag) nanocomposite. This RGO–Ag nanocomposite was prepared using a green and facile one-step synthesis approach utilizing the extract of a medicinal mushroom, *Ganoderma lucidum*. The higher content of polysaccharides in this extract makes it a potent reducing agent for the combined reduction of GO and $AgNO_3$ to produce the RGO–Ag nanocomposite. The properties of the RGO–Ag obtained were characterized by UV-Vis spectroscopy, SEM, TEM, XRD, FT-IR and XPS techniques. The RGO–Ag modified electrode showed good electrocatalytic activity towards H_2O_2 when compared to other modified electrodes. Furthermore, it showed an LOD of 136 nM, which was determined using the LSV technique. The amperometric *i–t* curve displayed two different linear ranges of 1–100 μM and 100–1100 μM with an LOD of 3 and 56 nM, respectively. This excellent electrochemical performance towards H_2O_2 detection could contribute to advances in current cancer diagnosis. The RGO–Ag nanocomposite was also explored as a potential antibacterial agent. Owing to its synergistic effects, RGO–Ag showed a comparable antibacterial activity to the standard antibiotic, chloramphenicol. The combined antibacterial effects and sensing potential make this RGO–Ag nanocomposite a promising candidate for future health care.

Received 1st February 2016
Accepted 24th March 2016

DOI: 10.1039/c6ra02928k

www.rsc.org/advances

Introduction

The exponential growth in the research of graphene and its derivatives during the past decade reflects its extensive attraction towards the global scientific community. The exceptional crystalline structure of graphene involves sp^2 hybridized carbon atoms, where the long range π conjugation in graphene contributes to its unique electrical, electronic, thermal, optical and magnetic properties.[1–3] The combination of graphene–metal nanoparticles has emerged as an exciting field of exploration, which has crucial applications in biomedicine, thermal expansion materials, nanocomposites, catalysts, sensors and energy conversion. The most frequently reported metal nanoparticles used in combination with graphene are silver, gold, platinum and palladium.[4–11] Among the noble metals, silver nanoparticles (AgNPs) have been extensively investigated due to their facile synthetic routes and unique physical, chemical, photochemical and biological properties. Furthermore, AgNPs possess outstanding properties such as high electrical and thermal conductivity, surface enhanced plasmon resonance effect, high catalytic activity, good chemical stability and antimicrobial properties.[12–14]

The antibacterial activity of silver is well documented; the properties of AgNPs vary based on their size and distribution. The antibacterial effects of AgNPs arise due to the following: (1)

[a]*Manufacturing and Industrial Processes Research Division, Faculty of Engineering, University of Nottingham Malaysia Campus, 43500 Semenyih, Selangor, Malaysia. E-mail: Sivakumar.Manickam@nottingham.edu.my*

[b]*School of Pharmacy, Faculty of Science, University of Nottingham Malaysia Campus, 43500 Semenyih, Selangor, Malaysia*

[c]*Low Dimensional Materials Research Centre, Department of Physics, Faculty of Science, University of Malaya, 50603 Kuala Lumpur, Malaysia*

† Electronic supplementary information (ESI) available: Information on the RGO–Ag nanocomposite regarding additional characterization data, antibacterial experiments and electrocatalytic responses. See DOI: 10.1039/c6ra02928k

International Journal of Nanomedicine

Dovepress
open access to scientific and medical research

Open Access Full Text Article

ORIGINAL RESEARCH

Conjugation of insulin onto the sidewalls of single-walled carbon nanotubes through functionalization and diimide-activated amidation

This article was published in the following Dove Press journal:
International Journal of Nanomedicine
18 April 2016
Number of times this article has been viewed

Chee Meng Ng[1]
Hwei-San Loh[2]
Kasturi Muthoosamy[1]
Nanthini Sridewi[3]
Sivakumar Manickam[1]

[1]Manufacturing and Industrial Processes Research Division, Faculty of Engineering, [2]Faculty of Science, School of Biosciences, University of Nottingham Malaysia Campus, Semenyih, Selangor, [3]Faculty of Science and Defence Technology, National Defence University of Malaysia, Kuala Lumpur, Malaysia

Purpose: The high aspect ratio of carbon nanotubes (CNTs) allows the attachment of compounds that enhance the functionality of the drug vehicle. Considering this, use of CNTs as a multifunctional insulin carrier may be an interesting prospect to explore.
Materials and methods: The carboxylic acid groups were functionalized on the sidewalls of single-walled CNTs (SWCNTs) followed by diimidation to form amide bonds with the amine groups of the insulin.
Results: Scanning transmission electron microscopy and transmission electron microscopy establish clear conjugation of insulin onto the surface of nanotube sidewalls. The incorporation of insulin further increased the solubility of SWCNTs in biological solution for the tested period of 5 months. Bicinchoninic acid assay confirms that 0.42 mg of insulin could be attached to every 1 mg of carboxylated SWCNTs.
Conclusion: With the successful conjugation of insulin to SWCNTs, it opens up the potential use of SWCNTs as an insulin carrier which in need of further biological studies.
Keywords: diimidation, CNT, SWCNT, increased solubility, carboxylation, drug carrier

Introduction

Carbon nanotubes (CNTs) are highly versatile materials due to their remarkable mechanical, thermal, and electronic properties. As a result, they have been used for applications across many different technological areas. Among the recently explored applications is the use of CNTs as multifunctional drug carriers. The high aspect ratio of CNTs means that it is possible to attach not only drug molecules but also other compounds that impart desired functionalities.

In the area of oncology, numerous efforts have been made to utilize CNTs to deliver drugs to cancerous cells without affecting the nearby noncancerous cells, thereby reducing the unwanted side effects that are common with conventional chemotherapy.[1–3] Previous study has shown that CNTs due to their nanometer dimensions inherently displayed increased tumor uptake through the leaky tumor vasculature.[1] The attachment of CNTs to targeting peptides and antibodies also significantly improved tumor uptake and displayed a higher overall toxicity to tumor cells without harming the normal cells.[4–7] In addition, the conjugation of radionuclides or fluorescent probes allowed the tracking of the drug vehicles for imaging purposes.[7,8] The potential of CNTs as drug delivery vehicles has also been demonstrated in other pharmaceutical applications such as the delivery of antifungal drugs, vaccines, and gene therapy.[9–15]

Correspondence: Sivakumar Manickam
Manufacturing and Industrial Process Research Division, Faculty of Engineering, University of Nottingham Malaysia Campus, Jalan Broga, 43500 Semenyih, Selangor, Malaysia
Tel +60 3 8924 8156
Fax +60 3 8624 8017
Email sivakumar.manickam@nottingham.edu.my

http://dx.doi.org/10.2147/IJN.S98726